

HEAT DISTRIBUTION BY NATURAL CONVECTION:  
A MODELLING PROCEDURE FOR ENCLOSED SPACES

by

Kalev Ruberg  
B.S.A.D. Massachusetts Institute of Technology  
1975

Submitted in Partial Fulfillment  
of the Requirements for the  
Degree of

MASTER OF ARCHITECTURE

at the

MASSACHUSETTS INSTITUTE OF TECHNOLOGY  
September 1978

Signature of Author.....

Department of Architecture  
August 28, 1978

Certified by.....

Timothy E. Johnson, Research Associate  
Thesis Supervisor

Accepted by.....

Imre Halasz, Professor of Architecture  
Chairman, Departmental Committee for Graduate Students

MASSACHUSETTS INSTITUTE  
OF TECHNOLOGY

©Kalev Ruberg 1978

FEB 15 1979

LIBRARIES



Room 14-0551  
77 Massachusetts Avenue  
Cambridge, MA 02139  
Ph: 617.253.2800  
Email: [docs@mit.edu](mailto:docs@mit.edu)  
<http://libraries.mit.edu/docs>

## **DISCLAIMER OF QUALITY**

Due to the condition of the original material, there are unavoidable flaws in this reproduction. We have made every effort possible to provide you with the best copy available. If you are dissatisfied with this product and find it unusable, please contact Document Services as soon as possible.

Thank you.

The images contained in this document are of the best quality available.

"A passive air system is part of a living system which makes our world a microcosmos again and re-establishes our bonds with the dynamics of our natural surroundings."

-Paul Davis

To Ingrid and my parents.

# Abstract

HEAT DISTRIBUTION BY NATURAL CONVECTION: A Modelling Procedure  
for Enclosed Spaces

by Kalev Ruberg

Submitted to the Department of Architecture, September 1978,  
in partial fulfillment of the requirements for the degree  
of Master of Architecture.

As the architect has begun to consider the thermal performance of his designs, a need for thermal performance simulation techniques has developed. Presently, a gap exists in the knowledge of slow, natural convective behavior, occurring in buildings due to passive gain or convection heating sources. The central theme of this thesis is the development and verification of a simple physical modelling procedure that would allow architects to determine temperature distributions and natural convection flows, developed due to design decisions.

The physical modelling procedure was established by a series of scaling laws, based on the mixing and heat conduction properties of air. The modelling procedure was verified using a test cell and a series of models. Although the scaling laws allowed for the modelling of both infiltration and dynamic heat transfer, these effects were not modelled or verified.

It was found that models between 1/6 and 1/12 scales modelled convective flows and temperature distributions well within a wide range of proportionally scaled model heat fluxes.

A simple modelling procedure uses rigid foam insulation as the skin material with heat loss proportionality established by the thickness of the insulation. Windows in the model must be tested for proportional heat loss. An attenuated light is used to illuminate suspended particles which describe the air flows in the model. Rigorous instrumentation comprising of multiplexed thermistors, or simple measurements with a thermometer yield temperature distributions within the model.

◀  
Thesis Supervisor: Timothy E. Johnson

Title: Research Associate  
Department of Architecture

## Acknowledgements

Two persons provided invaluable guidance and support during the preparation of this thesis: Timothy Johnson of MIT's solar architecture group, and Ain Sonin, Professor of Mechanical Engineering. Their helpful comments and criticisms were greatly appreciated.

The following people and organizations are thanked for their co-operation and assistance:

Frank Durgen and Al Shaw, from the Department of Aeronautics and Astronautics, provided bubble machines and fog juices; Professor R. E. Thornton and Professor H. Edgerton, from the Department of Electrical Engineering, provided help on instrumentation design and lighting; Professor W. Smith, from the Cryogenics Laboratory, provided gas regulating equipment. Professor C. F. Dewey, from the Mechanical Engineering Department, provided lasers and video equipment; The MIT Center for Advanced Engineering Studies loaned video and lighting equipment; Bonnie Blanchard typed the manuscript; and Professor Ed Allen, from the Department of Architecture, provided a marvelous test cell, and endured the cold.

This research was funded in part by a CMHC Scholarship and a Graham Fund Grant.

I extend a special thanks to Ingrid, my wife, who endured a great deal of loneliness during the past year, and whose editing patience and skill is unsurpassed.

ERRATA AND ADDENDUM TO M.ARCH THESIS  
 HEAT DISTRIBUTION BY NATURAL CONVECTION:  
 A MODELING PROCEDURE FOR ENCLOSED SPACES  
 M.I.T. SCHOOL OF ARCHITECTURE 1978 SEPTEMBER

An abstracted version of this thesis was published as a paper in:

"Heat Distribution by Natural Convection: Modeling Procedure for Enclosed Spaces", PROCEEDINGS OF THE THIRD NATIONAL PASSIVE SOLAR CONFERENCE, San Jose, CA., AS/ISES, Newark, NJ, January, 1979.

Questions have been raised about the procedure outlined in Chapter III. The discussion below should clarify some of this.

ERRATA and ADDNEDUM

PAGE	ERROR	CORRECTION
10	Eq. 4	$(gLdT/Tr)^{0.5}$
12	Eq. 8	$K = \frac{h_c}{\rho c} (gLdT/Tr)^{0.5}$
79	Eq. 27 $L = (Q_m * (Q_{fs} * D_f)^{-1})^{0.4}$	Discussion: $(q_m/q_r * L^{0.5}) = D_f$ $Q_m = q_m * A_m$ $Q_r = q_r * A_m / L^2$ from eq. 9a $q_m = q_r * L^{0.5} * D_f$ $q_m * A_m = (q_r * A_m / L^2) * L^{0.5} * L^2$ $Q_m = Q_r * D_f * L^{2.5}$ $L = (Q_m / Q_r * D_f)^{0.4}$ where L=scale $q_m$ =heat flux/area model $q_r$ =heat flux/area fl.sc. $Q_m$ =total model heat flux $Q_r$ =total fl.sc. heat flx $A_m$ =heat conduction area in the model. $D_f$ =departure factor (definded on pg. 16)



# Table of Contents

INTRODUCTION	1
CHAPTER ONE: Thermal Scaling of Convective Flows.....	5
CHAPTER TWO: Experimental Method and Results.....	19
CHAPTER THREE: A Procedure for Simplified Thermal Modelling.....	71
CONCLUSIONS.....	101
Appendix I: Model Descriptions and Test Results.....	103
Appendix II: Experiments and Experimentation.....	127
Appendix III: Dimensionless Parameters.....	141
BIBLIOGRAPHY.....	148

## Introduction

Alternative energy systems are becoming increasingly viable for the heating and cooling of buildings. These systems may employ a mechanical approach, providing predictable heating and cooling in various areas of a building, or they may be incorporated into the design of the building, allowing natural forces to distribute heat gain occurring in a specific area. With the increased use of these alternative energy systems, thermal behavior prediction techniques that respond to the subtleties of natural heat distribution must be used in the architectural design process.

Computer-based simulations are one of these prediction techniques and are used in simple geometries to determine the thermal behavior of designs which rely on passive solar heating or wood stoves. In this method, the convection component of the heat transfer process in a building design is included in the conduction factor and thus the simulations indicate heat balances between the building interior and exterior. However, computer-based simulations<sup>1</sup> cannot

---

1. The complexity of convection currents in buildings discourages the use of computer modelling as a simulation device. Heat transfer computer models are able to deal with thermal equilibrium at present, but cannot accurately predict air movement through complex spaces.

identify the effective distribution of heat that would occur due to heat gain in complex spaces. As interior geometries influence the flow of air, complex designs might result in the stratification of temperatures, and uncomfortable thermal conditions.

It is generally understood among architects that a potential remedy to this situation lies in the control of natural convection currents through the careful arrangement of a building's spatial geometry, thoughtful positioning of building openings, and judicious use of materials. However, there is no clear cut way of determining conclusively whether or not a design will actually work as intended. Where an architect does attempt to harness these air currents to the advantage of his building's thermal environment, he is forced to rely largely on his own "gut feeling" or the more informed intuition of his consultants, and must keep his fingers crossed until the completed structure proves failure or success.

The purpose of this thesis is to develop a method whereby natural convective flows in a proposed building may be tested before actual construction. It is based on the initial hypothesis that scale models of proposed building designs may successfully be used

to simulate actual convection currents. As an experimental approach was used to test this initial hypothesis, this paper is largely concerned with a discussion of the process of experimentation followed, as well as forming conclusions and recommendations. It is organized into three chapters. Chapter I discusses scaling relationships, the understanding of which is essential in thermal modelling, for if the scaling is faulty, any subsequent conclusions drawn on the behavior of resulting air currents is challengeable. Chapter II describes the actual process of experimentation conducted for the purpose of proving the validity of the initial hypothesis. Chapter III describes the final recommended modelling technique developed as a result of the experimentation process.

Physical models have traditionally been employed extensively by architects as a familiar design and communication device, and their use in wind tunnel modelling and the monitoring of lighting effects is becoming more and more commonplace. It is hoped that thermal modelling will ultimately prove to be a useful design tool in building designs where convective heat flow is an important issue. As such, this thesis is directed at architects as well as engineers

who have a particular interest in design applications and research in the field of passive solar energy. As the nature of the experimentation process requires a good deal of instrumentation, an elementary knowledge of electricity and thermodynamics is assumed.

# Chapter I

## Thermal Scaling of Convective Flows

Convection in buildings may be described as fluid dynamic behavior in a specific physical context. The way in which physical context affects fluid behavior determines the factors influencing convection in buildings, and an understanding of these factors enables the formulation of scaling relationships. It is a basic premise here that valid small scale simulation of full scale generic convection in buildings may be achieved by the use of simplified scaling, where the most important fluid dynamic behavior is related to the governing physical parameter. Thus, rigorous scaling, where all of the factors influencing fluid behavior in confined spaces are identified, is not necessary for modelling general air flows.

## FACTORS INFLUENCING CONVECTION IN BUILDINGS

Convective heat and mass transfer in buildings occurs due to the separation of heat sources from cooling surfaces. The convective flows formed are influenced by the following 3 factors:

1. Thermal behavior of the building skin
2. Temperature and humidity differences between bulk air and convective air flows
3. Transfer of infiltration momentum to convective flow.

The characteristic air flow developed in a building is a product of these effects.

Thermal Behavior of Building Skin. Convective flow is influenced by the temperature of the building skin near which it develops. As the air adjacent to the skin is slowed by friction at the skin surface, heat from the skin is transferred to the air flow by conduction. The rate of heat transfer to the building skin is dependent upon the heat flux through the building envelope and is determined by the conduction properties and the thermal storage capacity of the materials of which the envelope is made.

Buildings lose from 75% to 80% of their heat by conduction through the building skin,<sup>2</sup> the remainder being lost by infiltration. Due to the thermal resistance of the materials, a temperature gradient occurs across the skin. The heat flux is denoted by:

$$\dot{Q}_{\text{building skin}} = h_c A (T_r - T_a) \quad (1a)$$

and

$$\dot{q}_{\text{building skin}} = h_c (T_r - T_a) \quad (1b)$$

where

$\dot{Q}_{\text{building skin}}$  = total heat flux through building skin

$\dot{q}_{\text{building skin}}$  = heat flux per unit area

$h_c$  = overall unit thermal conductance of building skin

$A$  = area of building skin

$(T_r - T_a)$  = temperature difference between inside and outside

---

2. A.D. Bryan, "Performance Studies of a Working Solar House," p. 51.



Under steady state conditions, the ratio of heat flux to temperature gradient through the building skin remains constant, and conduction through the skin is the governing thermal parameter. This is also the case under dynamic conditions for a wall with negligible thermal storage capacity, even though surface temperatures may vary. But under dynamic conditions a wall with great thermal storage capacity will not resemble steady state behavior, because the thermal flywheel effect stabilizes wall temperatures during variable heat fluxes. This influences the wall to air heat transfer and consequently the air flow adjacent to the wall.

Typical well-insulated wood construction has low thermal capacities, and conduction through the skin is thus the governing thermal parameter. On a larger scale the building skin defines an actual space where a convection system develops. This happens because heat is conducted from skin surfaces to the adjacent air layers in the space. The air moves due to the rise in temperature, and is cooled when its heat is in turn conducted from the air layers to adjacent cooler skin surfaces. The cooled air consequently falls and the cycle is repeated. The space limits the possible paths of the flows developed in this cycle.

Temperature Differences. At constant pressure, a change in the temperature of air is proportional to a change in its density.<sup>3</sup> This relationship is expressed as follows:

$$\frac{\Delta T}{T_r} \sim \frac{\Delta \rho}{\rho_r} \quad (2)$$

where

$\Delta T$  = change in temperature

$T_r$  = average room temperature

$\Delta \rho$  = change in density

$\rho_r$  = average room air density, and

$\sim$  denotes equality in terms of orders of magnitude.

The product of the density ratio and gravity yields buoyancy:

$$F_b \sim g \frac{\Delta \rho}{\rho_r} \sim g \frac{\Delta T}{T_r} \quad (3)$$

- 
3. Changes in water vapour content also cause changes in air density. At 60°F an increase in humidity from 30% to 60% will create a force of 0.21 ft/lb/sec<sup>2</sup> per ft<sup>3</sup> of air. A rise in temperature from 60°F to 70°F will create a 0.47 ft/lb/sec<sup>2</sup> force per ft<sup>3</sup> of air.

where

$F_b$  = buoyancy force

$g$  = force of gravity

Exerting the buoyancy force ( $F_b$ ) over a distance ( $L$ ) yields:

$$V_{\text{mix}} \sim \frac{\sqrt{gL\Delta T}}{T_r} \quad (4)$$

where  $V_{\text{mix}}$  = the mixing velocity of air.

Thus, temperature differences are proportional to the square of the mixing velocity of air. Further, if heat is mixed via turbulent and convective processes, and if the motion is induced by buoyant air flows the diffusivity may be expected to scale with velocity as follows:

$$D_{\text{mix}} \sim V_{\text{mix}} L \quad (5)$$

where  $D_{\text{mix}}$  = effective thermal diffusivity

The heat transferred by convection ( $\dot{q}_{\text{conv}}$ ) is expressed

$$\dot{q}_{\text{conv}} = \rho_c c V_{\text{mix}} \Delta T \quad (6)$$

where

$\rho_c$  = density of air

$c$  = specific heat of air

$\Delta T$  = temperature difference between room air and convective air

Infiltration. Infiltration currents account for 20% to 28% of the heat loss from a full scale building. The momentum and heat of a typical infiltrating air jet diffuses into the bulk interior air within one meter of the point of origin, but the momentum transfer may have effects on bulk air movement beyond this limit.<sup>4</sup> The velocity of the infiltration is proportional to the velocity of the flow.

---

4. The diffusion limit is based on a crack width of 1/16 in.x4 ft., with  $Re \approx 1000$ , and  $\Delta T = 20^\circ F$ . See D. J. Crome and B. M. Roberts, Air Conditioning and Ventilation in Buildings, p. 370.

### SCALING RELATIONSHIPS FOR SIMPLIFIED CONVECTION MODELS

The hypothesis that simple building models may be used to determine full scale generic natural convective flows is based on the simple relation between geometric scale and steady state heat flux through building walls. This relation is shown as follows:

$$\dot{q}_{\text{conv.}} \sim \dot{q}_{\text{wall}} \quad (7)$$

$$\dot{q}_{\text{wall}} = h_c \Delta T \quad (1b)$$

$$\dot{q}_{\text{conv}} = \rho_c c V_{\text{mix}} \Delta T \quad (6)$$

$$\frac{\dot{q}_{\text{wall}}}{\dot{q}_{\text{conv}}} = \frac{h_c \Delta T}{\rho_c c V_{\text{mix}} \Delta T} =$$

$$K = \frac{h_c}{\rho_c c \sqrt{gL\frac{\Delta T}{T}}} \quad (8)$$

Based on the above, the parameter K is kept the same in the model as in the full-scale system, and the temperature differences in the model will be the same as in the full scale system. This is our basic scaling hypothesis.

Under the constraint that K is kept constant, the imposed parameters must be scaled as follows:

$$\dot{q}_{in} \sim \sqrt{L} \quad (9a)$$

$$h_{out} \sim \sqrt{L} \quad (9b)$$

$$V_{ext} \sim \sqrt{L} \quad (9c)$$

where

$\dot{q}_{in}$  = heat flux/unit area<sup>5</sup>

$h_{out}$  = unit thermal conductance of model building skin

$V_{ext}$  = external wind velocity applied to infiltration effects.

The independent variables are to be scaled as:

$$X \sim L \quad (9d)$$

$$t \sim \sqrt{L} \quad (9e)$$

where

X = geometric scaling

t = time<sup>6</sup>

5. if a model is 1/6 the full scale, then  $\dot{q}_{in}$  for the model =  
 $\dot{q}_{in}$  full scale  $\times \sqrt{1/6} =$

$\dot{q}_{in}$  full scale  $\times 0.41$

6. The time factor refers to the periodicity of flows, and not to dynamic wall response.

The dependent variables scale as:

$$\Delta T = T - T_{av} = \text{constant} \quad (9f)$$

$$V_{\text{inside}} \sim \sqrt{L} \quad (9g)$$

where

$T_{av}$  = average outside temperatures

$T$  = model temperature

$V_{\text{inside}}$  = interior room velocity

These scaling relationships are an approximation based on the scaling implied in Eq. 4 and are also incomplete in that dynamic wall effects and radiation heat transfer have not been included in the scaling parameters.<sup>7</sup> Furthermore, even though the modelling of infiltration effects is possible according to the scaling relationships, it was not attempted in this thesis, as the use of simple experimental models was deemed adequate.

---

7. It is theoretically possible to include dynamic wall effects in this series of scaling relationships by judicious scaling of the local thermal capacitance of the building element. It can be shown, from the first law of thermodynamics, that the effects of interior thermal mass will properly scale if the product  $mc$  is scaled as  $L$  where:  $m$  = mass of wall/unit area  
 $c$  = specific heat of wall

Scale models built strictly according to the scaling relationships and which maintain the equality of the parameter (K) may prove to be economically impractical as simple design tools. This is because the scaling relationship specifies a decrease in the building skin unit thermal conductance at the smaller scale, which in turn, increases the amount of insulation required. Therefore a 1:6 model of a simple dwelling, would require rigid insulation at about 10% the cost of that of a full scale dwelling, and would also be extremely bulky due to the large amount of insulation necessary.

Models with thin building skins are less cumbersome (as well as cheaper) as design tools but have greater heat flux than called for by the scaling relationships. In order to develop a practical simplified modelling technique, an investigation was made of the similitude of convection behavior in models that had a greater heat flux than that required for a proper scaling. Experiments were performed on models which maintained the scaling relationships but had heat fluxes larger than specified by Eq. (9a).<sup>8</sup> A departure factor ( $D_f$ )

---

8. The temperature difference between the inside air and ambient air was similar for both the models and the test cell.



was defined that related the model heat flux to the heat flux defined by the scaling law:

$$\frac{\dot{q}_{\text{in model tested}}}{\dot{q}_{\text{in model required by scaling law}}} = D_f \quad (10)$$

By testing a series of models, with various  $D_f$  values, the sensitivity of the similitude to  $D_f$  can be established.

## PROPOSALS FOR RIGOROUS SCALING

Rigorous scale modelling is a complex procedure. It implies that the models comply with all parameters developed in a set of scaling relationships. These include parameters that describe wall surface to fluid conduction effects, dynamic wall effects, and infiltration effects. Appendix III describes dimensionless parameters.

Experiments performed by Suter and Choulat<sup>9</sup> on forced air and natural convection systems in models indicate that dimensionless numbers (Reynolds, Grashof, Strouhal, and Prandtl), describing fluid properties and dynamics at a specified scale, must be similar to their full scale counterparts. Additional parameters describing wall behavior must also be defined. In order to retain similarity between full scale and model parameters, Freon 12 may be used at 1/5 scale under standard pressure conditions. With this gas the interaction between wall surface and fluid models well.

Infiltration in buildings may be modelled with the use of a wind tunnel.<sup>10</sup> The Reynolds numbers for full scale infiltration may range

9. "Essais sur Modèle Réduit Concernant la Dynamique de Locaux Chauffés à Similitude Rigoureuse," in Air Conditioning of Rooms and Vehicles, p. 117.
10. See R. E. Bilsborrow and F. R. Fricke, "Simulation of Building Ventilation in Wind Tunnels," Building Science, Vol. 10, 1975.

from 0 to 1000 and the effect of surface orientation to wind velocity models well. Experiments relating building interior thermal plume effects to infiltration have not been found in the literature reviewed. Rigorous scaling is a complex and expensive procedure, and not well suited to the architectural design process.

## Chapter II

# Experimental Method and Results

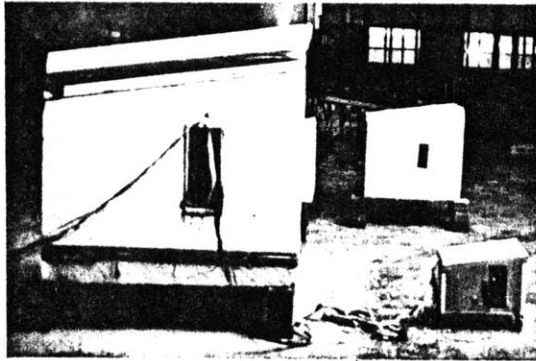


Fig. 1a. Thermal Models

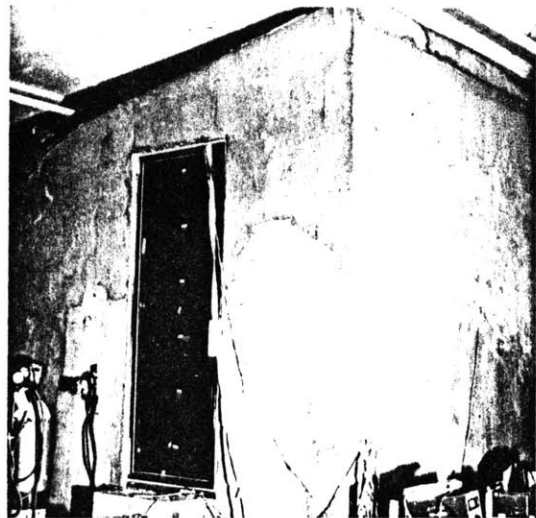


Fig. 1b. Full Scale Test Cell

A series of models (Fig. 1a), geometrically similar to a full scale test cell (Fig. 1b), was built and tested for temperature distribution similitudes in order to determine the applicability of the scaling relationships developed in the previous chapter. Air temperature fields provided the basis for comparison between the full scale test cell, which served as a control for model behavior, and the models. These fields represent air temperatures sampled in a vertical plane of the test cell, as pictured in Fig. 2. The test cell had heat loss characteristics that were proportional to those of typical dwellings.

Experiments for the 1/6 and 1/12 scale models and test cell were performed under steady state conditions with no infiltration which limits rigorous similitude to real life conditions but provides adequate approximations for the context intended. Three different heating configurations provided a variety of comparable temperature fields in the test cell and the model.

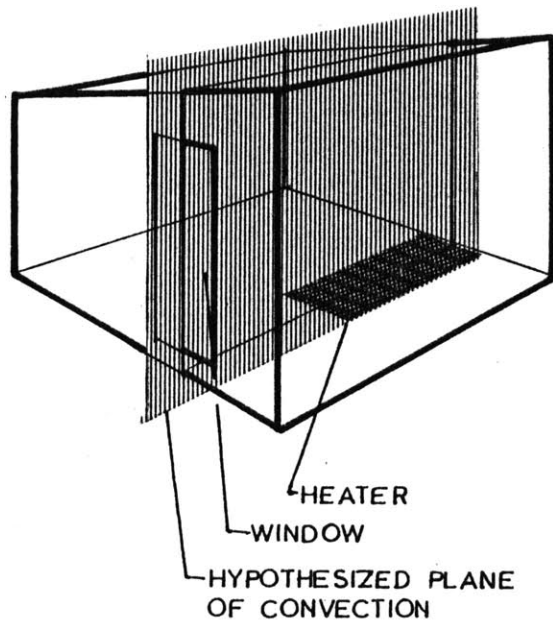


Fig. 2 Temperature fields were measured in the hypothesized plane of convection.

#### TEMPERATURE FIELD INTERPRETATION

Figure 3 represents the temperature field within a section of the test cell and models.<sup>11</sup> The grids in the figure represent 60 cm. by 60 cm. squares, and the isotherms are drawn at 0.2°C temperature differences with the 0°C isotherm representing the mathematical mean of sampled values. The spacing of the isotherm lines in the temperature field, and the relative geometric position of isothermal

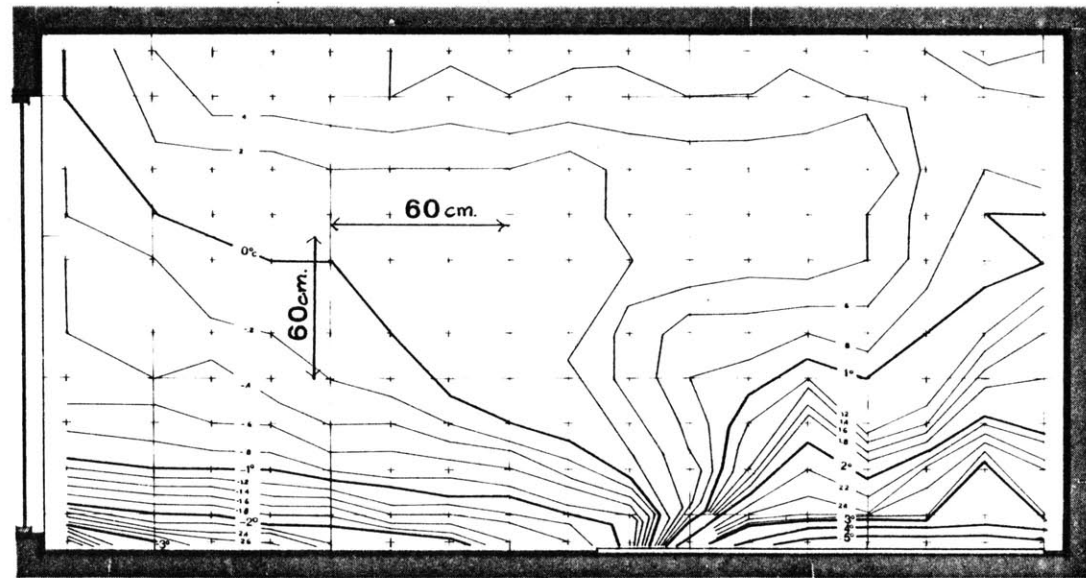


Fig. 3 Temperature fields in a section along hypothesized plane of convection

11. The plotting method necessitated an exaggeration in the length of the room pictured in the figure.

features, form the basis for subjective evaluation of similarity between the models and the full scale test cell.

A formalized method for heat flow evaluation from isotherm plots has been developed for heat conduction in solid materials.<sup>12</sup> In this method, the heat flow always occurs perpendicular to the isotherms, and the distance between these is related to heat flow by the following equation:

$$\dot{q} \sim \frac{\Delta T}{\Delta n}$$

where

$\dot{q}$  : heat flux

$\Delta T$  : difference in temperature between isotherms

$\Delta n$  : difference in distance between isotherms

The greater the distance between the isotherms, the less heat flow is present. Fig. 4 indicates heat flows applied to the isotherms.

Discretion must be used in applying this method to convection systems, as it is not applicable where mass transfer occurs in conjunction with heat transfer. But as heat transfer by conduction and local

---

12. F. Kreith, Principles of Heat Transfer, p. 79.

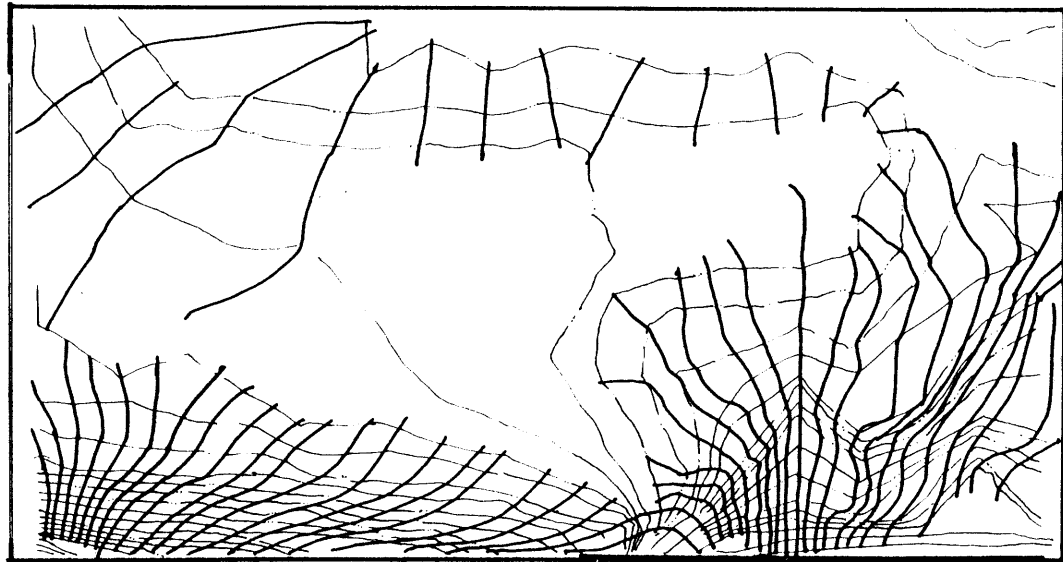


Fig. 4 Idealized heat flow lines; as if conduction only was occurring

diffusion occurs at the boundaries of flows, the heat flow accross the isotherms in these boundary areas may be roughly evaluated by this method. Interpretation of isotherm configurations relating to the natural convection developed in experiments is shown in Figure 5. A generic flow field as shown in Fig. 6 may be construed from the interpretation of the isotherms. Similitude between the model and the test cell may be evaluated on the basis of this perceived generic flow and temperature distribution correlations.

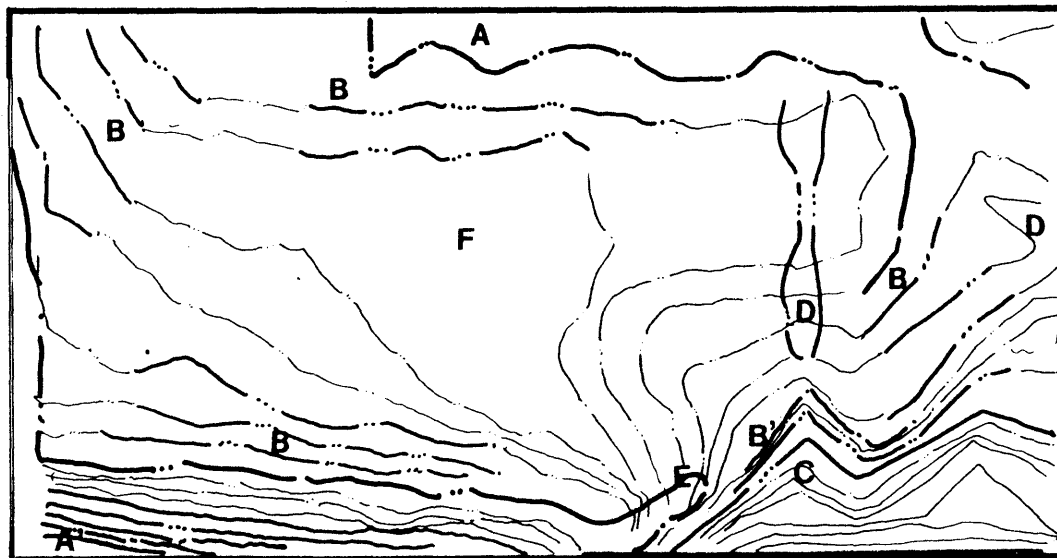


Fig. 5. Typical isotherm configurations and interpretations: (A) Long isothermal areas represent isothermal flows with (B) bordering diffusion and mixing of air. (A') Thermal areas of dense isothermal spacing indicate laminar air flows. Cone configurations indicate plume development. When cool air flows develop over warm air flows, vigorous eddying is likely to occur, as in (B') and (E). Large isothermal areas (F) act as reservoirs for air entrainment into plumes (D).



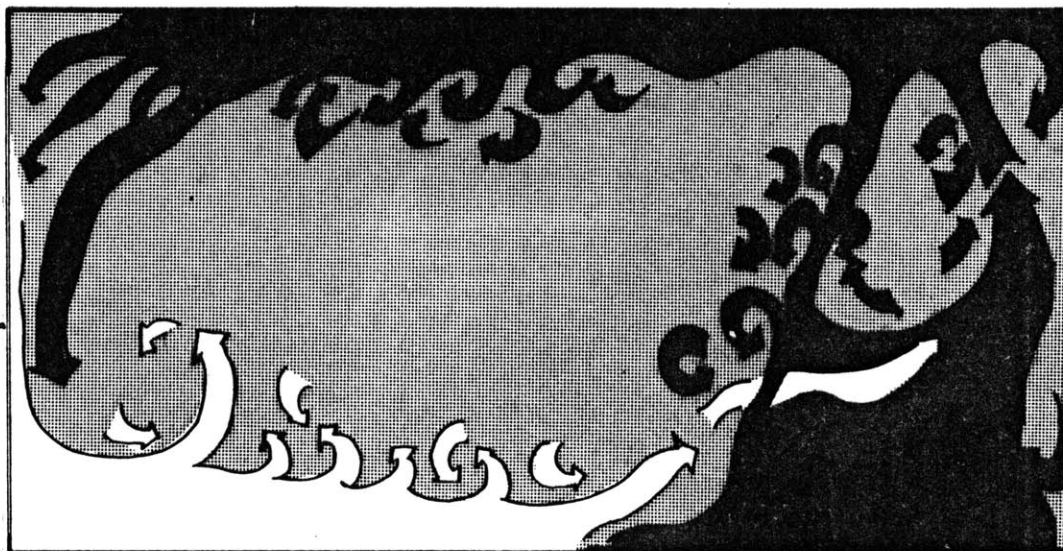


Fig. 6. Generic flow field, interpreted from temperature fields. Dark to white represents warm air flows to cool air flows.

## THE TEST CELL

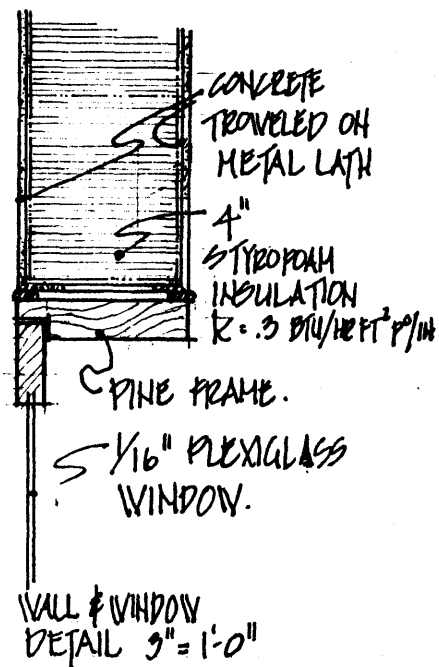


Fig. 7. Detail of test cell wall and window

To establish confidence that similitude of full scale real world convection flows may be achieved in models, a control with typical heat loss characteristics was used in the experiments. This test cell was located in an empty warehouse space where stable ambient conditions were possible. (Refer to Appendix II for a complete description) Although smaller in area and volume than a typical dwelling, the test cell had proportionally similar heat loss characteristics (See Table 1).<sup>13</sup> Its area was similar to that of an average bedroom. Table 2 indicates proportional heat losses for the test cell and the typical dwelling.

The construction of the test cell, however, differs from the construction of the typical dwelling. The building skin, shown in Fig. 7, was formed with styrofoam-concrete sandwich panels, 4 inches being used for the walls, and 6 inches for the roof and floor. Due to the elevated temperatures used during the experiments

( $T_{\text{room test cell}} \gg T_{\text{room typical}}$ ) and due to the thickness of the

13. The standard typical dwelling is a four bedroom townhouse as defined by the National Bureau of Standards. See B.A. Peary et al., Comparison of Measured and Computer-Predicted Thermal Performance of a Four Bedroom Wood-Frame Townhouse.

TABLE 1. VOLUMES AND AREAS OF TYPICAL DWELLING AND TEST CELL

Typical Dwelling ft <sup>3</sup>		Test Cell ft <sup>3</sup>
Volume	9000	873.1
Floor area	1200	128.4

TABLE 2. PROPORTIONAL HEAT LOSSES OF TYPICAL DWELLING AND TEST CELL

	TYPICAL DWELLING		TEST CELL	
	Building Component Area as a Percent of Total Building Skin Area	Building Component Heat Loss as a Percent of Total Building Skin Heat Loss	Test Cell Component Area as a Percent of Total Test Cell Skin Area	Test Cell Component Heat Loss as a Per- cent of Total Building Skin Heat Loss
	%	%	%	%
Window	6	33	2	22
Wall	46	38	53	52
Floor	24	12	22	12
Roof	25	17	22	14

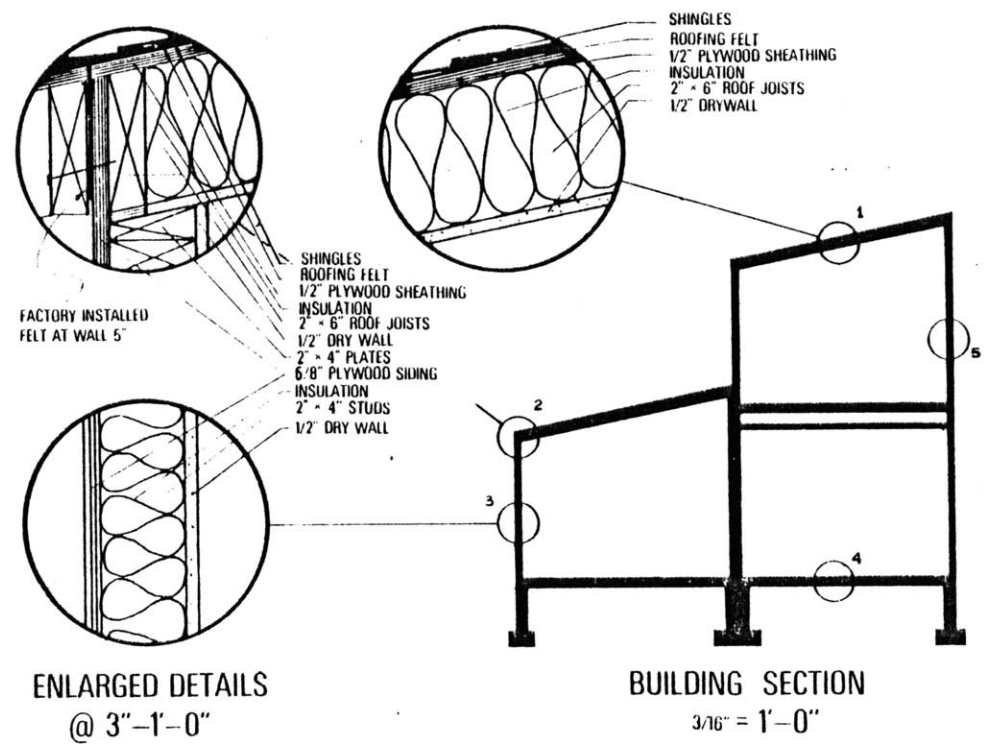


Fig. 8. Section and details of NBS typical dwelling

styrofoam, (refer to Proportional Heat Loss Test, P.32) the overall unit conductance of the test cell wall was found to be 7% higher than that of the 4 inch fiberglass batt wall of the typical dwelling (Fig.8). Although the percentage of window area in the test cell was smaller than that of the typical dwelling (window to floor ratio for the test cell was 9.4% as compared to 16.2% for the dwelling) it lost more heat per unit area. This was due to the use of 1/16 in. plexi-glass glazing in the test cell while the typical dwelling had double glazed window units.

The test cell was heated by electric resistance wiring evenly distributed below a 1/16 in. steel plate,  $1.16 \text{ M}^2$  in area and geometrically proportional to the window. The shape of the plate and the energy flux into it ( $448.3 \text{ W/M}^2$  or  $142 \text{ BTU/hrft}^2$ ) resembled solar gain on a floor with low thermal storage capacity. The floor of the cell was located 2 feet above the warehouse floor allowing the ambient air to remove heat from this surface as well as from the walls and roof. This situation is comparable to that of a typical dwelling with a crawl space beneath. On the other hand, infiltration was negligible in the test cell but accounted for 21% of the losses in the typical dwelling, and in this aspect the test cell did not resemble real world conditions.

#### PERFORMANCE OF THE TEST CELL

The proportional heat losses of the test cell building skin and the data for the plotting of the test cell temperature fields were determined from experiments on the thermal performance of the test cell. Three different heating configurations were monitored and are described below.

Configuration A. The heater plate was located at the rear wall of the test cell, opposite the window, as shown in Fig. 9. The heat

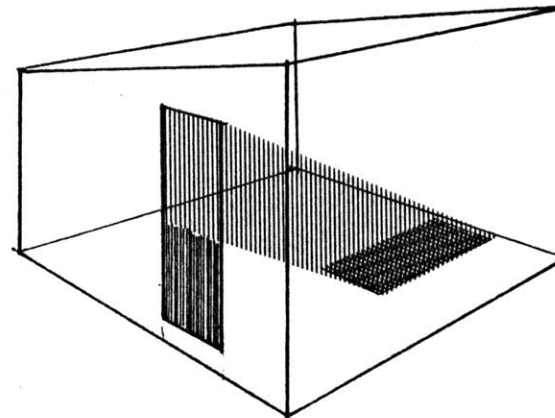


Fig. 9. Configuration A with solar gain simulated as shown.

input simulated solar gain on November 21 at 45°N latitude through a single glazed window with a ceramic frit on the bottom portion. Steady state conditions in the cell were similar to noon solar conditions, which were determined by computer-based simulations.<sup>14</sup> The effect of low power density on convection was assessed.

Configuration B. While the heater plate was located in the same position as in Configuration A, a baffle was raised between the heater plate and the window, as shown in Fig. 10. The dimensions of

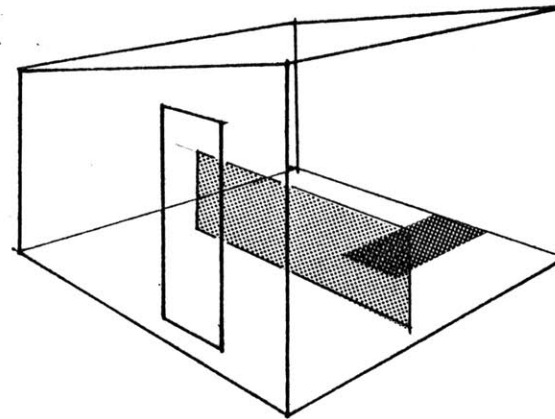


Fig. 10. Configuration B with baffle separating heat sink from heat source.

<sup>14</sup>. See R. Lebens, "Passive Design Background and Workbook."

the baffle, 0.76 Mx2.9 M (or 2 ft. 9 in. x 9 ft 6 in.), resembled those of a sofa. The effect of changing interior geometries was assessed.

Configuration C. The heater plate in this configuration was placed below the windows, thus simulating equinox solar gain through a reflecting window on March 21 at 45°N latitude, as shown in Fig. 11.

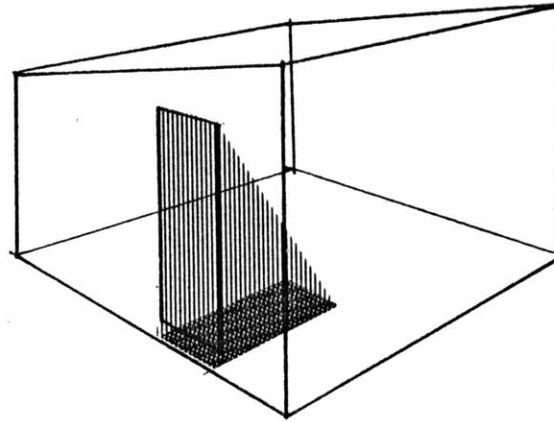


Fig. 11. Configuration C with solar gain as shown.

The effect of contiguous heating and cooling was assessed. Steady state conditions, which simulated solar gain in the test cell, implied that the solar gain was occurring either on a surface of low thermal storage capacity, or on the same surface throughout the day.<sup>15</sup>

---

15. This is the case in passive solar buildings where long glazed areas permit constant solar gain on one area in the building.



Three sets of measurements were taken using Configuration A, while only temperature fields were sampled with Configurations B and C. The three tests and their results follow.

Proportional Heat Loss Test. The window of the test cell was replaced with 4 in. styrofoam insulation to determine the actual unit conductance of the walls. Average inside air and average ambient air temperatures were used to determine the conductivity of the styrofoam which was found to be 0.043 W/M°C (or 0.3 BTU/hrft<sup>2</sup>/in).<sup>16</sup> The total heat loss rate was 20.7 W/°C (or 39.3 BTU/hr°F). The ratio of heat lost by the test cell with window removed, to the heat lost with the window in place, defined the proportional heat loss factor ( $P_f$ ).

$$P_f = \frac{\dot{Q}(T_r' - T_a)}{\dot{Q}(T_r - T_a)} = 0.84 \quad (11)$$

---

16. According to tests performed by D. Bryan at MIT in 1977, this is 7% above the prescribed value at 95°F. W. F. Cammerer, in "Insulating Values as a Function of Thickness," indicates that discrepancies may be due to the thickness of the sample, (in International Institute of Refrigeration, Some Thermophysical Properties of Refrigerants and Insulants, p. 189)

where

$$\begin{aligned}\dot{Q} &= 520 \text{ W} && = \text{power input to the test cell} \\ T_r &= 40.2^\circ\text{C} && = \text{temperature of test cell wall with windows in place} \\ T_r' &= 44^\circ\text{C} && = \text{temperature of test cell wall with window removed} \\ T_a &= 20^\circ\text{C} && = \text{ambient temperature}\end{aligned}$$

The proportional heat loss factor was used in the design of the simplified scale models to maintain the proper proportion of heat losses through the window areas.

Velocity Measurements. Velocity measurements of the natural convection flows in the test cell were made with a directional hot wire anemometer. These measurements provided the data base for the velocity fields plotted for the test cell shown in Figs. 12a and 12b. (Refer to Appendix II for details on instrumentation.) The velocity fields were used to confirm the intuitive evaluation of flows from the temperature fields and to develop an understanding of the magnitude of the flows that were being generated by the low density heat flux.

As only one component of the velocity could be measured at a time, the true velocity was arrived at by vector addition of the measured horizontal and vertical components. The highest computed velocity

Fig. 12a. Horizontal velocities and direction measured in the hypothesized convection plane of the test cell.

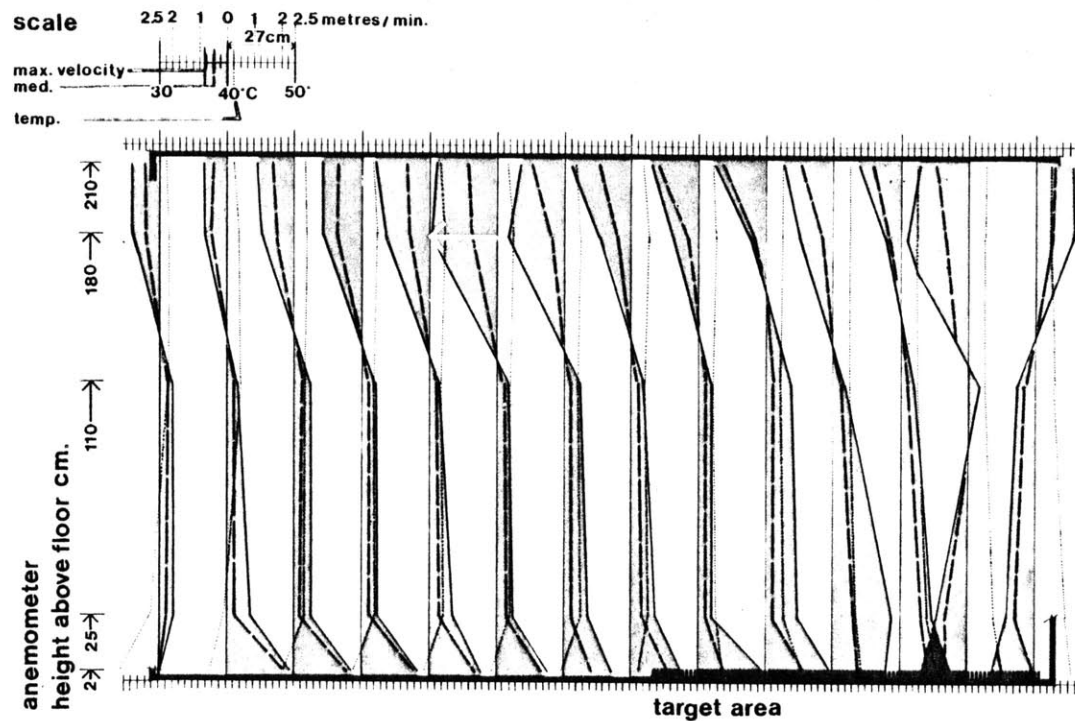
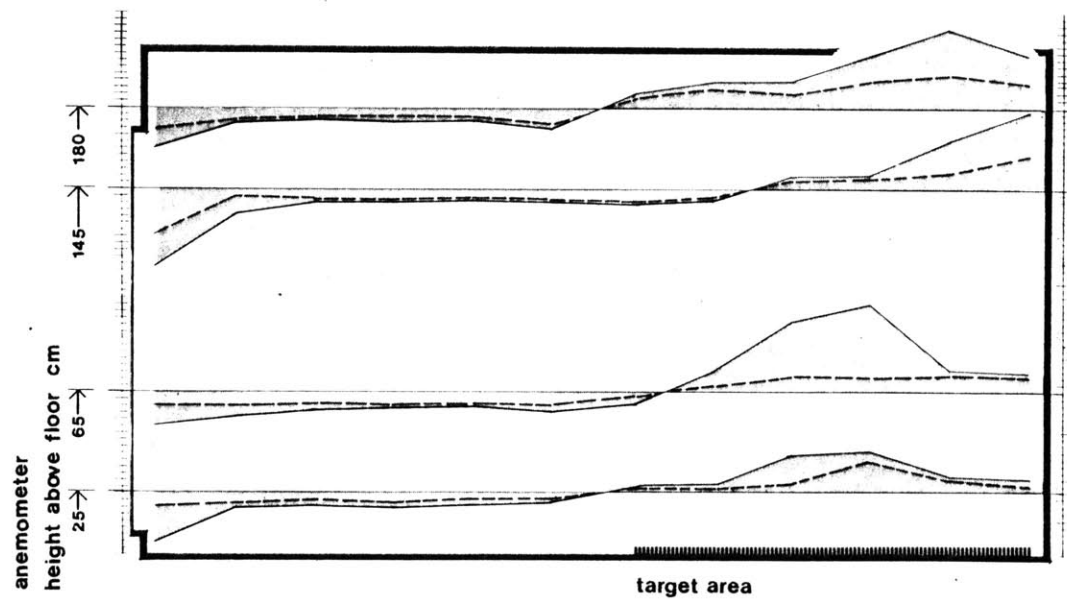


Fig. 12b. Vertical velocities and directions measured in the convection plane.



was 5M/min. (or 16.5 ft/min) and occurred over the heater plate. The same vertical plume velocities were visually timed at 7 M/min. (or 23 ft/min.).<sup>17</sup> Typical horizontal velocities measured with the hot wire anemometer were in the 2.5 M/min. range along the ceiling and floor. Velocities were also indicated in the middle of the room, but these were below the threshold of the instrument.

A periodic flow developed over the heater plate in the test cell. The 1 min. 25 sec. period had 3 distinct phases:

- 1) a calm phase, lasting ca. 1 minute, characterized by a wave configuration of warm laminar flow along the back wall.  
(Fig. 13a)
- 2) an acceleration phase, lasting ca. 20 seconds, characterized by an unsteady rise in velocity and the disappearance of the wave configuration (Fig. 13b)
- 3) a high velocity phase, lasting ca. 5 seconds, characterized by fluctuating velocities and entrainment of flow close to the plate (Fig. 13c)

---

17. Velocities of 3 M/min. (10 ft/min.) are common in rooms heated by forced air systems. Forced air systems for equivalent sized rooms operate with twice the outlet velocity (14 M/min.) that developed with the low power, limited space natural convection system described here.

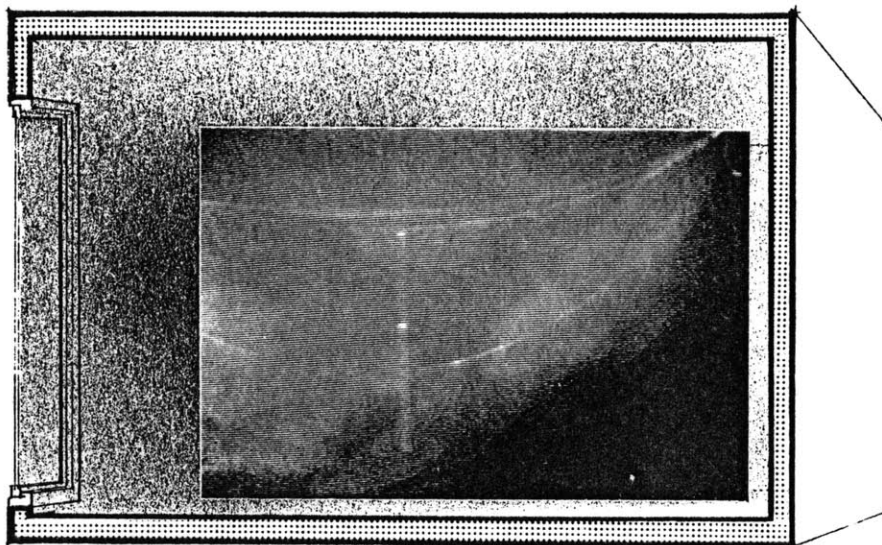


Fig. 13a. Wave configuration, calm phase.

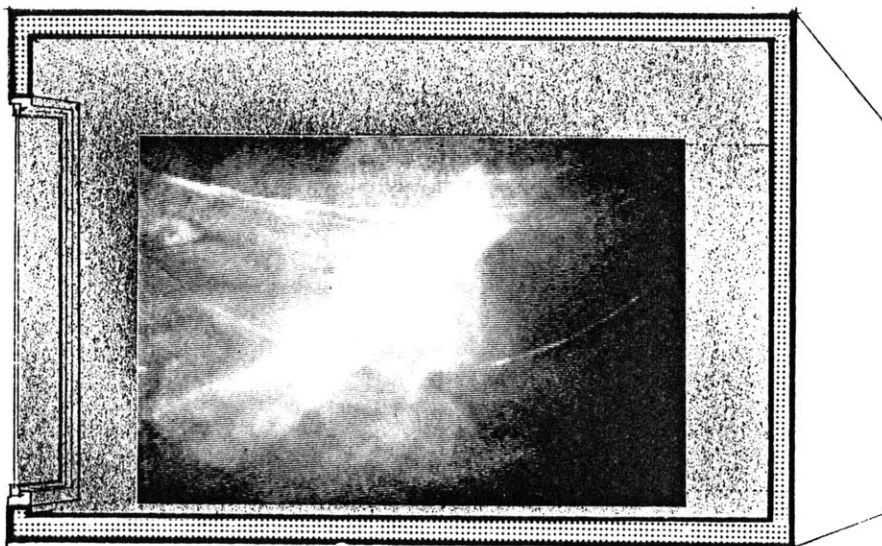


Fig. 13b. Acceleration phase, wave configuration changes.

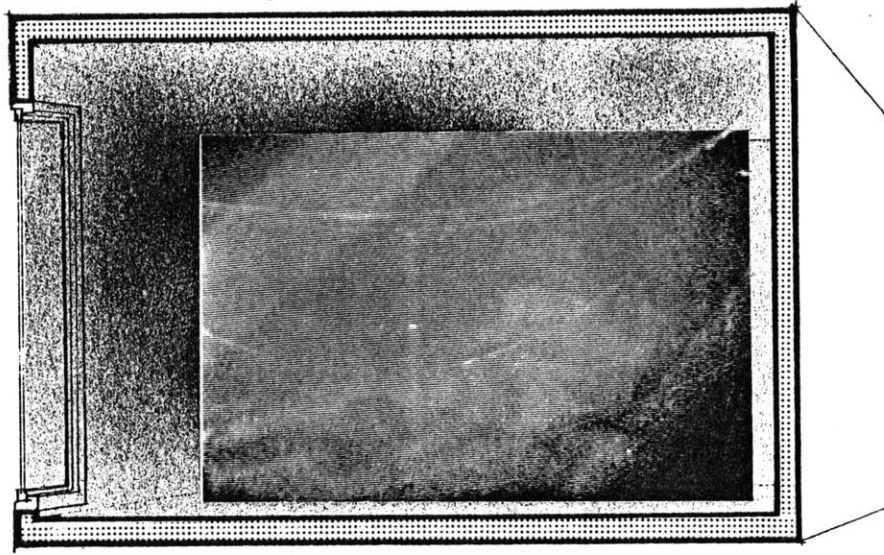


Fig. 13c. Final plume rise and high velocity phase.

The pulse in the flow created by this periodicity was propagated along the ceiling but dissipated at the window area. In contrast to the periodicity observed in the heat flows above the heater plate, the cool air flows along the window surface and the floor had a fairly constant velocity. Fig.13d illustrates the major flow regimes that were found in the test cell.

Temperature Measurements. Air temperatures and the temperatures of various surfaces in the test cell were determined for all configur-

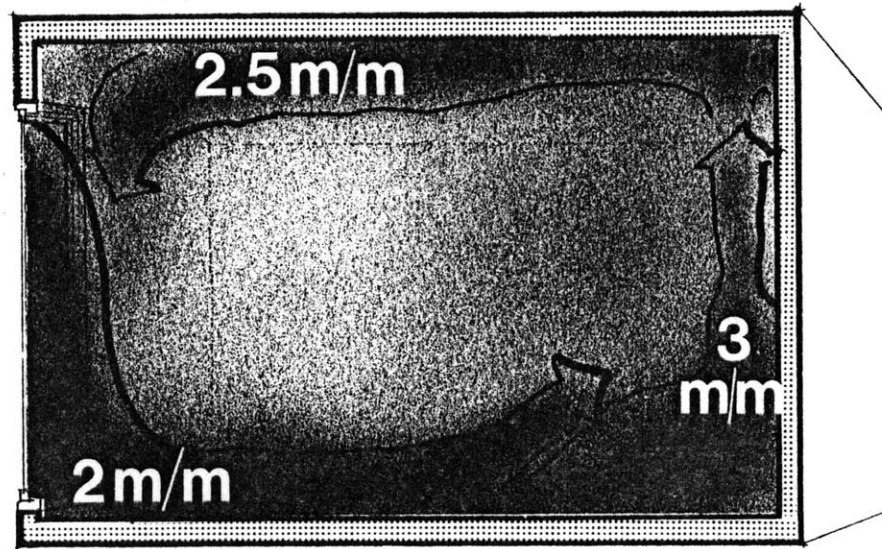
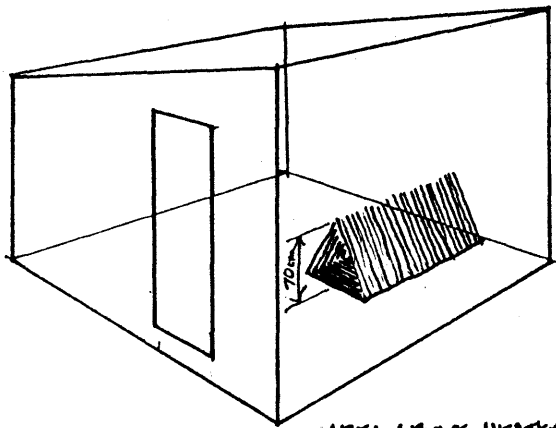


Fig. 13d. Generic velocity regimes in the test cell.

ations. The air temperature was measured by a regular distribution of YSI thermistor beads on a vertical boom. (See Appendix II for a complete description of measurement techniques.) The boom was moved across the room, thus providing a sample of air temperatures within its movement plane, which provided the data base for the isotherm plots. The movement plane was along the hypothesized plane of convection shown in Fig. 2, p. 20. As the scaling relationships developed in Chapter I do not provide parameters for heat conduction



AREA ABOVE HEATER  
PLATE NOT INCLUDED  
FOR COMPARISON.

Fig. 14. Area of conduction heat transfer not included in temperature field comparisons.

from a surface to the air, the area directly above the heater plate to a height equal to the width of the plate was not included in determining average temperatures. It was also discluded from discussions concerning air temperature ranges and thermal fields within the test cell and models. It was assumed that in this area conduction from the heater plate to the air was taking place. (Fig. 14).

The temperature measurements were employed to determine radiation and convection transfers from the heater plate, using standard heat transfer equations.<sup>18</sup> A high proportion of radiation heat transfer from the plate (ca. 64% of the total heat transfer) was attributed to the elevated temperatures used for measurements in the test cell. Table 3 gives some typical temperatures found during the experiments. The convection heat transfer coefficient of the heater plate varied with the method of computation used. Using Grashof\* ( $Gr^*$ ),<sup>19</sup> the

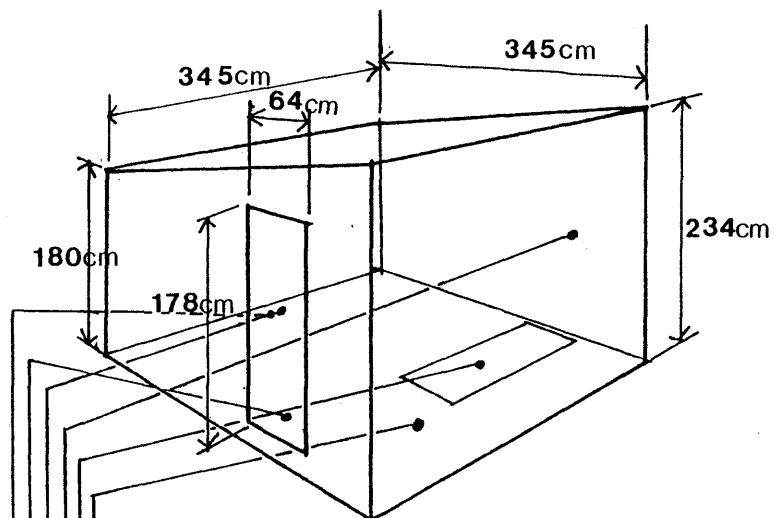
18. For standard heat transfer equations, see Kreith,

$$19. Gr^* = Gr_x Nu_x = \frac{g\beta qL^4}{kv^2}$$

This definition is from J. P. Holman, Heat Transfer, p. 217. For other definitions of  $Gr$ , see Appendix III.



TABLE 3. TYPICAL TEST CELL TEMPERATURES



POSITION	C°	F°
Ambient air temperature	21.4	70.5
Room air temperature	40.6	105.1
Heater plate temperature	64.7	148.5
Rear wall temperature (+1M)	42.8	109
Inside window temperature (+1.5M)	36.8	98.2
Inside Window temperature (+.25M)	34	93.2
Outside window temperature (+1.5M)	23.7	74.7

heat transferred by convection was 33% of the total heat transferred from the plate. Typically, 46% of the heat is transferred upward by convection from a horizontal surface.<sup>20</sup>

The temperature field plots generated from the temperature measurements in the test cell and models were used to evaluate the similarities between them.

The three series of tests described above gave insight into the convection process and heat transfer occurring within the test cell. These tests provided a basis for comparing the thermal behavior of the cell with that of the models. Multiple temperature measurements indicated a correlation coefficient of 0.88 between tests of similar flows. (For a complete description of the models and the tests performed, refer to Appendix I.)

---

20. Lebens, p. 78.

## COMPARISON OF TEMPERATURE FIELDS

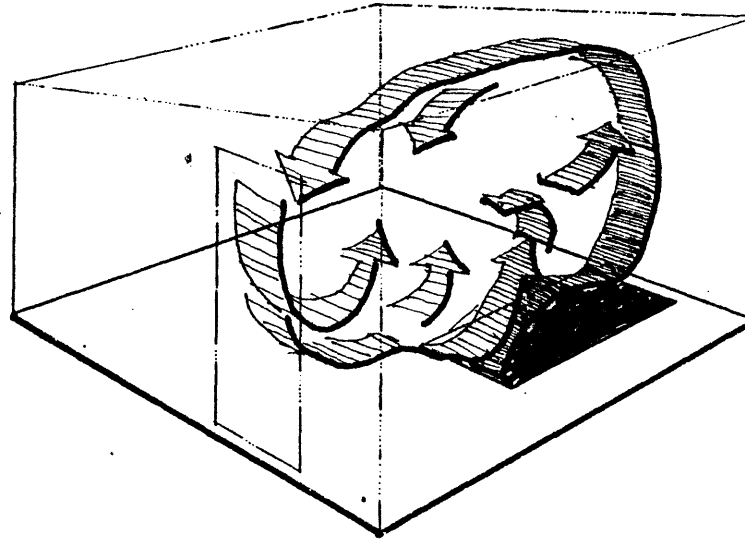
Of all the models tested, the 1/6 scale model with a  $D_f = 2$  proved to have convective flows most similar to those of the test cell.<sup>21</sup> The temperature field patterns and the high correlation of model to test cell temperature distribution (correlation coefficient = 0.87) indicated similitude of bulk air flows. This similitude was established for all configurations, although in Configuration A, the best similitude was achieved.

### Configuration A

The heat source in this configuration was located at the rear wall, opposite the window, as previously described. It was hypothesized that, in the section where temperature fields were sampled, the distinct separation of heating and cooling areas would reinforce the convection flow. (See Fig. 15).

---

21. Of all the models, this one departed least from the scaling relationships.  $D_f$  (departure factor) expresses conformity to scaling relationships. For explanation, see Chapter I p. 16.

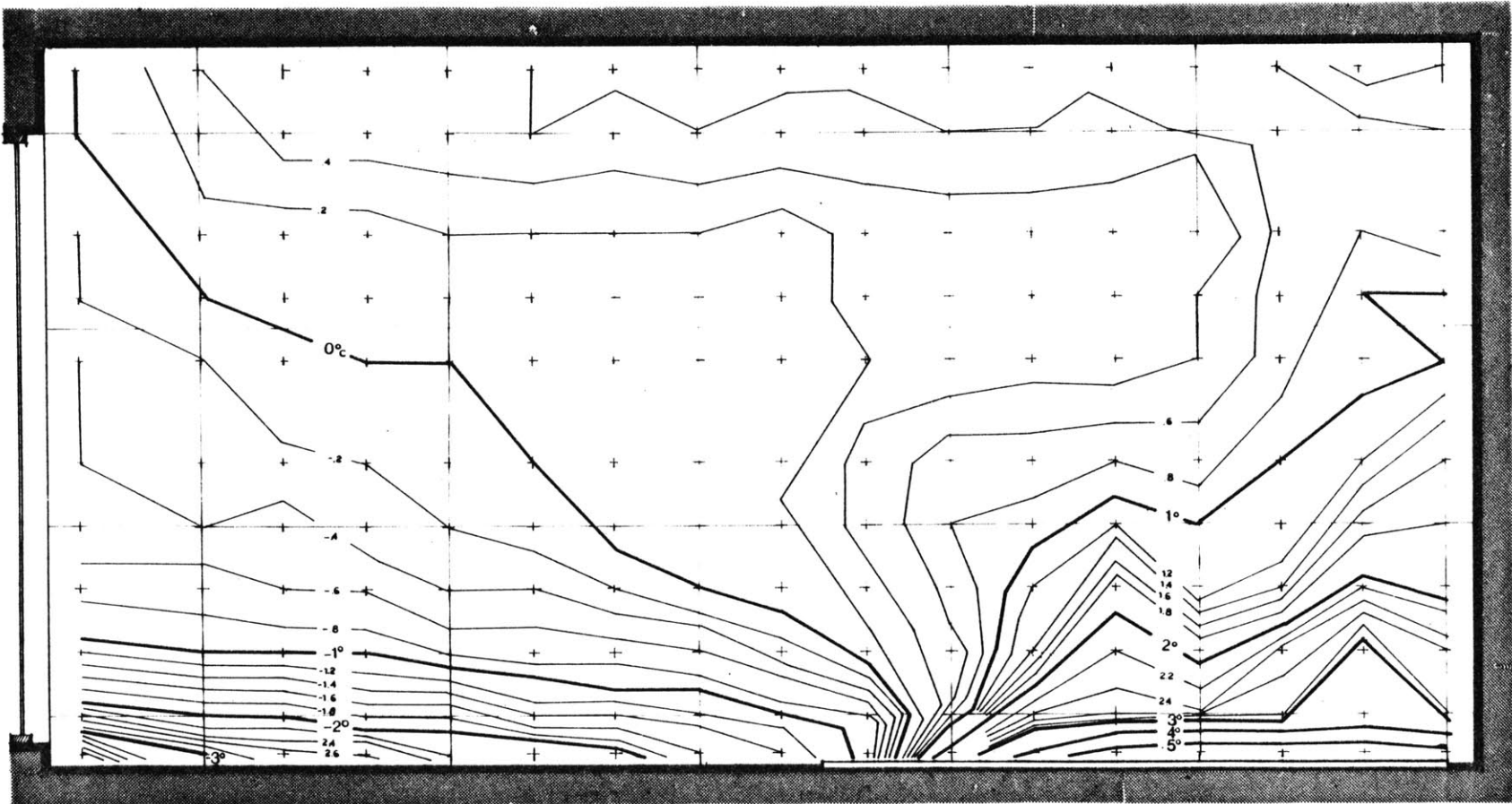


## CONFIGURATION A

### HYPOTHESIZED TEST CELL FLOW

Fig. 15.

Test Cell Interpretation. The temperature field in the full scale test cell, as shown in Fig. 16a, indicates 2 distinguishable thermal flows; the first created by the heater plate, and the second, by cooling at the window surface. The warm air flow, generated at the heater plate, rose along the rear wall and was deflected toward the front of the test cell at the ceiling (See Fig. 16b). At the front of the heater plate a wave configuration developed, as the plume was pushed toward the rear wall by the cool air flow from the window



**A scale 1·1**

Fig. 16a. Temperature field of full scale test cell, Configuration A. + indicates thermistor locations. Grid is 60 cm. x 60 cm.



Fig. 16b. Warm air flows in test cell. (A 1.1) indicates Configuration A, Scale  $1, D_F \cdot l$ . + indicates 60 cm x 60 cm grid. White number is the average temperature of the warm air flow in °C above the mean temperature. Black number indicates the average temperature of the cool air flow, °C below mean temperature.

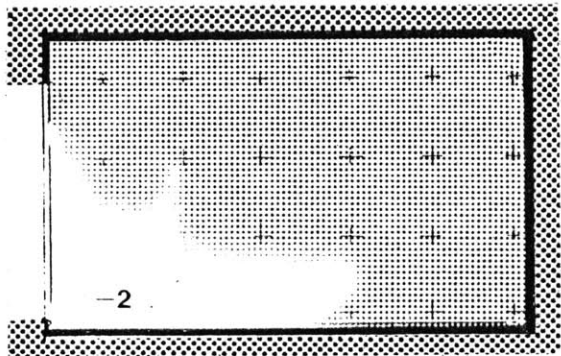


Fig. 16c. (A 1.1) cool air flows.

surface. Eruptions of hot air, corresponding to the high velocity phase described on p. 35 occurred so as to separate the plume from the rear wall. The cool air flowed toward the heater plate where a layer of hot air was built up by conduction and diffusion until the force of buoyancy was great enough to cause it to flow upward rapidly. Both the slower laminar plume and the eruptions entrained cooler air as they rose through the isothermal midroom area. An isothermal flow developed at the ceiling as a result of the deflection of the heater plume. The ceiling flow was characterized by diffusion and eddying at the flow boundaries and at its termination above the window area.

The ceiling flow was entrained at this point into the cool air flow developing across the window surface, and continued along the floor toward the heater plate. A transient eddy occurred halfway down the window and extended into the isothermal midroom area. In all other aspects this flow proved laminar as it proceeded down the window area and across the floor (Fig. 16c). A boundary layer with diffusion and some eddying developed between the top of the flow and the isothermal area. The cool air flowed over the heater and pushed the warm air toward the rear, forming a small temperature inversion

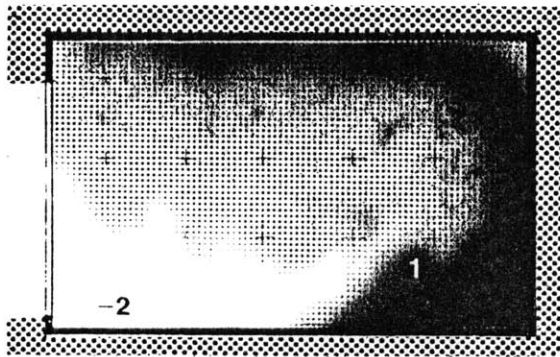


Fig. 16d. (A 1.1) generic air flows.

at the front of the heater. At this point diffusion and entrainment of the cool air flow into the warm air plume occurred rapidly. The midroom isothermal area was a reservoir for entraining air into flows. The general movement of air in this area was toward the rear of the room as entrainment into the plume was most vigorous.

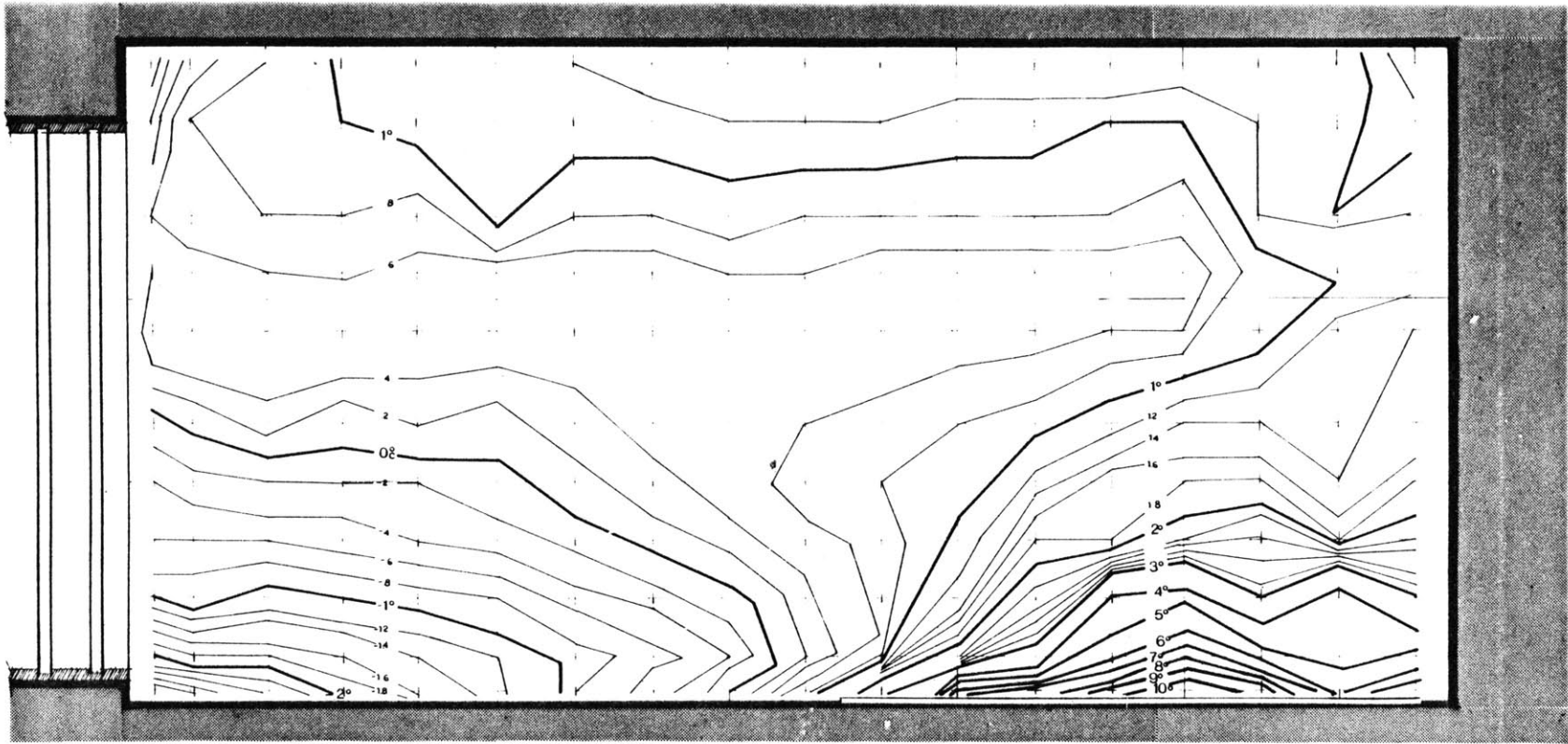
The complete convective flow (Fig. 16d) was viewed as a product of the warm and cool air flows and entrainment from a large isothermal area. The overall temperature range in the test cell was  $5.7^{\circ}\text{C}$  ( $10.2^{\circ}\text{F}$ ).

Model Interpretation. The temperature field of the  $(1/6 \cdot 2)^{22}$  scale model (Fig. 17a) closely matched that of the full scale test cell. Two major flows were discovered: 1) a warm air flow generated at the heater plate, swept along the rear wall to the ceiling, and deflected toward the window, and 2) a cool air flow which moved down the window and across the floor. Although the generic flows were similar to those of the test cell, differences in detail could be discerned.

The warm air flows in the model (Fig. 17b) did not exhibit the dramatic periodic instability found in the larger system of the test

---

22. This notation is used in this thesis to identify models. The first number refers to the geometric scale; the second indicates  $D_f$ .



A scale  $1/6 \cdot 2$

Fig. 17a. Temperature field in (1/6·2) model



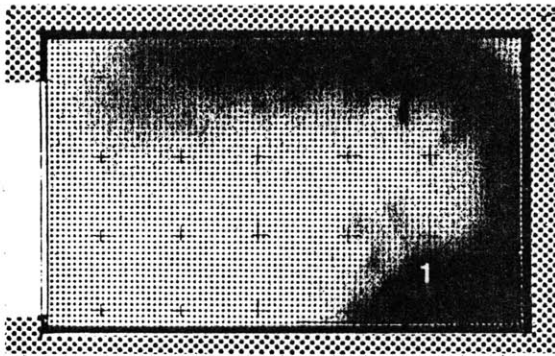


Fig. 17b. (A 1/6·2) warm air flows.

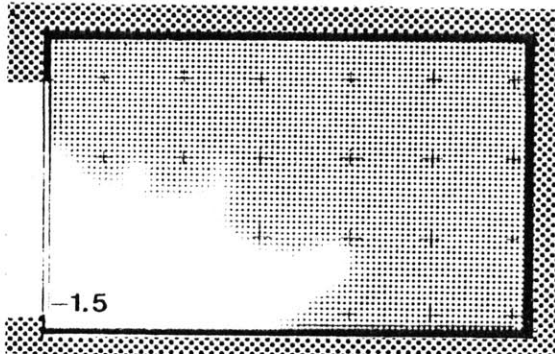


Fig. 17c. (A 1/6·2) cool air flows.

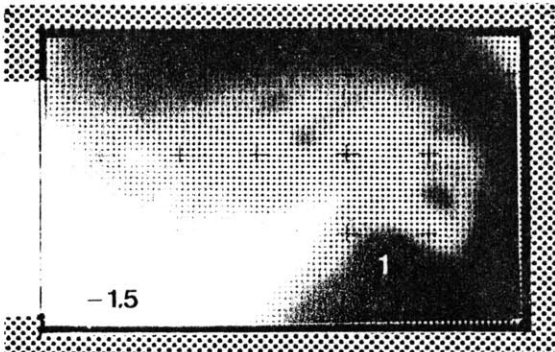


Fig. 17d. (A 1/6·2) generic air flows.

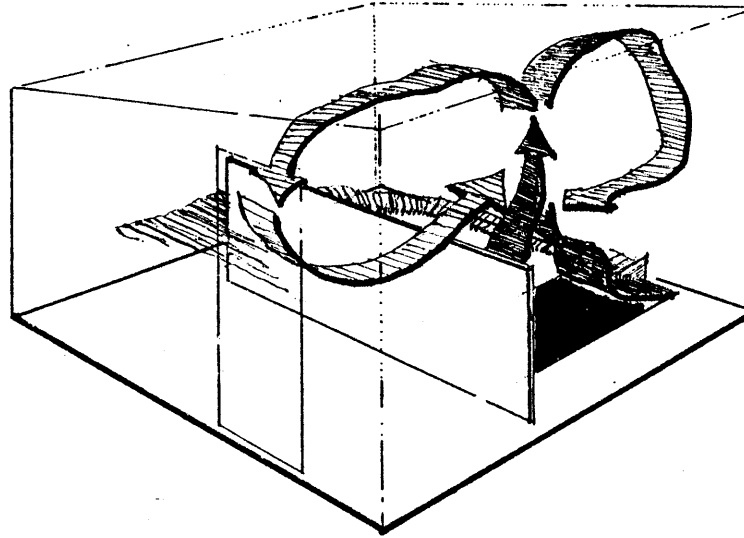
cell. The ceiling flow was thicker, and the cool air flow (Fig. 17c) across the floor diffused and began its mixing process with the warm air before it reached the heater plate area. This indicated some turbulent mixing in the model where laminar flow was occurring in the test cell. A smaller temperature gradient in the floor flow was also developed.

The hotter temperature flows of this model were very similar to those of the test cell in terms of temperature distributions. The generic flow patterns (Fig. 17c) also resembled those of the test cell, and a premature diffusion of the flow across the floor was the only difference. The overall temperature range in the model was 5.1°C.

Convection systems where the thermal flows reinforced each other (as in Configuration A) developed fairly rigorous similitudes of flows and temperature distributions with the full scale test cell.

#### Configuration B

The heat source in this configuration was separated from the window by a baffle, as previously described. This separation caused a distinct change in the interpreted flows in the test cell, as shown in Fig. 18. With two of its ends open to air movement, the baffle



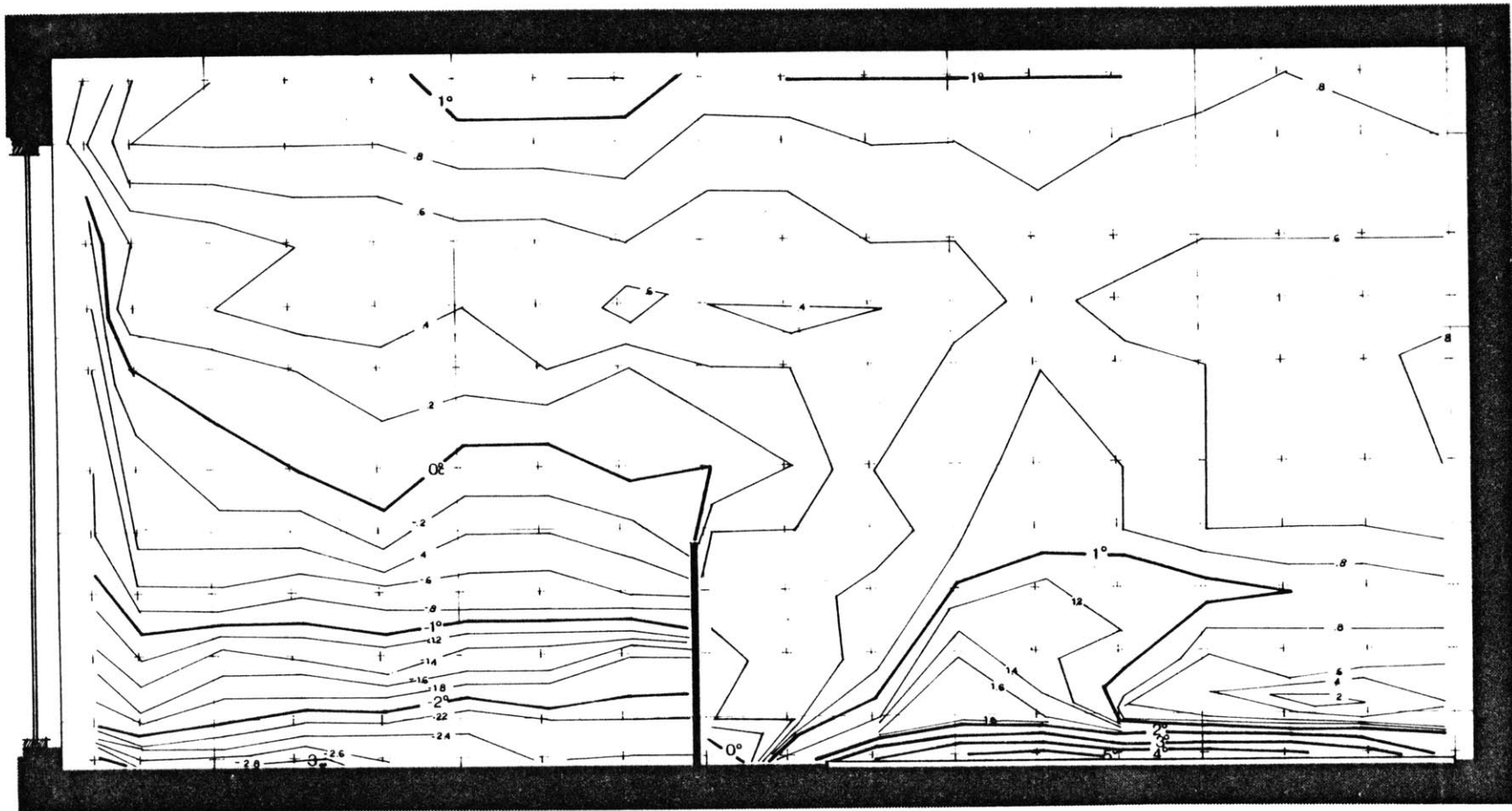
## CONFIGURATION B

HYPOTHESIZED TEST CELL FLOWS.

Fig. 18.

created a third dimension in the flow around it. The length of free flows along the floor was limited by the complexity of the new geometry.

Test Cell Interpretation. Two thermal flows were discernible on the temperature field of the test cell (Fig. 19a): 1) a warm air flow which rose near the front of the heater plate, split at the ceiling, and flowed toward the window and toward the rear of the



**B scale 1:1**

Fig. 19a. Temperature field in test cell, with baffle.

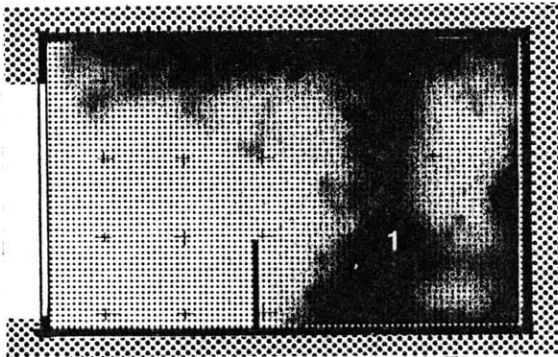


Fig. 19b. (B 1.1) warm air flows.

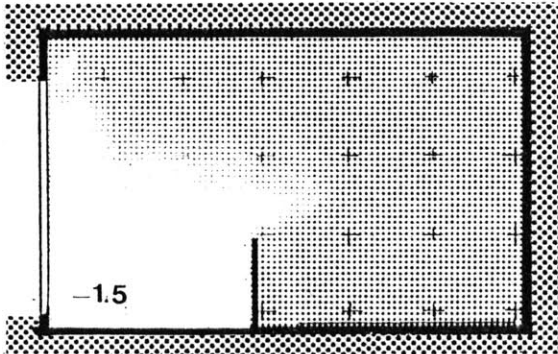


Fig. 19c. (B 1.1) cool air flows.

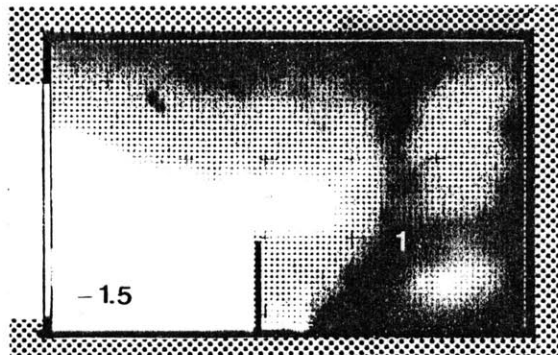


Fig. 19d. (B 1.1) generic air flows.

room, and 2) a cool air flow which developed across the top and around the side of the baffle. Complexity of the warm air flow increased with the addition of the baffles (See Fig. 19b). The warm air flow lacked the periodicity evident in the flow of Configuration A. Instead, the plume, generated about 120 cm from the rear wall, occurred randomly over time. The isotherms representing the plume had unstable characteristics. The plume was similar in nature to plumes observed over large flat plates, developing without constraints or impinging flows.<sup>23</sup>

The shifting of the plume from the rear (where it was found in Configuration A) toward the front, and the change in characteristics, was due to the absence of a strong cool air flow at the floor level. This shift in plume location affected the ceiling flows, in that the plume rose through the isothermal area and dispersed at the ceiling. A warm blob of air under the ceiling characterized the deflection point for the plume. The flow toward the rear wall, at the ceiling, formed part of a warm air vortex that extended down the rear wall and across the heater plate before being entrained into the plume.

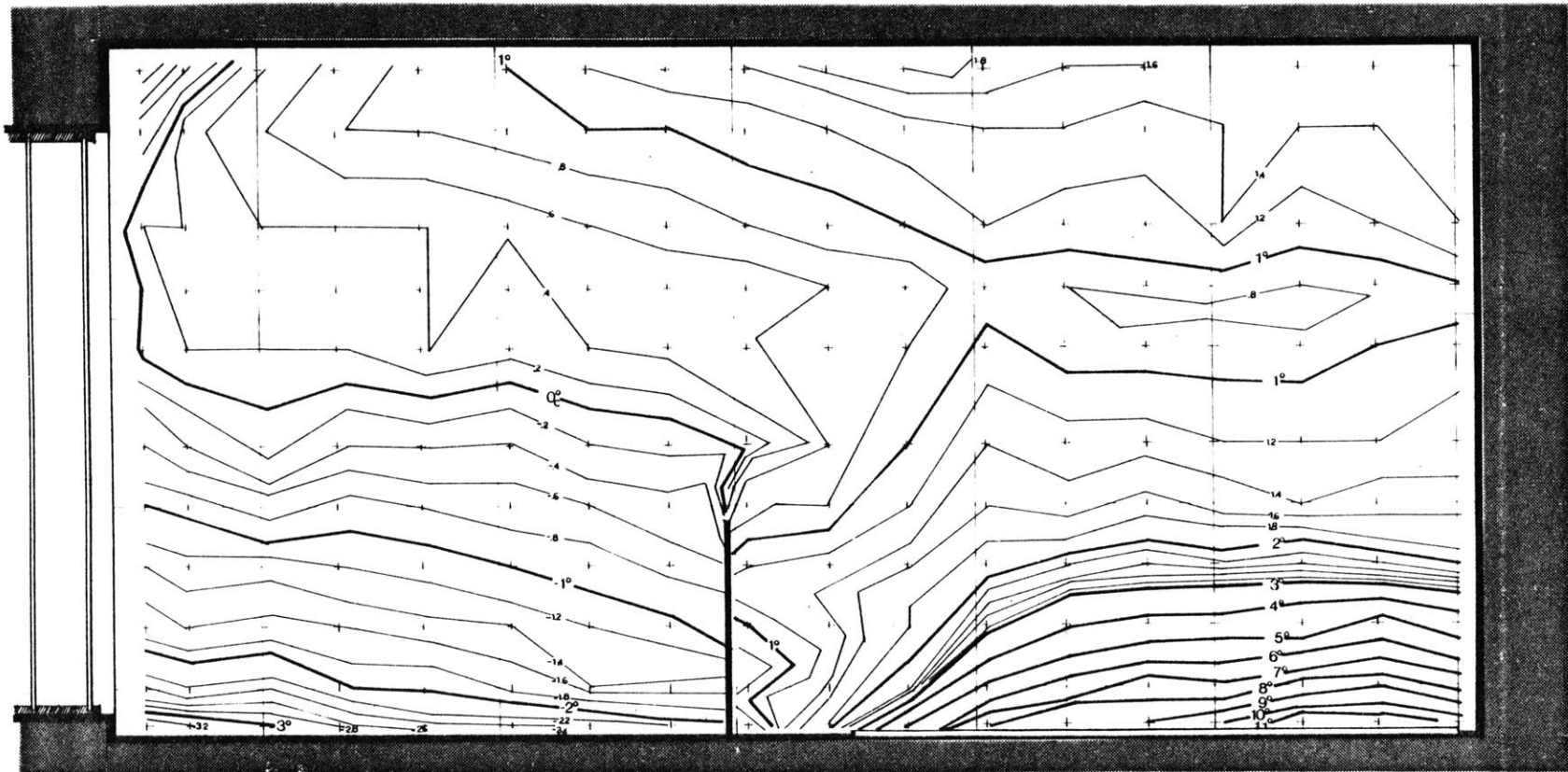
23. See D. J. Tritton, Physical Fluid Dynamics, p. 47.

The ceiling flow toward the window was characterized by diffusion and eddying at the lower boundary of the flow until it dispersed above the window.

The baffle prevented the cool air flow, generated at the window surface, from flowing across the floor (See Fig. 19c). A stable pool of cool air gathered in front of the baffle and a slow cool air flow of 1 M/min. (3.3 ft/min.) formed over the top of the pool, continuing over the baffle until it was entrained in the plume. A second cool air flow developed around the end of the baffle, moved along the floor, and was entrained over the middle and front of the heater thus reinforcing the plume position. The midroom isothermal area acted as a boundary layer as the warm and cool air flows occurred so close to each other.

The baffle caused a radical change in the generic flows of the test cell (See Fig. 19d). A cool air pool with slow movement over the top of the baffle was entrained into a plume which rose and split into two flows at the ceiling. The temperature range in the flow was 4.9°C.

Model Interpretation. Similitude in temperature fields was established between the model (Fig. 20a) and the test cell. Two



**B** scale  $1/6 \cdot 2$

Fig. 20a. Temperature field in model with baffle.

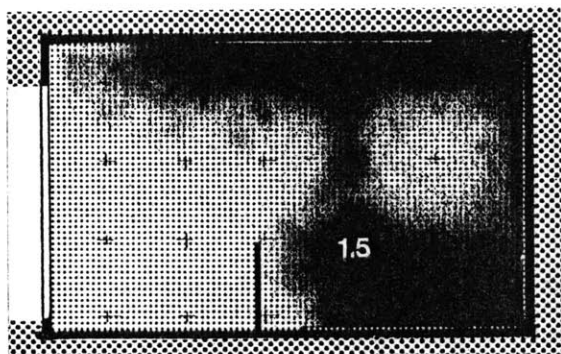


Fig. 20b. (B 1/6.2) warm air flows.

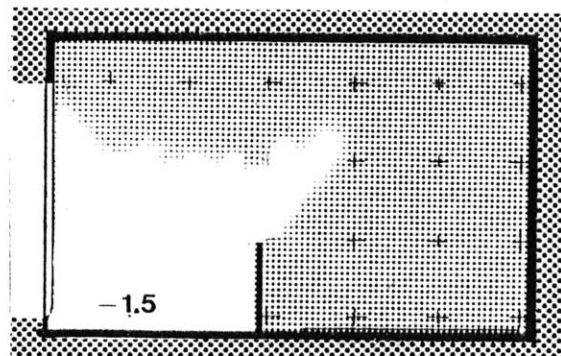


Fig. 20c. (B 1/6.2) cool air flows.

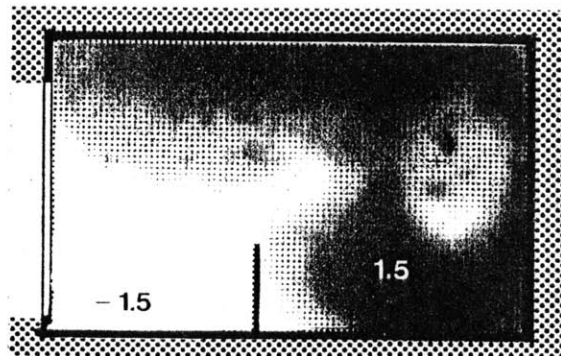


Fig. 20d. (B 1/6.2) generic air flows.

major flows were identified: 1) a warm air flow which ascended at the front of the heater and split at the ceiling into a flow toward the window and a flow toward the rear of the room, and 2) a cool air flow which formed at the window and flowed over and around the baffle. The generic flow patterns were similar to those of the test cell, but the temperature distributions of the flows exhibited differences.

The differences found in the warm air flows (Fig. 20b) were: 1) the formation of a conduction layer at the heater<sup>24</sup> and 2) the development of a thicker flow at the ceiling. The ceiling flow indicated the development of a conduction layer adjacent to the ceiling. Differences in the cool air flow (Fig. 20c) occurred in the entrainment of the floor flow at the side of the heater rather than over it as was the case in the test cell.

The generic flow patterns (Fig. 20d) in the small scale proved similar to the full scale flows. Temperature range in the model was 5°C. Variations occurred in the warm air flows, and interpretation indicates that the baffle slowed the convective flow regimes in the 24. This conduction layer occurred within the relative 70 cm. boundary delineated as the conduction area, and does not bear on the evaluation of similitude.

model to a point where conduction through the air layers was occurring, thus creating a temperature stratification of  $0.8^{\circ}\text{C}$  at the ceiling (the stratification was  $0.2^{\circ}\text{C}$  in the test cell). Thus convection systems where the thermal flows were deflected by physical barriers developed slower flows and the rigorous similitude of the modelled system deteriorated.

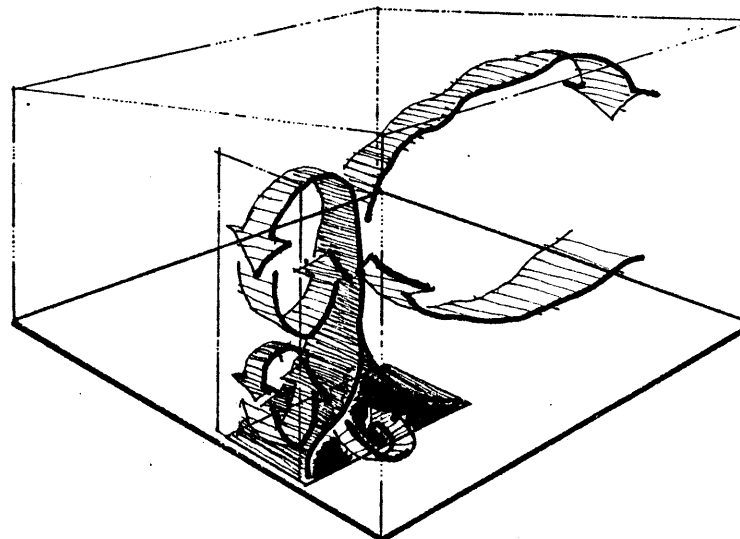
#### Configuration C

In Configuration C the heater plate was located below the window, as previously described, in a position similar to that recommended for forced air heat outlets to prevent cold drafts.<sup>25</sup> In the test cell this configuration created smaller flows and prevented cool air flows from forming by immediately mixing the cold flow with the rising warm air (See Fig. 21). The smaller flows were used to assess the model's ability to simulate detail.

Test Cell Interpretation. The temperature field in the test cell (Fig. 22a) was seen as having 2 flows: 1) a warm air plume that ascended from the middle of the plate, creating 2 convective cells at the window and a weak flow at the ceiling, and 2) a cool air flow

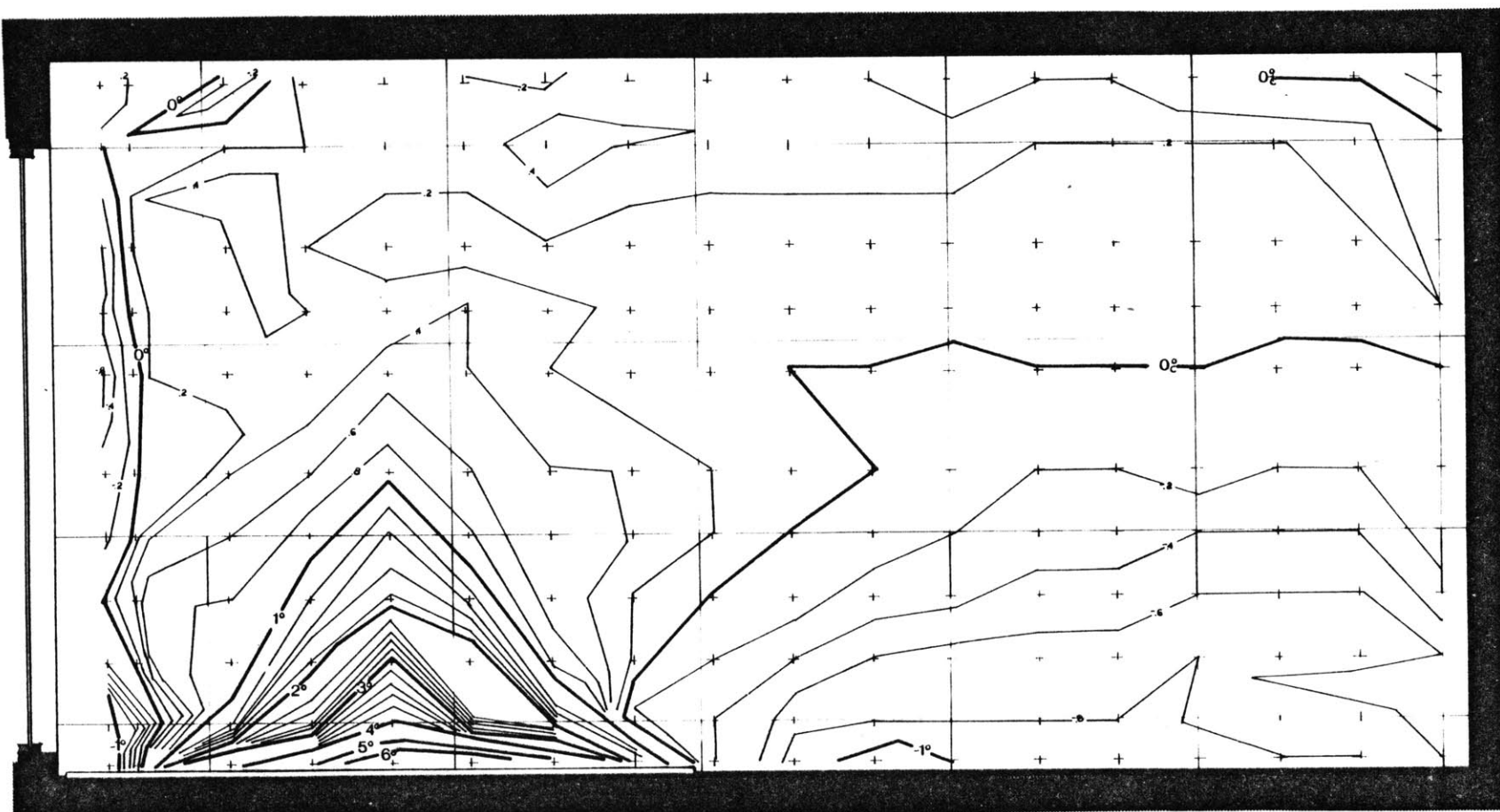
25. W. J. McGuiness and B. Stein, Mechanical and Electrical Equipment for Buildings, p. 251.





**CONFIGURATION C**  
*HYPOTHESIZED TEST CELL FLOWS.*

Fig. 21.



**C scale 1:1**

Fig. 22a. Temperature fields in test cell with heater under window.

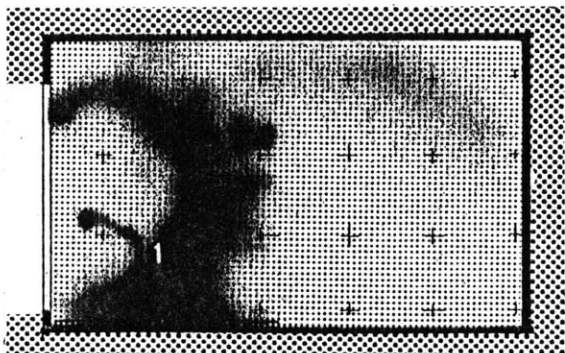


Fig. 22b. (C 1.1) warm air flows.

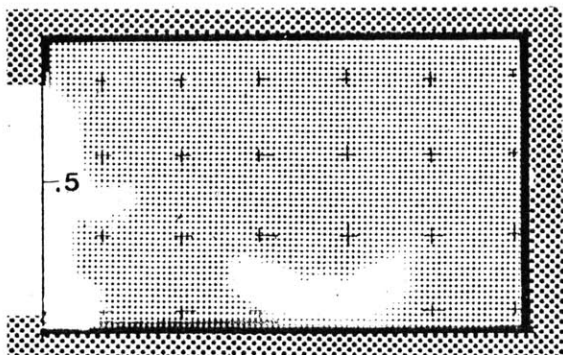


Fig. 22c. (C 1.1) cool air flows.



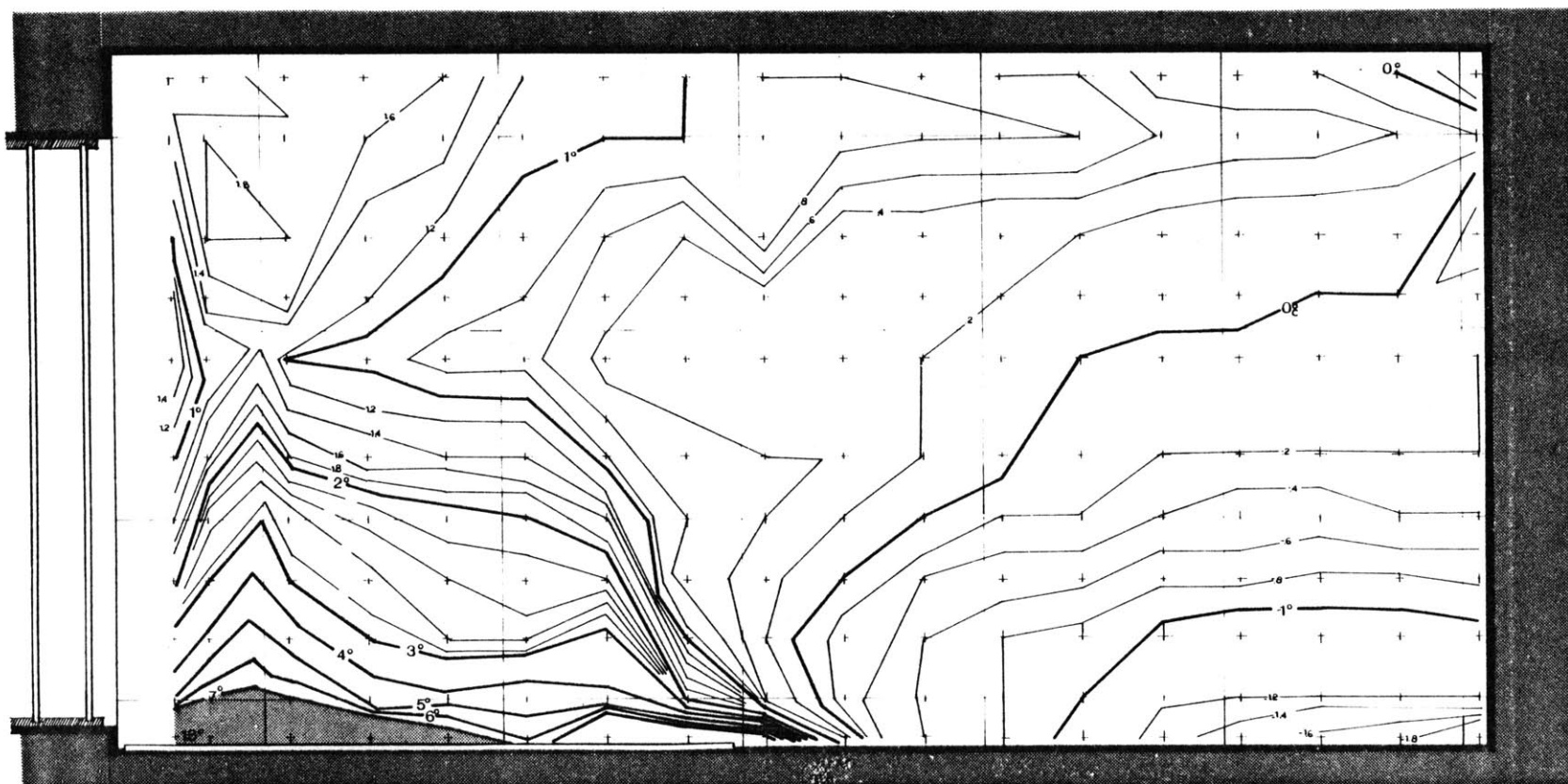
Fig. 22d. (C 1.1) generic air flows.

reinforced the convective cells created by the plume. The warm air flow, as shown in Fig. 22b, ascended from the middle of the heater plate, entraining air into itself as it rose. Part of this flow peeled off toward the window at a height of ca. 60 cm. The largest flow portion turned toward the window at a height of 200 cm. The remainder of the plume was deflected at the ceiling toward the rear of the room forming a weak flow under the ceiling.

Air being cooled at the window is confined to the window area. Two cool air flows are formed in conjunction with the flows formed by the plume (Fig. 22c). Some cool air was also entrained from the side of the heater. An isothermal area was located at the rear of the test cell, and the air from this area was entrained into the plume causing a slow air drift from the rear to the front.

The generic flows of Configuration C in Fig. 22d illustrate a detailed mixing process at the window and an isothermal area at the rear of the room. A temperature range of  $3.3^{\circ}\text{C}$  was present in the system.

Model Interpretation. In the model, the patterns established by the isotherms (Fig. 23a) were similar to those of the test cell. As in the test cell, a warm air flow ascended at the front end of the



**C** scale  $1/6 \cdot 2$

Fig. 23a. Temperature fields in model with heater plate under window.

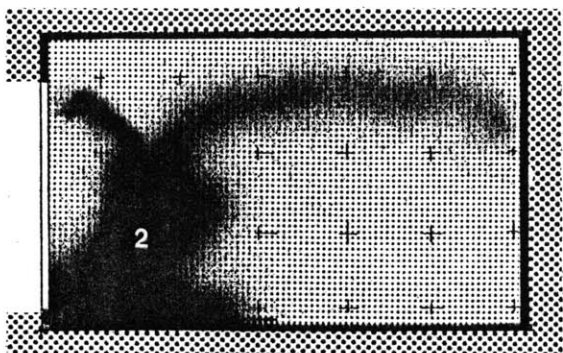


Fig. 23b. (C 1/6.2) warm air flows.

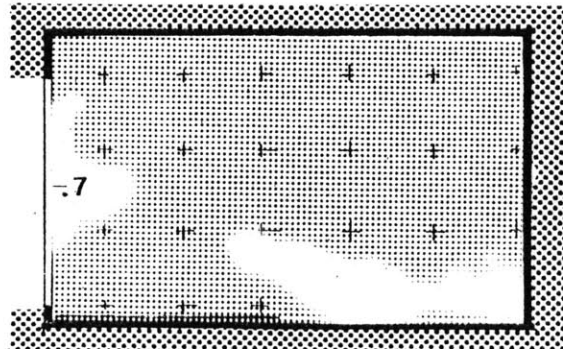


Fig. 23c. (C 1/6.2) cool air flows.

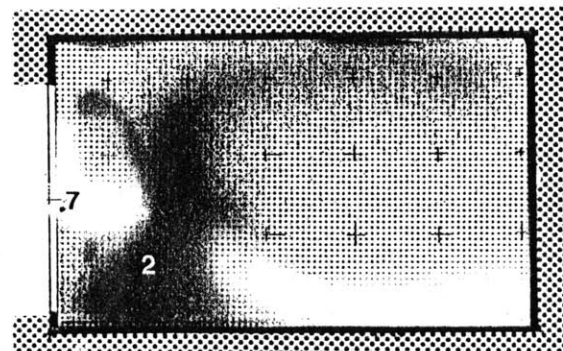


Fig. 23d. (C 1/6.2) generic air flows.

heater, and created a convection cell at the window and a flow at the ceiling. The cool air flows, as they mixed with the warm air, were restricted to the window area. However, differences in temperature fields occurred in the conduction area over the heater; the plume was located further forward; and the smaller vortex that had developed in the test cell was not present in the model.<sup>26</sup> A more distinct ceiling flow toward the rear of the room developed in the model, and the isothermal area exhibited a  $1^{\circ}\text{C}$  greater temperature gradient than was present in the full scale system. From this, it was deduced that the isothermal area in the model had a relatively stronger flow than the test cell counterpart. A single cool air flow at the window was formed in conjunction with the plume flow, as opposed to the double flow formed in the test cell, (See Fig.23c).

Beyond the conduction limit of the heater plate, the generic flow patterns (Fig. 23d) were similar to those of the test cell. Rigorous similarity of temperature distributions was not achieved in the rear room area. The temperature range in the model was  $4.4^{\circ}\text{C}$ .

26. The plume position, in a second test of the model in this configuration, was more centrally located over the heater plate.

TABLE 4. SYNOPSIS OF EXPERIMENTAL RESULTS

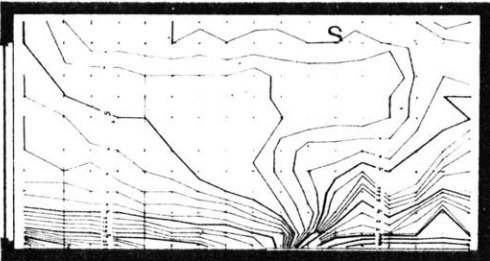

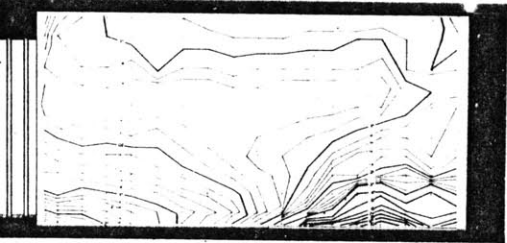
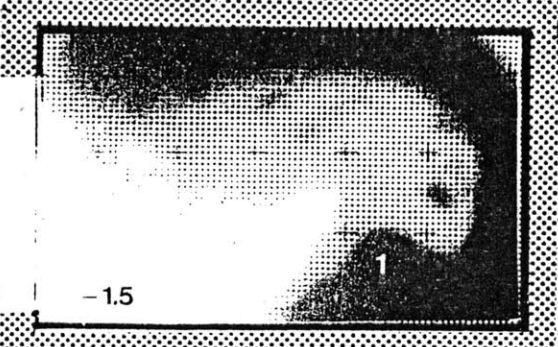
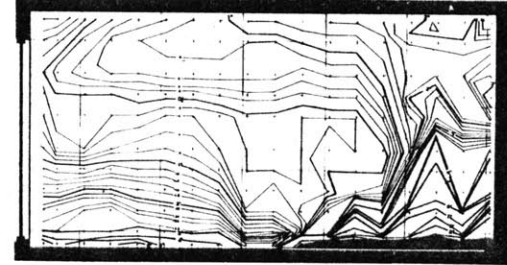

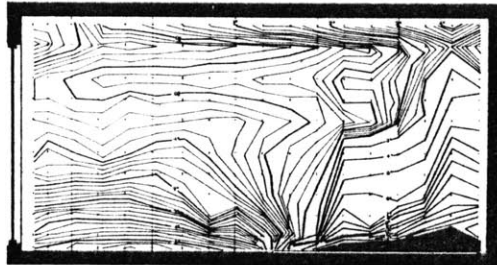
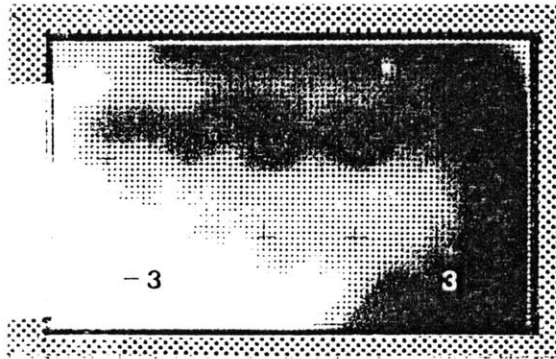
TEMPERATURE FIELD	GENERIC FLOW	INTERPRETATION
 <p data-bbox="201 561 296 581">A scale 1-1</p>	 <p data-bbox="814 570 852 589">-2</p>	<p data-bbox="1295 289 1908 412">Two air flows; a warm air flow formed at the rear wall and along the ceiling, and a cool air flow formed at the window, and along the floor.</p> <p data-bbox="1295 448 1850 477"><math>\Delta T</math> (gradient in test cell) = <math>5.7^\circ\text{C}</math></p> <p data-bbox="1295 493 1908 522"><math>Gr^*</math> heater = <math>7.2 \times 10^{11}</math></p> <p data-bbox="1295 539 1908 568"><math>Gr^*</math> window = <math>2.2 \times 10^{11}</math></p> <p data-bbox="1295 591 1866 656">correlation coefficient (R) between similar experiments = .92</p>
 <p data-bbox="226 938 331 958">A scale 1/6-2</p>	 <p data-bbox="800 954 858 974">-1.5</p>	<p data-bbox="1295 704 1877 828">Similar air flows to test cell; the warm air flow was thicker and the cool air flow diffused before reaching the heater plate.</p> <p data-bbox="1295 850 1877 880"><math>\Delta T</math> (gradient in the model) = <math>5.1^\circ\text{C}</math></p> <p data-bbox="1295 896 1908 925"><math>Gr^*</math> heater = <math>5.1 \times 10^8</math></p> <p data-bbox="1295 941 1908 971"><math>Gr^*</math> window = <math>1.5 \times 10^8</math></p> <p data-bbox="1295 993 1877 1029">R (between model and test cell) = .88</p>
 <p data-bbox="201 1347 348 1367">A scale 1/6-3.8</p>	 <p data-bbox="806 1341 844 1360">-3</p>	<p data-bbox="1295 1127 1908 1224">Similar air flows; the warm air plume was slightly separate from rear wall. Ceiling flow was thicker.</p> <p data-bbox="1295 1247 1908 1276"><math>\Delta T</math> = <math>11.9^\circ\text{C}</math></p> <p data-bbox="1295 1292 1908 1321"><math>Gr^*</math> heater = <math>9.6 \times 10^8</math></p> <p data-bbox="1295 1338 1908 1367"><math>Gr^*</math> window = <math>3.0 \times 10^8</math></p> <p data-bbox="1295 1390 1839 1419">R = .87</p>

TABLE 4 (Continued)

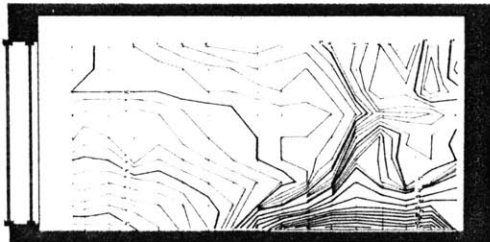


A scale 1/6-85

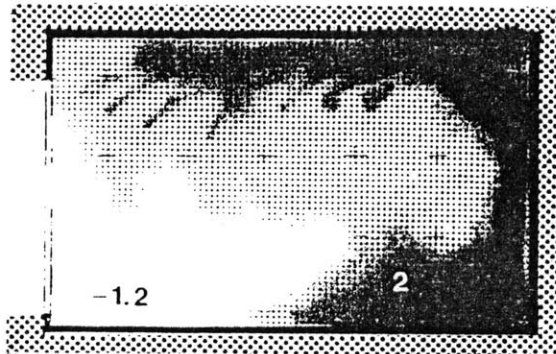


Dissimilar air flows; the warm air flow beneath the ceiling is split (or possibly cellular).

$$\begin{aligned}\Delta T &= 14^{\circ}\text{C} \\ \text{Gr}^* \text{ heater} &= 2 \times 10^9 \\ \text{Gr}^* \text{ window} &= 6.6 \times 10^8 \\ R &= .83\end{aligned}$$

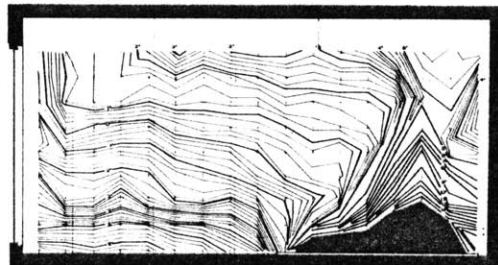


A scale 1/12-21



Similar air flows; more pronounced wave form over the heater plate and premature diffusion occurred along the cool air floor flow.

$$\begin{aligned}\Delta T &= 4.9^{\circ}\text{C} \\ \text{Gr}^* \text{ heater} &= 2.4 \times 10^7 \\ \text{Gr}^* \text{ window} &= 7.0 \times 10^6 \\ R &= .85\end{aligned}$$



A scale 1/12-159



Dissimilar air flows; plume use is further from wall causing a small vortex.

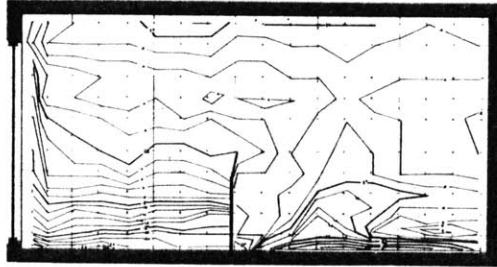
$$\begin{aligned}\Delta T &= 18^{\circ}\text{C} \\ \text{Gr}^* \text{ heater} &= 1.6 \times 10^8 \\ \text{Gr}^* \text{ window} &= 5.3 \times 10^7 \\ R &= .84\end{aligned}$$

TABLE 4 (Continued)

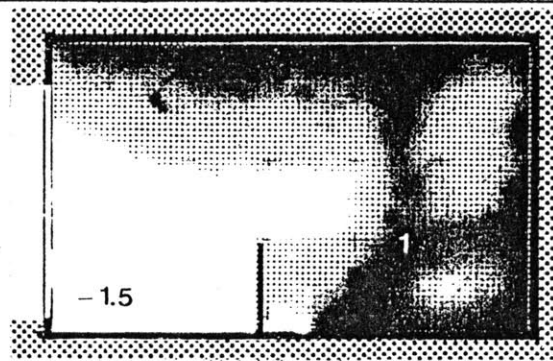
## TEMPERATURE FIELD

## GENERIC FLOW

## INTERPRETATION



B scale 1:1

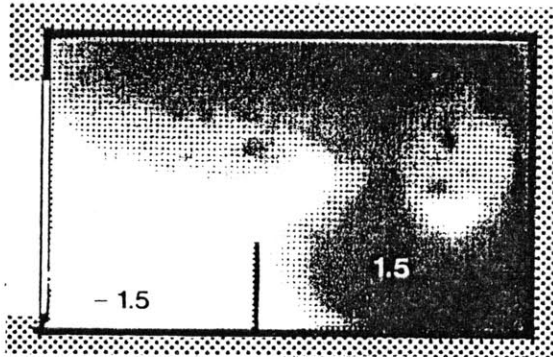


Two air flows; a warm air flow at the front half of the heater plate, splitting at the ceiling, and a cool air pool behind the baffle with a flow over the top.

$$\Delta T = 4.9^{\circ}\text{C}$$



B scale 1/6:2

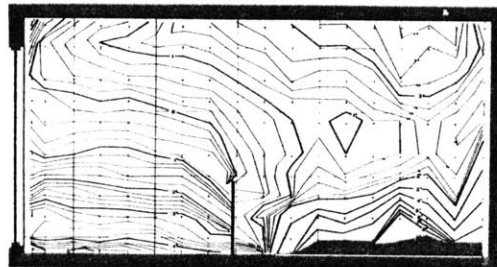


Similar flows developed beyond the conduction range of the heater, the ceiling flow was thicker indicating conduction through that layer.

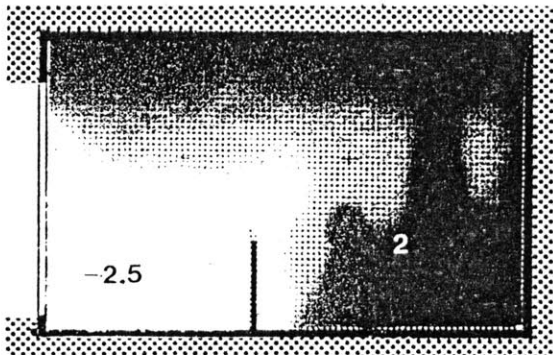
$$\Delta T = 5^{\circ}\text{C}$$

$$R = .86^*$$

\*between test cell and model



B scale 1/6:38



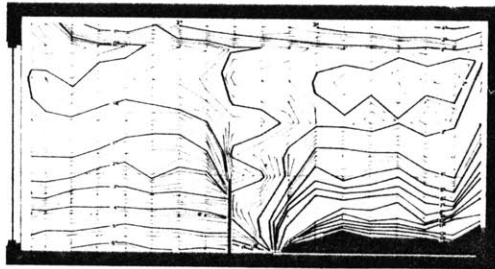
Similar air flows; the main plume rises towards the rear half of the heater plate. A thicker hot layer at the ceiling was evident.

$$\Delta T = 9.8^{\circ}\text{C}$$

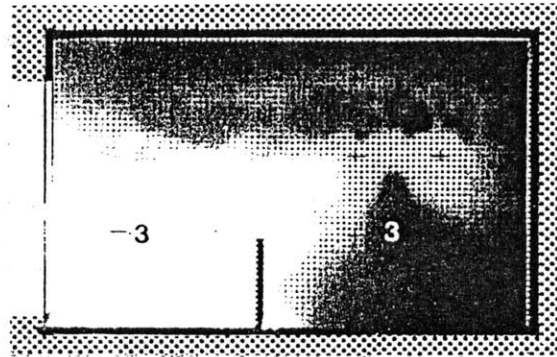
$$R = .9$$



TABLE 4 (Continued)



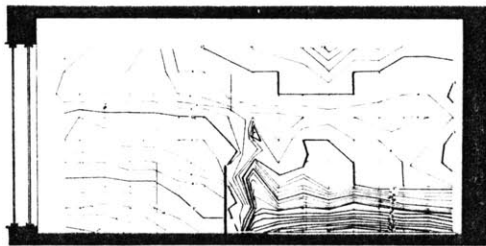
B scale 1/6-85



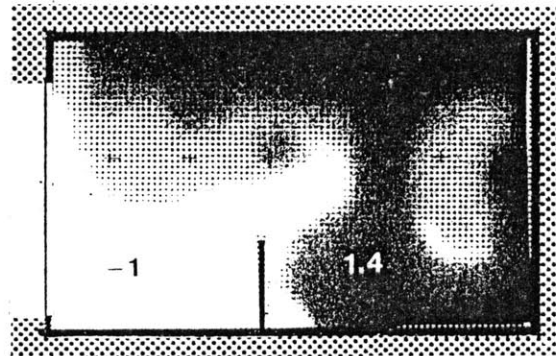
Dissimilar air flows; the warm air flow indicated a split flow or cellular development. A long vortex was formed from the baffle flow to the rear wall.

$$\Delta T = 13^{\circ}\text{C}$$

$$R = .84$$



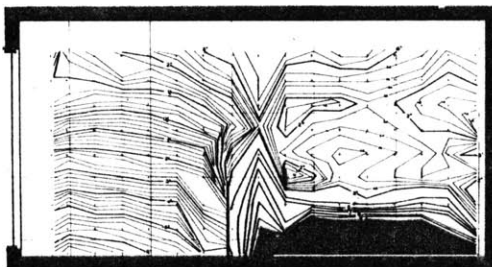
B scale 1/12-21



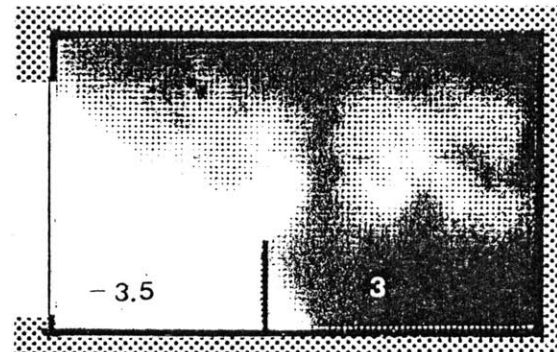
Similar air flows; the warm air ceiling flows are thicker.

$$\Delta T = 3.9^{\circ}\text{C}$$

$$R = .8$$



B scale 1/12-159

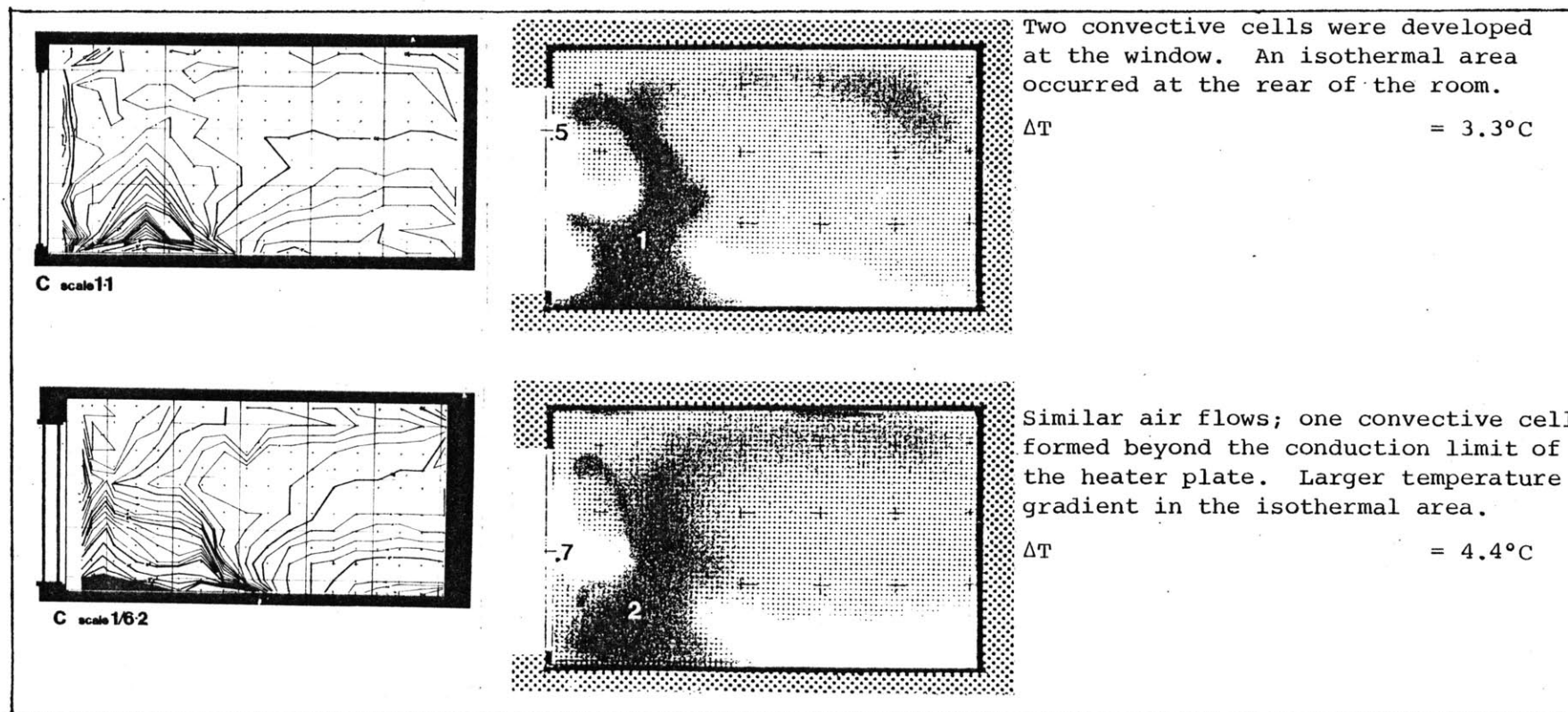


Dissimilar air flows; the warm air flow was characterized by a plume rise at the baffle and turbulent thermal development over the heater plate

$$\Delta T = 13.8^{\circ}\text{C}$$

$$R = .76$$

TABLE 4 (Continued)



## CONVECTIVE FLOW SIMILITUDES IN MODELS

Although it was not possible to precisely define similitudes of convective flows found in the tested models, the scaling relationships as defined in Chapter I proved to yield reasonable similarity between the generic flows in the models and the test cell. (Table 4 relates the temperature fields and generic flows of the models to the full scale counterparts.) As rigorous modelling was not attempted, precise temperature correlations were not expected. The model temperature distributions, however, correlated well with the temperature distributions found in the test cell. The correlation coefficients found in the entire range of models was above 0.8, except for the (1/12·15.9) model, while correlations between experiments of similar conditions in the test cell were 0.92.

As the modelling procedure departed from scaling relationships, it was expected that similitude of the models with a smaller  $D_f$  would yield better similitudes.<sup>27</sup> This proved to be the general case. But the more rigorous similitude of temperature distributions seemed to depend on the Grashof\* numbers (the convection to conduction

---

27. The higher the  $D_f$  the greater the departure from the heat flux specified by the scaling relationships.

ratio) of the convection flow. At 1/6 scale the most similar flows occurred where the Grashof\* number was in a range between  $2.5 \times 10^8$  and  $1 \times 10^9$ . At 1/12 scale, the most similar flows were found where the Grashof\* number was in the approximate range of  $8 \times 10^6$  to  $1 \times 10^8$ ,<sup>28</sup> (See Fig. 24). The window flows had lower Gr\* values than the heater plate flows due to the lower heat flux through the windows. The models with a lower  $D_f$  had lower Gr\* values. Thus the cool air window flows in the models with a low  $D_f$ , the (1/6·2) model and the (1/12·2) model, did not model as well as the warm air flows. Conversely, the models with high  $D_f$  factors, the (1/6·8.5) model and the (1/12·15.9) model, had fairly good representations of the cool air flows, but the warm air flows modelled poorly. With an increase in  $D_f$ , the temperature ranges within the models increased. Fig. 25 shows the temperature factor,  $T_f$ ,<sup>29</sup> as a function of the model scale.

Similarity to the generic flows in the test cell was better in the simple models (Configuration A) than in the models with the

---

28. Full scale  $Gr^* = 7.5 \times 10^{11}$  at the heater flow.

29.  $T_f = \frac{\text{temperature range of model}}{\text{temperature range of the test cell}}$  (12)

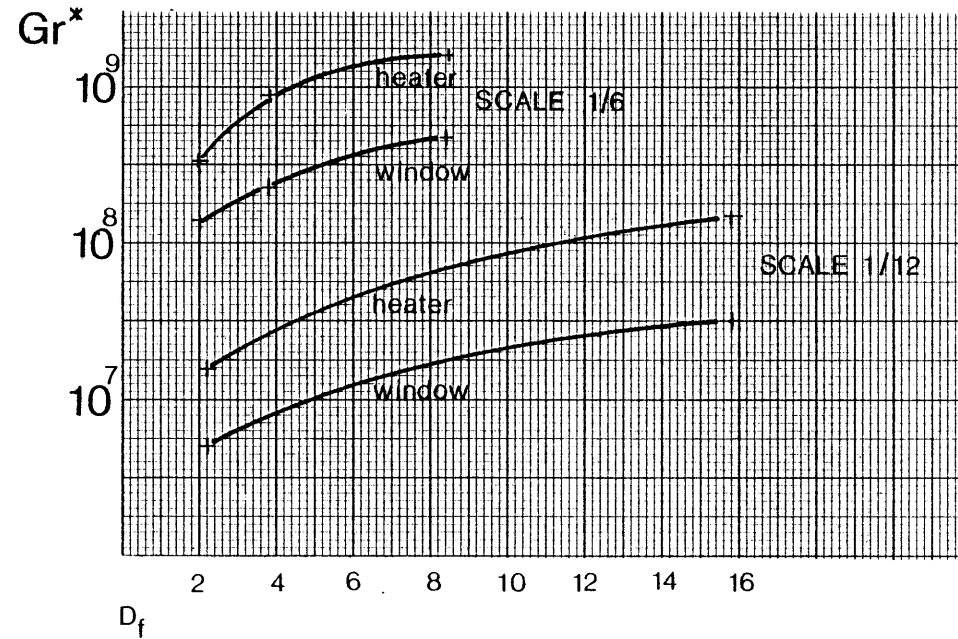


Fig. 24.  $Gr^*$  values as a function of scale and  $D_f$ .

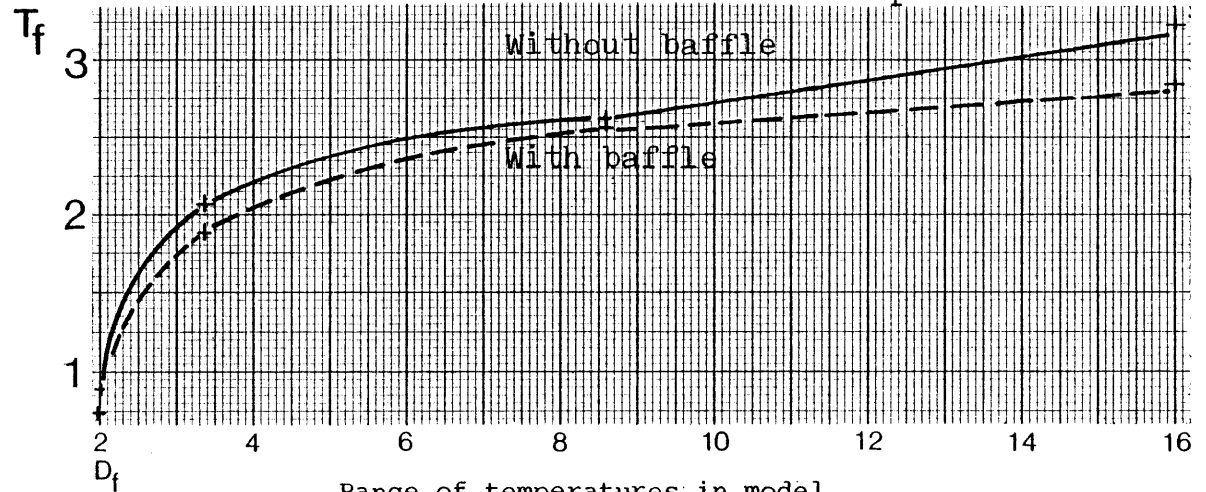


Fig. 25.  $T_f = \frac{\text{Range of temperatures in model}}{\text{Range of temperatures in test cell}}$  as a function of  $D_f$ .

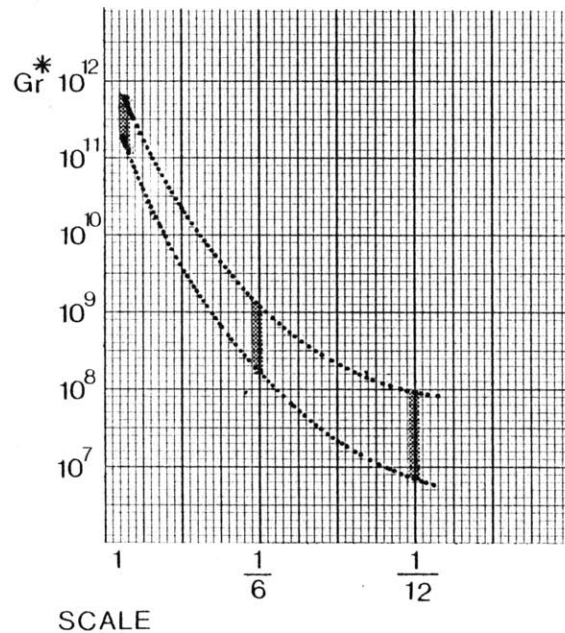


Fig. 26.  $Gr^*$  values that yield good similitude as a function of scale.

baffles (Configuration B). The complexity of interior spaces due to the addition of baffles seemed to cause more acute divergence from similarity. The following general observations were made concerning scale modelling of convection flows:

- 1) The similitude of convection flows was best in a specific range of Grashof\* numbers. (The  $Gr^*$  values which best modelled the flows are shown as a function of scale in Fig. 26.) The more similar a heat source and a heat sink are in terms of convection to conduction ratios ( $Gr^*$ ), the better the similitudes.
- 2) The larger the free volumes and surfaces, the less complex were the flows. Neither greater  $D_f$  factors nor smaller geometric scales affected the similitude of the flows found in the models with simple configurations. Conversely, models with complex flow patterns did not model as well with higher  $D_f$ 's and smaller scales.

From observation of the models, it seemed that the departure factor ( $D_f$ ) did not crucially affect modelling of convection flows, provided that, in the model and the test cell, the average temperature difference between interior and exterior, and the proportional

heat loss from building skin elements were similar. Thus it was concluded that at model scales between 1/6 and 1/12, and with departure factors between 2 and 10, reasonable similitudes of temperature distributions and generic flows could be obtained for fairly complex flows.

# Chapter III

## A Procedure for Simplified Thermal Modelling

The results of the modelling experiments explained in Chapter II predicate the use of simple scale models for determining bulk air movements in buildings. The use of this physical modelling is suggested for the prediction of convection flow in building designs where natural convection is used for heat distribution, and is most suitable for buildings with small thermal storage capacities or buildings where large thermal storage capacities are the primary heat source.

Modelling convection flows in scale models is a process that begins with an analysis of the thermal characteristics of a building design, followed by the construction and subsequent testing of a model, and the recording of convection flows. This procedure is explained in this chapter, and is illustrated by an example of a simple sketch design.



ANALYSIS OF THE THERMAL CHARACTERISTICS  
OF THE DESIGN

In the modelling procedure, information regarding the thermal characteristics of a given building design is required before a model can be built. Different levels of analysis are necessary for different types of heat inputs in a specific building design. The process for developing this information follows.

Unit Thermal Conductance. The unit thermal conductance of building elements and their areas must first be determined.

$$h_{ci} = \frac{1}{R_{if} + R_{ins} + R_{of}} \quad (13)$$

where

$h_{ci}$  = unit thermal conductance of building skin component

$R_{if}$  = thermal resistance of inside finish

$R_{ins}$  = thermal resistance of insulation

$R_{of}$  = thermal resistance of outside finish

Overall Conductance. The overall conductance must also be determined.

$$h_c A = \sum_{i=1}^n h_{ci} A_i \quad (14)$$

where

$h_c$  = overall unit thermal conductance

$A$  = total building skin area

$A_i$  = building skin component area

Overall Windowless Conductance. A large portion of the heat lost by conduction is typically lost through a relatively small window area. The greater heat flux at these areas may be a crucial factor in the development of convection flow. In order to develop similarity of flows in the model the heat loss from the window areas must be proportionally similar to that of the building design. In order to determine the overall windowless conductance of the design, the window areas must be added to the area of the building component in which they were found.

$$h'_c \times A = \sum_{i=1}^{n-1} h_{ci} A'_i \quad (15)$$

$$A'_i = A_i + A_w \quad (16)$$

where

$h'_c$  = the overall windowless unit thermal conductance

$A'_i$  = windowless building component area

$A_w$  = window area in building skin component  $A_i$

The Proportionality Factor. The ratio between the overall windowless unit thermal conductance and the unit thermal conductance defines the proportionality factor  $P_f$ .

$$P_f = \frac{h'_c}{h_c} \quad (11)$$

where

$P_f$  = proportionality factor

The Energy Flux into the Design. For natural convection to occur, a heat source is required. This may be a point heat source, such as a stove or radiator, or a planar heat source, such as a radiant ceiling or a floor experiencing solar gain. Heat sources that maintain a constant interior temperature typically have a designed heat flux capacity high enough to maintain comfortable room temperatures when minimum ambient temperatures are experienced. The heat flux can be assumed constant during heating periods.

$$\dot{Q}_{fs} = \dot{Q}_{hs} \quad (17)$$

$$\dot{Q}_{hs} = h_c A (T_r - T_{md}) \quad (18)$$

where

$\dot{Q}_{fs}$  = heat flux into full scale design

$\dot{Q}_{hs}$  = designed heat flux of the heat source

$T_r$  = average room temperature

$T_{md}$  = minimum design temperature

As the energy flux due to solar gain is not a steady state phenomenon, the model may only be used to define convection occurring at specific periods in the day. In the case of solar gain onto surfaces with low thermal storage capacities, the heat flux into the design is determined from the vertical component of the transmitted solar energy.

$$\dot{Q}_{fs} = I_v \quad (19)$$

$$I_v = (I_n \cos A_z \cos W) \tan P \quad (20)$$

where

$I_v$  = vertical component of solar flux

$I_n$  = energy flux on surface normal to solar rays

$A_z$  = zenith angle

$W$  = azimuth angle to normal of the wall

$P$  = profile angle

If the solar energy flux is occurring onto an area of large thermal storage capacity then, only the component of energy influencing air temperatures must be determined. The solar gain on an

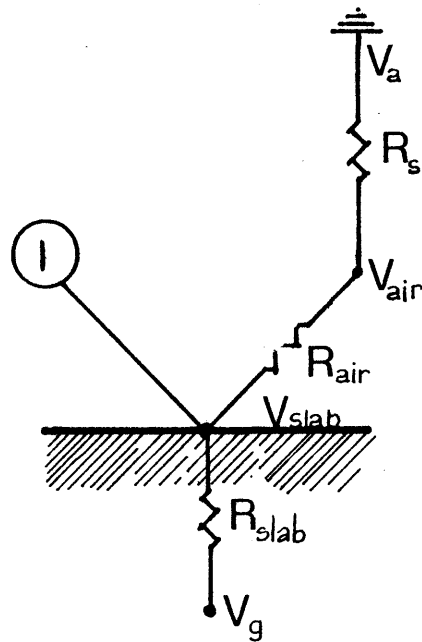


Fig. 27. Analog circuit representing direct solar gain.

interior building surface may be determined by a simple analog circuit (Fig. 27). The air temperatures, the thermal resistance of surface to air conduction, and the thermal resistance of the storage area, determine the amount of heat that is convected and radiated into a space.

$$I_v = \frac{V_{\text{slab}} - V_g}{R_{\text{slab}}} + \frac{V_{\text{air}} - V_a}{R_s} \quad (21)$$

$$\frac{V_{\text{slab}} - V_g}{R_{\text{slab}}} = I_v \frac{R_{\text{air}}}{R_{\text{slab}} + R_{\text{air}}} \quad (22)$$

$$\frac{V_{\text{air}} - V_a}{R_s} = I_v - I_v \frac{R_{\text{air}}}{R_{\text{slab}} + R_{\text{air}}}$$

$$h_c (T_r - T_a) = I_v - I_v \frac{R_{\text{air}}}{R_{\text{slab}} + R_{\text{air}}} \quad (23)$$

where

$V_{\text{slab}}$  = voltage equivalent of slab temperature

$V_g$  = voltage equivalent of ground temperature

$V_{\text{air}}$  = voltage equivalent of room air temperature

30. For a 6 inch concrete slab,  $\frac{R_{\text{air}}}{R_{\text{slab}} + R_{\text{air}}} = 0.54$

$V_a$  = voltage equivalent of ambient air temperature

$R_{slab}$  = resistance of thermal storage material

$R_s$  = overall resistance of building skin

$R_{air}$  = resistance of heat transfer to air layer

$T_a$  = ambient temperature

$$I_{conv} = I_v - I_v \frac{R_{air}}{R_{slab} + R_{air}} \quad (24)$$

$$\dot{Q}_{fs} = I_{conv} = h_c A (T_r - T_a) \quad (25)$$

where

$I_{conv}$  = energy flux into air from thermal storage

By determining the difference between the room air and the ambient air temperatures, the heat flux influencing convection may be determined.

$$\dot{Q}_{fs} = h_c A (T_r^* - T_a) \quad (26)$$

where

$T_r^*$  = room temperature determined from solar simulations

A simple solar gain simulation program developed for a Texas Instrument 59 Calculator provides hourly air temperatures for given

ambient conditions and solar gain.<sup>31</sup> From a daily average difference between interior and exterior temperatures, an equivalent steady state heat input representing an average heat flux due to solar gain on large thermal masses may be derived.

---

31. See Lebens, p. 134. Note that infiltration losses must be set to zero while using this program.

## MODEL DESIGN

Once the thermal characteristics of the proposed building have been obtained as outlined above, the design of the model may begin. This design is dependent on the complexity of the space where convection is hypothesized to take place, and is also influenced by the level of precision desired in the determination of convection flows and temperature distributions.

Choice of Geometric Scale and Departure Factor. As the scaling relationships determine the heat fluxes within a model, the choice of a geometric scale and a departure factor ( $D_f$ ) influences its performance and cost. Scales between 1/6 and 1/12 may be expected to model convection flows well. With larger scales better similitudes may be obtained.

$$L = \left( \frac{\dot{Q}_m}{\dot{Q}_{fs} D_f} \right)^{2/5} \quad (27)$$

where

$L$  = model scale

$D_f$  = departure factor

$\dot{Q}_{fs}$  = full scale heat flux

$\dot{Q}_m$  = model heat flux



Similarly, the choice of a departure factor influences similitudes achieved in a model. Lower departure factors may be expected to yield better similitudes. (Departure factors between 2 and 10 have proved to work well.)

$$D_f = \frac{\dot{Q}_m}{\dot{Q}_{fs} L^{5/2}} \quad (28)$$

The building skin conductance, as well as the heat flux in the model is dependent on the departure factor  $D_f$ .

$$h_m = h_c D_f L^{1/2} \quad (29)$$

where

$h_m$  = model building skin unit thermal conductance.

Rigid insulation of polyurethane, with  $k = 0.02$  W/M°C/ (or 0.14

BTU/hrft<sup>2</sup>°F/in.) or polystyrene, with  $k = 0.04$  W/M°C (or 0.25

BTU/hrft<sup>2</sup>°F/in.) may be used as the model building skin.<sup>32</sup> Any in-

crease in  $D_f$  increases the heat flux and decreases the model building component thicknesses.

---

32. Because their cost/W transmitted are similar, the prices of these two materials are equivalent.

$$t_{mi} = \frac{k_{mi}}{h_{ci} D_f L^{1/2}} \quad (30)$$

where

$t_{mi}$  = thickness of model building skin component

$k_{mi}$  = conductivity of the model building skin component

As the window areas must lose heat proportionally to the other building skin components,  $D_f$  also affects the type of window required in the model. From a determination of the window unit thermal conductance in the building design, and an application of the scaling relationship:

$$h_{mw} = h_{fsw} L^{1/2} D_f \quad (31)$$

where

$h_{mw}$  = unit thermal conductance model window

$h_{fsw}$  = unit thermal conductance of full scale window

a preliminary model window design may be interpreted from Fig. 28.

Model windows with higher unit thermal conductances than single glazing may be achieved by crimping a larger area of material into a geometrically scaled window opening. This provides a larger ratio between window conduction area and window opening area.

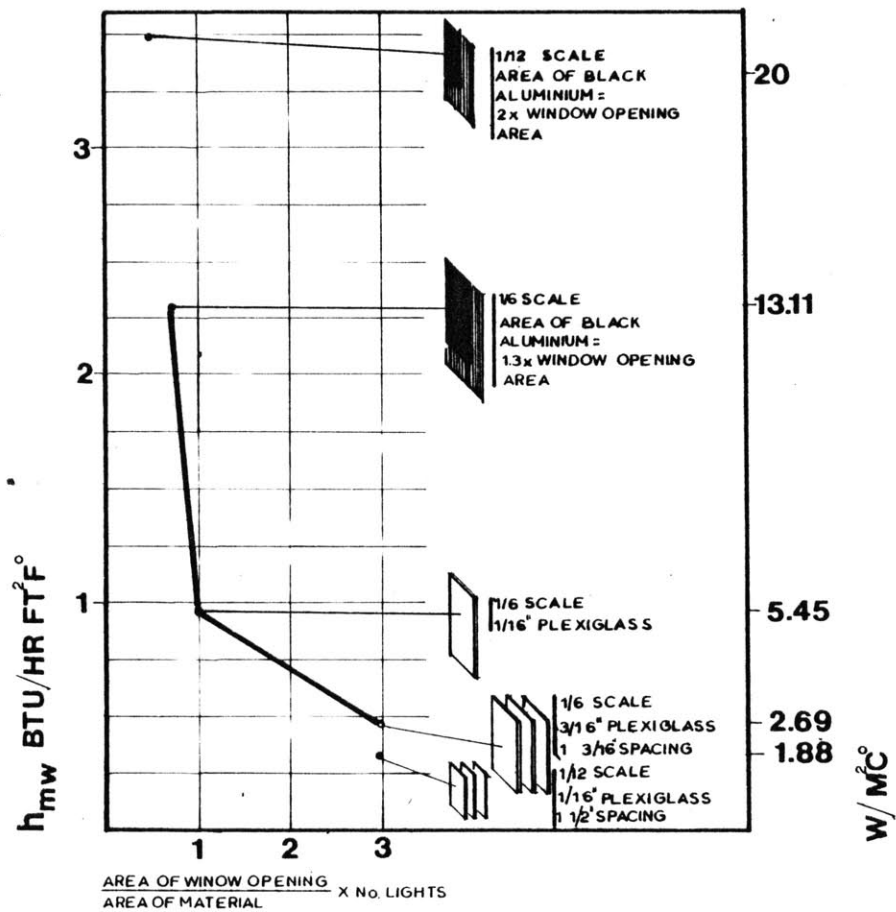


Fig. 28. Window designs for various scales and conductances. Area of material in the case of the crimped aluminum is larger than the geometrically scaled window opening area.

Due to the sensitivity of similitude to scale and  $D_f$ , models of complex spaces (where projections and passageways in the path of a hypothesized flow are less than 1M. in any dimension) require larger scales with thicker building components in order to develop flows similar to full scale flows.

Building the Model. The thickness of the model building skin is determined by geometric scale and departure factor  $D_f$ . Areas in the design which are not involved in the convection modelling may be replaced in the model by a building skin component of equivalent overall unit thermal conductance. Thus, garages and vestibules which may not have a role in the convection flows of a particular design may be replaced by a single piece of insulation.

The model building skin components are cut and loosely assembled to enclose a space geometrically similar to that of design. No windows are cut at this stage, but outlines should be drawn on the walls. As recording and interpreting of convection is the major purpose for building the model, viewing ports must be provided so that the convection process inside may be seen. (This is necessary where windows do not occur at convenient locations.) These ports should be parallel to the hypothesized plane of convection, and are

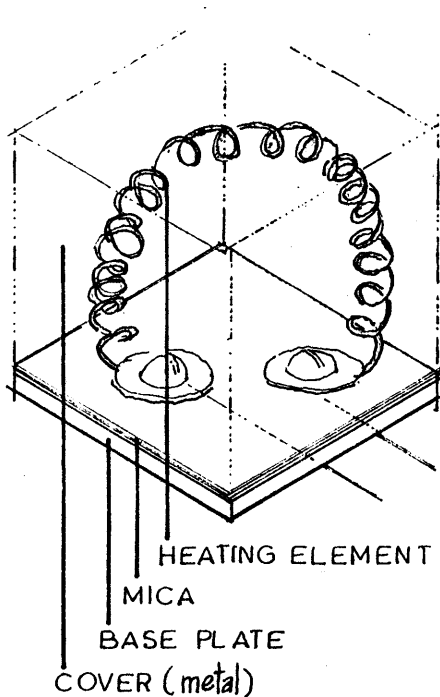


Fig. 29. Design of point heat source, simulating wood stove.

built by inlaying a 1/8 in. piece of glass into the inside surface of the insulation and sealing the edges with silicone sealant. The insulation on the outside is cut to expose the glass, but the cut-out is kept as a cover for the viewing port. At this point the model components are assembled and the joints are caulked with silicone sealant. The model is now ready for a heat source.

Building a Heat Source. Electric resistance heating elements are used as heat sources for the model. A point source may be built using a toaster resistance element (Fig. 29) and a planar source may be fashioned from resistance wiring or heater tape applied to the back of a thin black metal plate (Fig. 30). A direct current power supply, capable of delivering 60 watts, may be used to heat the resistance wires. Model railroad transformers are available in these power ranges, but it is cheaper to build a power supply oneself.

A potentiometer, located between the power supply and the model heat source (0-50 ohms) will allow fine tuning of the power input to the heat source. A multimeter is used to measure the voltage and current input to the model and thus monitor the heat flux.

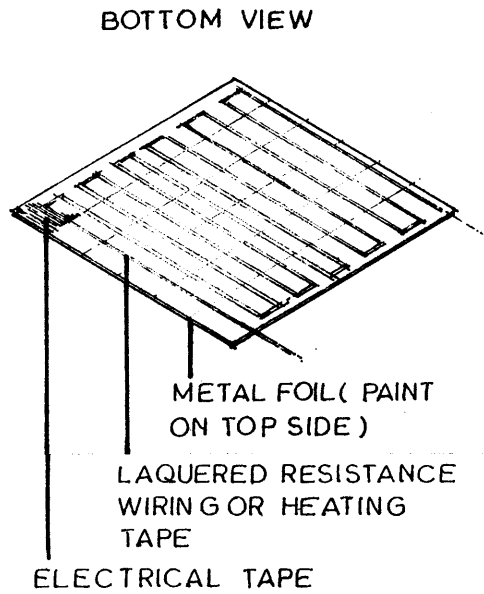


Fig. 30. A planar heat source.

$$W_m = V^2 R_h \quad (32)$$

$$W_m = VI \quad (33)$$

where

$W_m$  = power input into model

$V$  = voltage across resistance heater

$R_h$  = resistance of heater

$I$  = current into heater

$$\dot{Q}_m = W_m \quad (34)$$

From the relationship of scale to heat flux:

$$W_m = \dot{Q}_{fs} D_f L^{5/2} \quad (35)$$

A simpler, but untried, method would use a heat lamp as a heat source to simulate solar gain. Plastics with high infrared transmission, such as Teflon, would then be required as windows.

#### TESTING THE MODEL

Once the model has been built as described above, a series of tests are required to determine its thermal behavior.

Balancing Model Heat Loss. The model building elements must lose heat in proportions similar to those of the full scale design. As window losses are particularly crucial to convective flow development, the proportionality between window losses and other conduction losses must be maintained. Further, as only empirical data is available concerning small scale window losses, and as the conductance of the model building components may vary due to test temperatures and sample thicknesses, the proportionality factor of the model,  $P_{fm}$ , must be empirically obtained. For similitude,  $P_{fm} = P_f$ . (36)

To determine  $P_{fm}$  empirically, the windowless heat flux is compared to the heat flux with windows. The model is heated to steady state conditions, and interior air temperatures are measured with a long stem thermometer poked through the building skin. (Alternative temperature measurement techniques are explained on p. 89.) A number of measurements are taken to provide an average reading for the room. The holes left in the skin are sealed after each reading. This process is repeated after the model windows have been installed and

sealed with silicone, and an empirical proportionality factor is found.

$$P_{fm}' = \frac{H_{cm}'}{H_{cm}} \quad (11)$$

$$H_{cm}' = \frac{W_m}{(T_{rm}' - T_{am})} \quad (36)$$

$$H_{cm} = \frac{W_m}{(T_{rm} - T_{am})} \quad (37)$$

where

$P_{fm}'$  = experimental proportionality factor

$H_{cm}'$  = overall windowless thermal conductance of model

$H_{cm}$  = overall thermal conductance of model (with windows)

$T_{rm}'$  = average windowless model room temperature

$T_{rm}$  = average room temperature of model (with windows)

$T_{am}$  = model ambient temperature

-if  $P_{fm}' = P_f$ , the model can be tested for convection flows.

-if  $P_{fm}' < P_f$ , the windows must be rebuilt and additional

plexiglass layers must be added to decrease the windows thermal conductance.

-if  $P_{fm}' > P_f$ , the windows must be rebuilt and the conductance increased.



The above procedure is repeated until  $P_{fm}' = P_f$ .

As the model conductivity may vary from calculated values, an empirical  $D_f'$  must also be determined.

$$D_f' = \frac{H_{cm} (T_{rm} - T_{am})}{\dot{Q}_{fs} L^{5/2}} \quad (38)$$

$$D_f' = \frac{\dot{Q}_m}{\dot{Q}_{fs} L^{5/2}} \quad (39)$$

where

$D_f'$  = experimental departure factor

$D_f'$  needs to be within only  $\pm 1$  of the original calculations of  $D_f$ , but it must be used to set the heat input for the final test.

$$W_m' = \dot{Q}_m' = \dot{Q}_{fs} D_f' L^{5/2}$$

where

$\dot{Q}_m'$  = corrected model heat flux

$W_m'$  = corrected model power input

Determining Convection Flow in Models. When  $W_m'$  is input to the model, the following condition should exist at steady state:

$$(T_{rm} - T_{am}) = (T_r - T_a) \quad (40)$$

The temperature differences may vary by ca. 5%.

To record convection in the model, the air must be rendered visible by suspending particles in it. Smoke or aluminum powder blown through a tube into the model allows enough matter to be suspended to facilitate visualization of the flows, provided there is an attenuated light source. A red laser beam projected through a glass rod creates a horizontal light plane, and may be used to reveal flows in specific sections of the model. A spotlight attenuated by a series of baffles and located about 3 meters from the model will also provide a good light plane. To view the convection flows, the insulation is removed from the viewing ports. For a brief period (about 10 seconds) the convection flows may be viewed and recorded, as the glass has enough specific heat to prevent the steady state from changing. The flows may best be seen when a slightly acute viewing angle is maintained with respect to the light plane.

Another approach to visualization in models is to pass a periscope camera attachment through the wall. This is an expensive method, but is less likely to upset the model's thermal equilibrium.

As the attenuated light levels are typically low, and as the natural convection systems are fairly slow-moving, long exposure times and fast film speeds will yield the best results. Video recordings should be made with a Nuvi-con camera due to its better resolution at lower light levels. If temperature distributions are determined in the model, these may be scaled, and the temperature factor  $T_f$  (from Fig. 25) employed, to yield expected temperature distributions in a building.

$$(T_r - T_{fs}) = (T_{rm} - T) \times T_f \quad (12)$$

where

$T$  = sampled room temperature of model at a specific location.

$T_{fs}$  = expected temperature in building design at same relative location as  $T$ .

This simplified model testing procedure is expected to predict the generic flows in a building design, and provide a rough estimate of temperature distributions.

Rigorous Instrumentation. Temperature fields in simplified models may be accurately determined by sampling the air temperature with thermistors. YSI thermistors (described in Appendix II) provide an accurate temperature reading in terms of voltage, and their lo-

cation in the model should minimize interference with the air movement in the hypothesized convection plane by reaching into this plane on long, thin probes.

For a large number of probes, a low-noise analog multiplexer is required to sequentially sample the voltages. These voltages may be read from a digital voltmeter, recorded on an FM recorder, digitized and recorded on a tape deck, or digitized and directly read into a microprocessor. This last option is considered most suitable when a large number of models are to be tested. Due to the empirical nature of the testing procedure, a microprocessor would be helpful to quickly define and analyze all the parameters necessary for the model. The microprocessor could store the empirical results for future reference. With rigorous instrumentation of simplified models, correlation of temperature distributions between the model and the full scale design results.

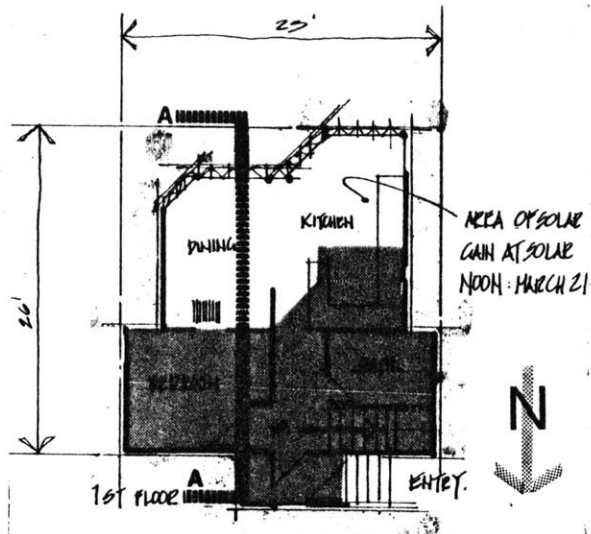


Fig. 31b. 1st floor plan.

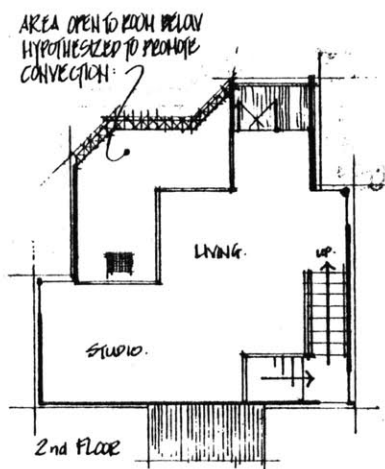


Fig. 31c. 2nd floor plan.

#### SIMPLIFIED MODELLING: AN EXAMPLE

A hypothetical example is used to illustrate the building design analysis and model design phase of the modelling procedure. This example is a sketch design of an 84M<sup>2</sup> cottage (Figs. 31a through 31d)

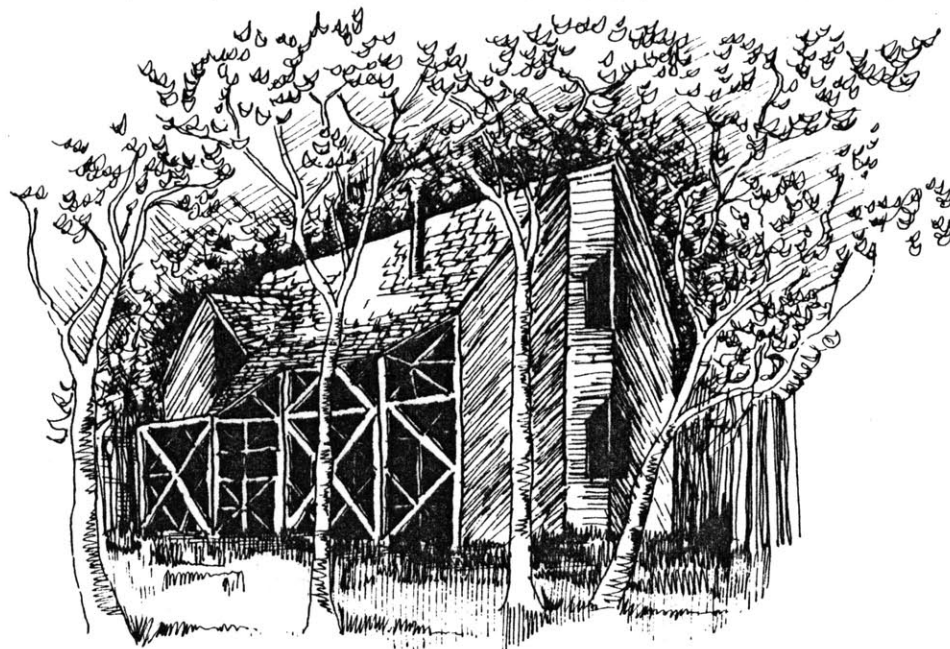


Fig. 31a. Perspective of passive solar sketch design, south elevation. which incorporates convective flow as a heat distribution method. The aim of the modelling procedure is to identify the convection flow fields and the general temperature distributions within the design which arise from solar gain through a large south-facing window. The hypothesized flow is shown in Fig. 32.

TABLE 5. BUILDING COMPONENT ANALYSIS

COMPONENT BUILDING AREAS	$h_c$				CONSTRUCTION
	Sq. ft.	M <sup>2</sup>	BTU/hrft <sup>2</sup> °F	W/M <sup>2</sup> °C	
Roof area	578	53.7	.034	.19	10" fiberglass batt, cedar shingles, plywood
Floor area					10" fiberglass, wood planking, building board
Target Area	200	19.6	0		6" concrete slab, gravel subgrade, insulated per.
Other	358	33.3	.034	.19	
Walls and	760				6" fiberglass, staggered stud wall, sypsum wallboard, wood siding
Windows	609 1369	127.2	.047	.26	
Windows	224	10.8*			two layers FEP between two glass layers transmission is 65% with 90° incidence.
	91	8.5**	.25	1.42	Solar gain window is a wood frame system

Note: \*solar gain window

\*\*others

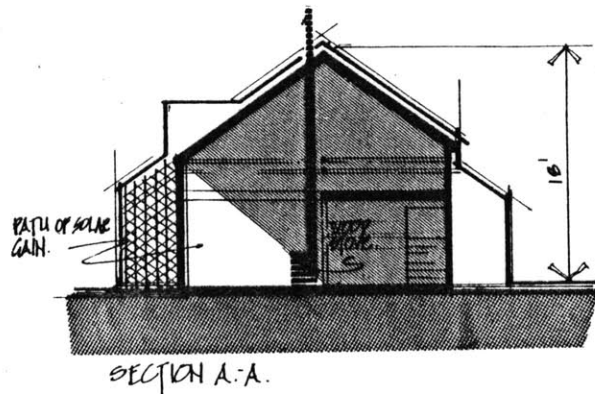


Fig. 31d. Section of sketch design.

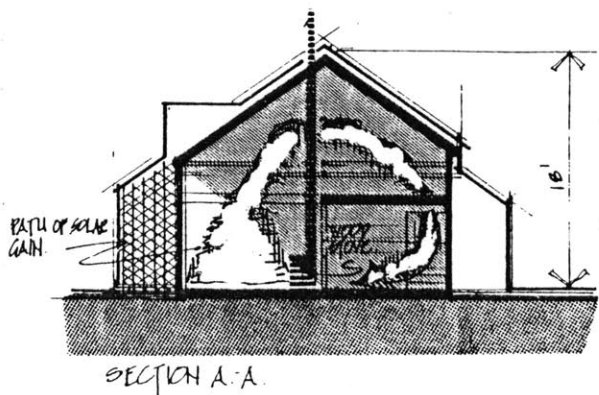


Fig. 32. Anticipated convection flow due to solar gain.

Analysis of Building Design. The building component parameters are given in Table 5. The  $h_c$  A values are:

$$h_c' A = 15.0 \text{ W/}^\circ\text{C} = 92.5 \text{ BTU/hr}^\circ\text{F} \quad (14)$$

$$h_c A = 28.9 \text{ W/}^\circ\text{C} = 177.0 \text{ BTU/hr}^\circ\text{F} \quad (14)$$

$$P_f = \frac{h_c' A}{h_c A} = \frac{92.5}{177.7} = 0.52 \quad (10)$$

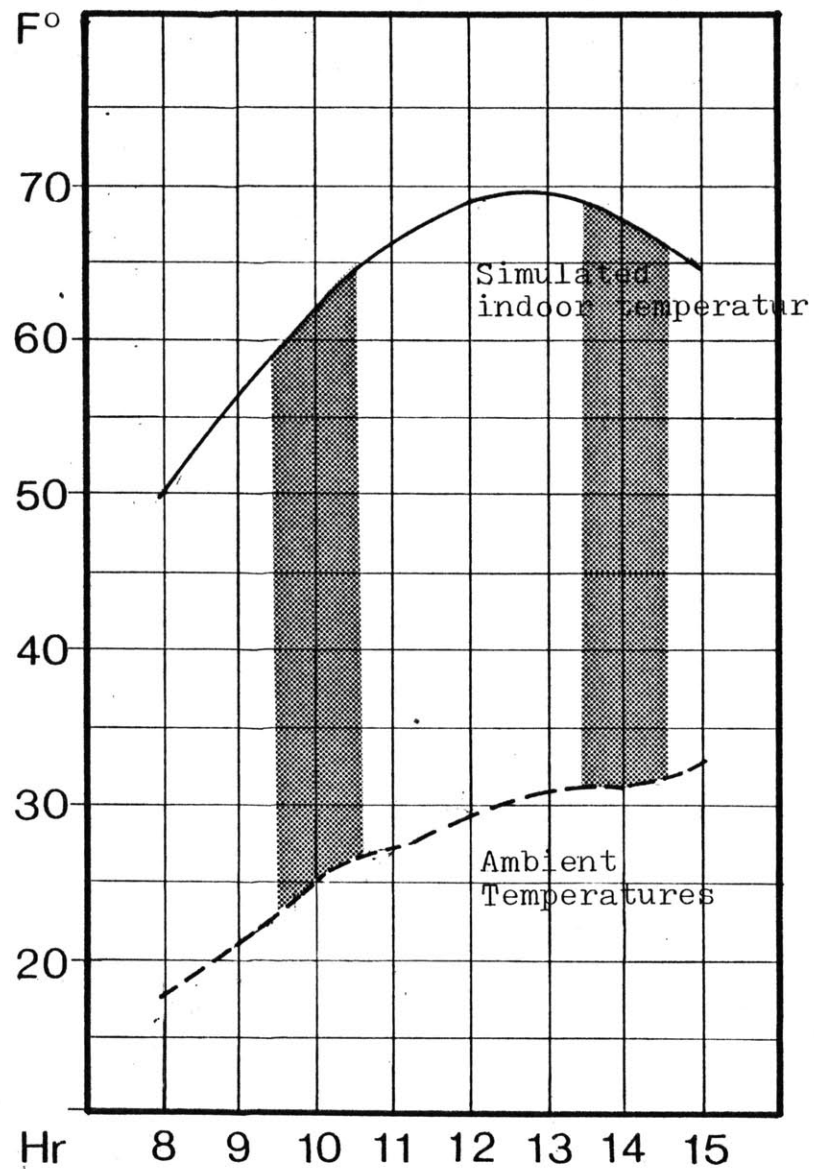
The designed dwelling is located in Central Quebec at latitude  $46^\circ\text{N}$ , longitude  $74^\circ\text{W}$ . The solar gain simulation is performed on a Texas Instrument 59 calculator for March 21 (equinox), clear day insolation. The room temperatures are shown in Fig. 33. Shown in Fig. 31b and Fig. 31d are the penetration of solar gain into the room, and the area of the floor experiencing solar gain through most of the day. The difference in average temperature of the inside of the dwelling and the ambient temperature,  $(T_r^* - T_a)$ , was  $20^\circ\text{C}$  or  $36.6^\circ\text{F}$ .

$$I_v = 2772.6 \text{ W} = 9467.0 \text{ BTU/hr}$$

$$I_{\text{CONV}} = 1904.8 \text{ W} = 6503.8 \text{ BTU/hr}$$

Model Design. As the spaces in the design are fairly complex and the passageway for the hypothesized convective flow is narrow

Fig. 33. Room temperatures as simulated by a Texas Instruments 59 Calculator for March 21st, clear day insolation. The shaded areas indicate times when the average temperature difference  $(T_r^* - T_a)_{avg}$  occurs. The steady state model would model convective flows during these times.





(See Figs. 31, p. 92), a fairly low  $D_f$  of 4 and a geometric scale of 1/9 are used. The material chosen for the model is polyurethane ( $k = .02 \text{ W/M}^\circ\text{C}$ ). The total surface area of the model is ca.  $3.3 \text{ M}^2$  (or  $35 \text{ ft}^2$ ). With a  $D_f = 4$ , the material thicknesses ( $t_m$ ) are calculated as follows:

$$\begin{aligned} \text{wall thickness} &= \frac{k_{mi}}{h_c D_f L^{1/2}} \\ &= \frac{0.14 \times 3}{0.047 \times 4} = 5.8 \text{ cm.} = 2.3 \text{ in.} \\ \\ \text{ceiling and} &= \frac{0.14 \times 3}{0.034 \times 1.3} = 8 \text{ cm.} = 3.15 \text{ in.} \\ \text{floor thick-} & \\ \text{ness} & \end{aligned}$$

The unit thermal window conductance is:

$$\begin{aligned} h_{mw} &= h_{fsw} D_f L^{1/2} \\ &= \frac{0.25 \times 4}{3} \\ &= 1.89 \text{ W/M}^2\text{ }^\circ\text{C} \text{ (or } 0.2 \text{ BTU/hrft}^2\text{ }^\circ\text{F)} \end{aligned}$$

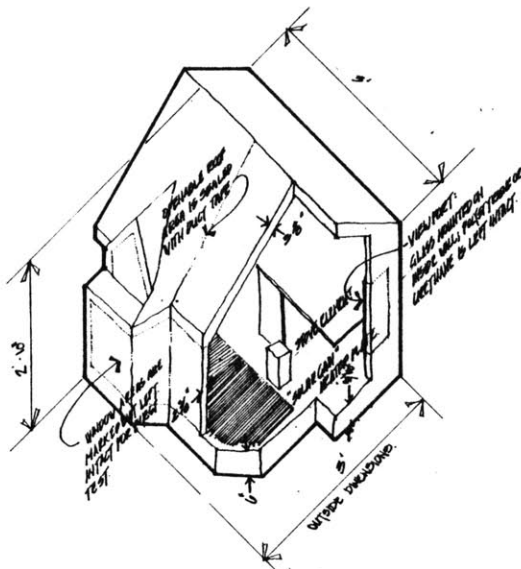


Fig. 34. Isometric of first phase in sketch design modeling, with polyurethane in all window areas.

From interpolation of Fig. 28, p. 82, a design incorporating 3 panes of plexiglass with 1.2 cm. separations should provide a reasonable close model proportionality factor.

Building Model. The heater plate simulating the solar gain is constructed of thin gauge aluminum. Its shape and size is geometrically similar to the outline created by the solar gain at noon (Fig. 31b, p. 92).

The building components are assembled with window areas marked, but not cut out, as shown in Fig. 34. The roof is left unsealed for access to the interior of the model, but is sealed with duct tape during tests. The joints are sealed with silicone, then the power is applied to the model heater.

$$W_m = \dot{Q}_m = \dot{Q}_{fs} D_f L^{5/2} \quad (35)$$

$$\begin{aligned} W_m &= 1905(4)(0.004) \\ &= 31.3 \text{ watts (or 106.9 BTU/hr)} \end{aligned}$$

Testing the Model. The model takes about 2 hours to reach steady state due to the specific heat of the walls. The ambient air temperature must be kept constant during this time. The  $P_{fm}'$  and  $D_f'$  are derived by comparison of the model windowless and window heat loss

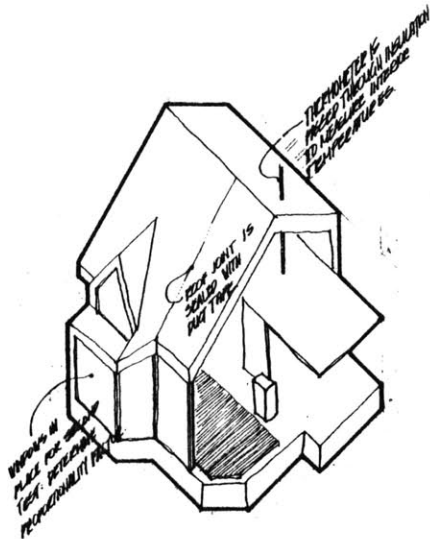


Fig. 35. The second phase of modelling occurs with the insertion of the windows and the determination of  $P_f'$  and  $D_f'$ .

tests. Fig. 35 illustrates the addition of windows to the model, and the final visualization tests are shown in Fig. 36. The simplified modelling technique is expected to indicate the convection flows of the design. According to Fig. 25, p. 68, with a  $D_f$  of 4, a  $T_f$  of 2 is interpolated. With this  $T_f$ , an approximation of the temperature ranges present in design may be interpreted using Eq. (12).

The Cost of the Model. The cost of the model here is the first-time cost for modelling the example sketch design, Many of the items are reusable, thus bringing down subsequent costs. The cost list is as follows:

Model Building Skin

Silicone sealant	-		= \$3.20
Polyurethane	- 83.2 B.F.	at 0.33/B.F.	= \$27.50
Plexiglass, 1/16 in.	- 11.0 ft <sup>2</sup>	at 0.53/ft <sup>2</sup>	= \$6.20

Heater

Aluminum sheet	2.4 ft <sup>2</sup>	at 0.34/ft <sup>2</sup>	= \$0.82
Resistance wire	154.0 ft	at 0.02/ft	= \$3.00
Power source			= \$20.00

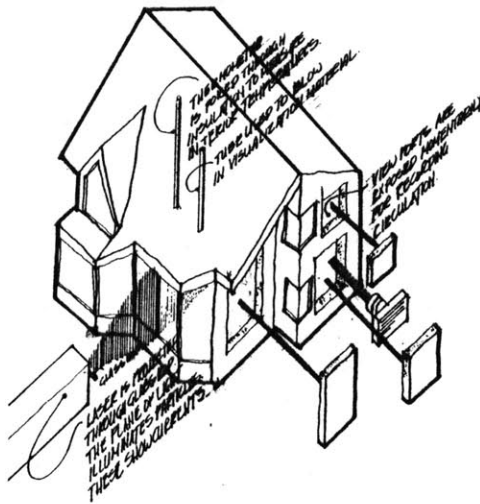


Fig. 36. Final phase of modelling occurs with flow visualization and measurement of temperature distributions.

#### Instrumentation

Multimeter	\$8.50
Thermometer	8.00
<u>Light and Baffles</u>	<u>4.00</u>
	\$81.22

#### Rigorous Instrumentation

Laser	\$180.00
Thermistors (10 @\$14/each)	140.00
Multiplexer and A/D Converter	200.00
Power supplies (3 @\$20/each)	60.00
Recorder	<u>30.00</u>
Total	\$691.22

Interpretation and Design Modification. If the sketch design does not behave as hypothesized, but rather develops air stratification instead of convection within the space (Fig. 37), it should be modified to increase the convective flow. For instance, a larger stairwell would increase the downflow area. "Hot spots" which have a lower specific heat than the surrounding thermal storage slab would increase the plume effect at the floor (Fig. 38). These area could be visually differentiated to become architectural events rather than mundane considerations of heat flow.

The model is useful in encouraging the designer's active participation and imagination while designing with natural convection.

Fig. 37. A hypothetical result from modelling might be stratification of air, (as opposed to convective flows). Design remedies would include enlargement of the staircase area.

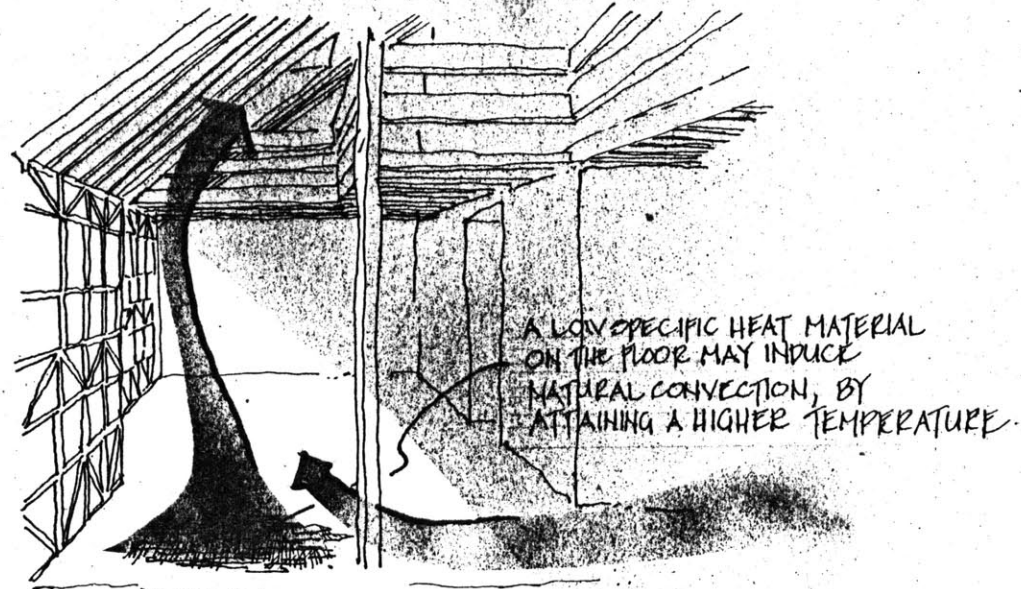
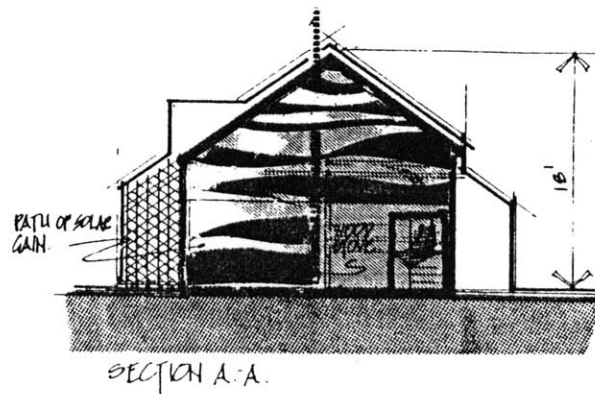


Fig. 38. "Hot spots" could be used to induce natural convection and heat distribution.

## Conclusion

The information developed in this thesis is only a starting point in the discovery of the subtle natural convection flow in buildings. The simple modelling technique developed was based on non-rigorous scaling laws, but provided good similitudes to full scale flows in a range of models tested.

It is expected that in building designs where conduction through the building skin is the primary heat loss method, and where thermal storage capacity of the building skin is fairly low, the simple modelling technique will indicate major natural convection flows and temperature distributions of the full scale building. The technique is best suited to designs where natural convection and thermal zoning of use spaces is an issue. In this context, the model may be useful for confirming hypotheses, or in finding solutions to problems of air flow. Both solar gain and point sources may be modelled in a steady state equivalent model.

However, as the experiments in this thesis were performed in a small space, with no infiltration and under thermal steady state conditions, the simplified modelling technique must be further proven for its applicability to modelling real life dynamic situa-

tions. To this end, building convection models of existing well-insulated buildings, such as A.D. Bryan's Hood House in Vermont where convective heat distribution was a design intent, would prove useful. With greater use of this technique, it is hoped that a larger body of knowledge concerning convective generic flows will form and that guidelines may then be developed.

Simplified modelling can theoretically be extended to include infiltration and dynamic effects. It is in these areas that further development of the modelling procedure is required.

## Appendix I

### Model Descriptions and Test Results

Five models of the test cell were constructed, the inside spaces of each model being geometrically similar to the inside space of the test cell. Three of these were 1/6 scale and had departure factors ranging from 2 to 8.5 and two were 1/12 scale with departure factors of 2.1 and 15.9. A summary of the models tested, the energy inputs, the departure factors and experiments carried out is given in Table A1. For each test, the temperature difference between the ambient air ( $T_{am}$ ) and the average inside air temperature of the model ( $T_{im}$ ) were maintained similar to the test cell temperature difference. The models also maintained the similarity between heat loss ratios of the different components. As all experiments were performed at elevated temperatures, the radiation component of heat transfer from the heater plate is higher than would typically be expected.



TABLE A.1. MODEL EXPERIMENTS

MODEL SCALE	AREA HEATER	POWER INPUT	POWER INPUT		TEST TYPE			TEMP. FIELD TEST		
			AREA	$D_f$	Heat Loss	Velocity	Dynamic	A	B	C
1:6	.032 M <sup>2</sup>	11.8 watts	366.2 W/M <sup>2</sup>	2	X	X	X	X	X	X
1:6		22.8	696.9	3.8	X			X	X	
1:6		50.1	1565.6	8.6	X			X	X	
1:12	.0081	2.22	275.4	2.1	X			X	X	
1:12		16.6	2054	15.9	X			X	X	
1:1	1.16	520	448.3	1	X	X	X	X	X	X

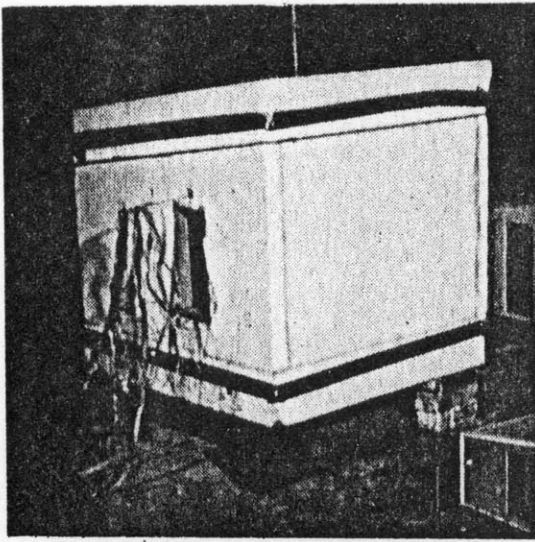


Fig. A-1. The (1/6·2) scale thermal model

#### THE (1/6·2) SCALE MODEL

This model (Fig. A-1) had 15.2 cm. polystyrene walls, 25.4 cm. ceiling and floors and was located 22 cm. from the floor. A triple glazed plexiglass window with 2.5 cm. spacing formed the window. A plexiglass slider, loaded with thermistors, sampled vertical air temperature distribution.

Heat Loss Test. The polystyrene conductivity was found to be higher than the prescribed value. ( $k_{\text{experimental}} = 0.042$ ;  $k_{\text{prescribed}} = 0.036 \text{ W/M}^\circ\text{C}$ ). The elevated temperatures are believed to be the source of variance. The heat loss of the model without the window was  $0.5 \text{ W}/^\circ\text{C}$  and with the window in place, the heat loss was  $0.58 \text{ W}/^\circ\text{C}$ , or 16% greater than without the window.

Velocity Test. The hot wire anemometer, due to its size, was used only to measure horizontal flow along the floor of the model. Results indicated a considerably steadier flow than in the full scale counterpart, even though it was occurring below the accurate threshold of the instrument (1 meter/min., 3.3 ft/min.).

Temperature Measurements. The (1/6·2) model had the best similitudes of temperature fields when compared with test cell fields. The description of thermal fields for this model is

found alongside the description of temperature fields in the full scale test cell (Chapter II, p. 46).

#### THE (1/6·3.8) SCALE MODEL

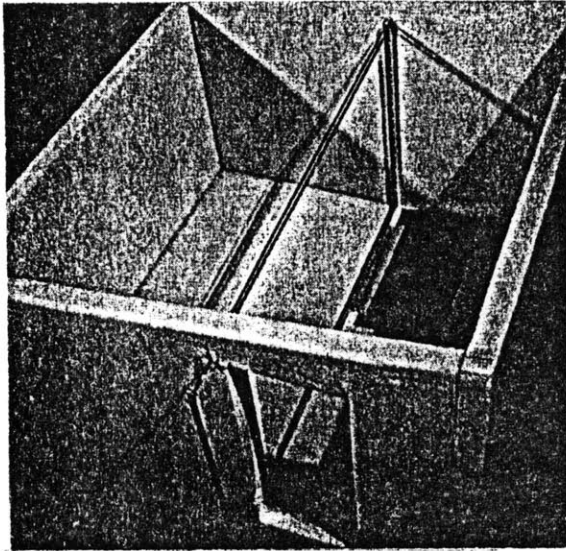


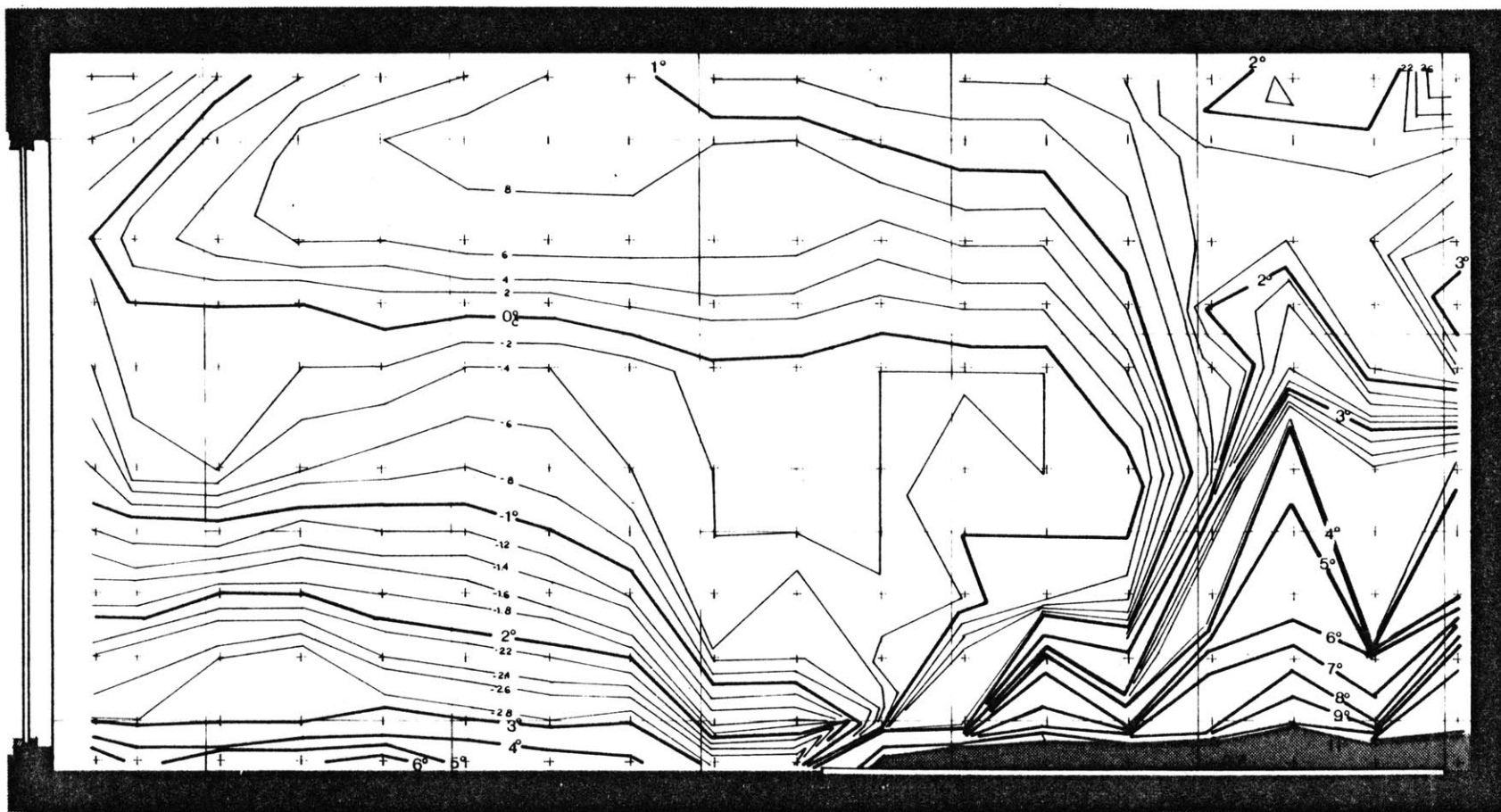
Fig. A-2. The (1/6·3.8) scale model; the model heater is located on the floor, and the probe boom is seen at the side of the heater.

The model (Fig. A-2) was located 9 in. from the floor with 3 cm. polyurethane wall and 4 cm. ceiling forming the spatial enclosure. A single .16 cm. plexiglass window formed the system's heat sink. An aluminum slider with thermistor spacing geometrically similar to the test cell provided vertical temperature distribution readings.

Heat Loss Test. The polyurethane conductivity was determined to be the prescribed value (0.02 W/M°C). The model heat loss with the window in place (1.13 W/C°) was 14% greater than the loss without the window, (0.97 W/C°).

Temperature Field of Configuration A. With a  $D_f$  of 3.8, the model's thermal field (Fig. A-3a) indicates minor differences with the test cell temperature field. Two major flows were discerned:

- 1) a warm air flow, generated at the heater plate, ascended slightly away from the rear wall and deflected towards the window at the ceiling.
- 2) a cool air flow formed at the window and flowed across the floor. Some differences in the detail of the flows were observed.



**A** scale  $1/6 \cdot 3.8$

Fig. A-3a. Temperature field of a 1/6 scale model with  $D_f = 3.8$  in Configuration A.



Fig. A-3b. (1/6·3.8) warm air flows.

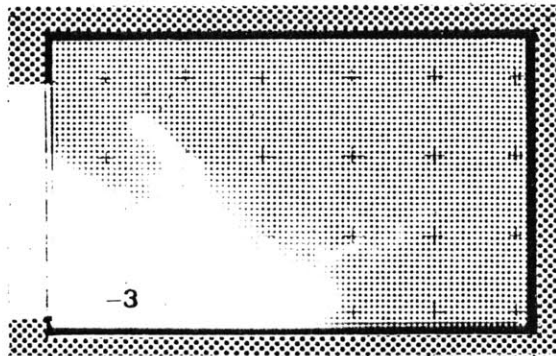


Fig. A-3c. (1/6·3.8) cool air flows.

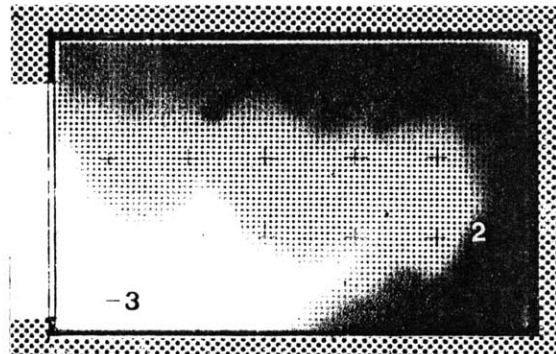


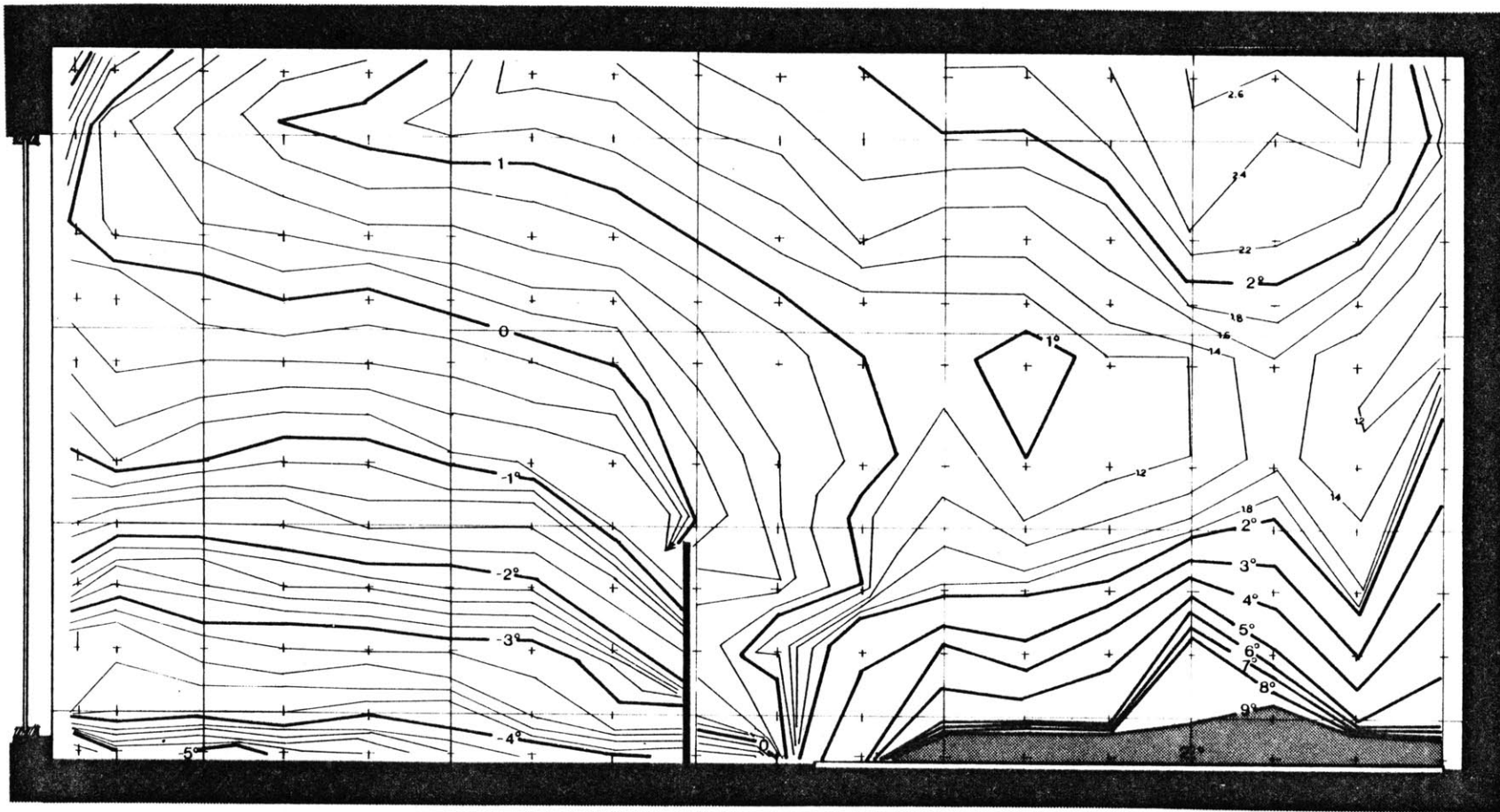
Fig. A-3d. (1/6·3.8) generic air flows.

Differences with the test cell warm air flow (Fig. A-3b) occurred with the slight separation of the plume from the rear wall, and the formation of a small vortex at the ceiling. Although generically similar, the ceiling flow was thicker. On the other hand, the cool air flows (Fig. A-3c) were very similar to those in the test cell, the overall relative temperature distribution and the generic flows (Fig. A-3d) were similar to their test cell counterparts. The temperature range was 11.9°C.

Temperature Field of Configuration B. Generic similitude in temperature fields was established between the model (Fig. A-4a) and the test cell. Two major flows were identified:

- 1) a warm air flow which ascended at the front and middle of the heater, then split at the ceiling into a flow toward the window and a smaller flow toward the rear of the room, and,
- 2) a cool air flow which formed at the window and flowed over and around the baffle. The generic flow patterns (Fig. A-4d) were similar to those found in the test cell, but flow details differed.

The differences found in the warm air flow (Fig. A-4b) were



**B** scale  $1/6 \cdot 3.8$

Fig. A-4a. Temperature field of (1/6·3.8) model with baffle.

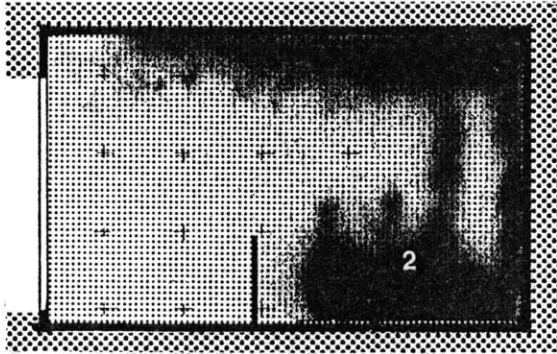


Fig. A-4b. (1/6·3.8) warm air flows with baffles.

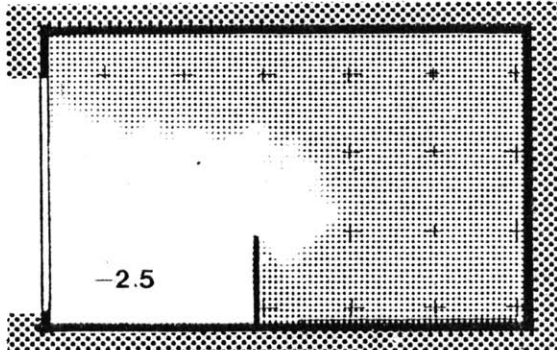


Fig. A-4c. (1/6·3.8) cool air flows with baffles.

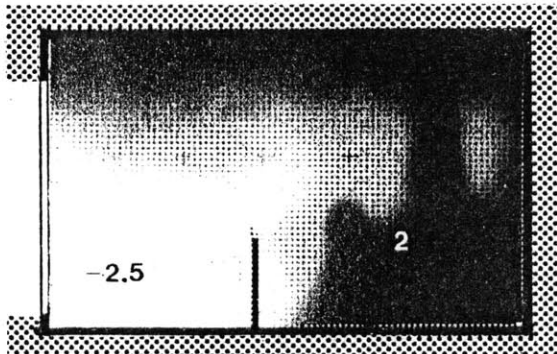


Fig. A-4d (1/6·3.8) generic air flows with baffles

- 1) formation of a conduction layer at the heater,
- 2) a shifting of the main plume towards the rear of the room, and
- 3) a thicker hot air layer at the ceiling. Differences in the cool air flow, (Fig. A-4c) occurred in the entrainment of the floor flow at the side of the heater rather than over it, as was the case in the test cell. The temperature range in the model was 9.8°C.



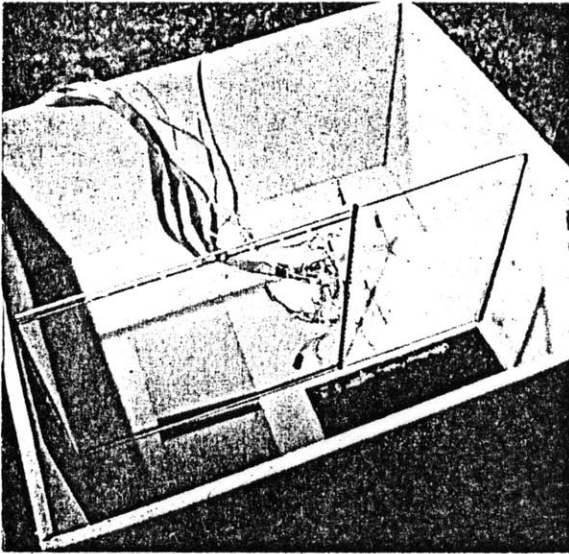


Fig. A-5. (1/6·8.5) scale thermal model. Baffle is shown in a down position with probe boom and thermistors located over the heater plate.

#### THE (1/6·8.5) SCALE MODEL

The model (Fig. A-5) was located 22.9 cm. from the floor and was built with 1.3 cm. polyurethane walls with 2 cm. polyurethane ceilings and floors. Black aluminum, 1.25x the size of the window opening, and crimped to fit into it, was used in order to establish the correct  $P_{fm}$  ratio.

Heat Loss Transfer. The windowless heat loss experiment indicated a polyurethane conductivity of .025 W/M°C. The deviation in the value may have been caused by long wave radiation transfer through the thin insulation. The heat loss rate was determined as 2.11 W/C° without the window. Addition of the window increased the heat loss by 16% to 2.48 W/C°.

Temperature Field of Configuration A. At this scale, marked differences occurred between the temperature fields of the model (Fig. A-6a) and the test cell. Two major flows were discerned in the model:

- 1) a warm air flow ascended at the rear of the wall and deflected toward the window at the ceiling in what seemed to be a split flow (Fig. A-6b).



**A** scale 1/6-8.5

Fig. A-6a. Temperature field of (1/6-8.5) model

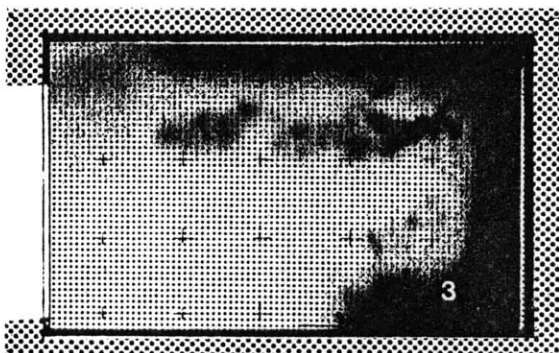


Fig. A-6b. (1/6·8.5) warm air flows, Configuration A.

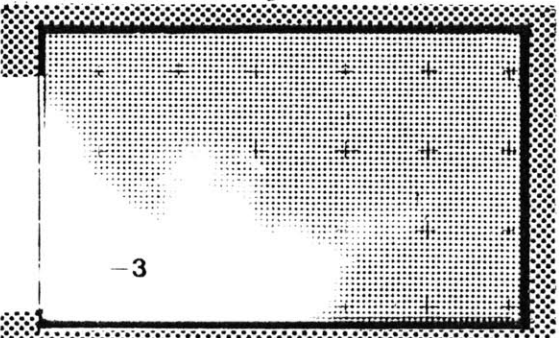


Fig. A-6c. (1/6·8.5) cool air flows.

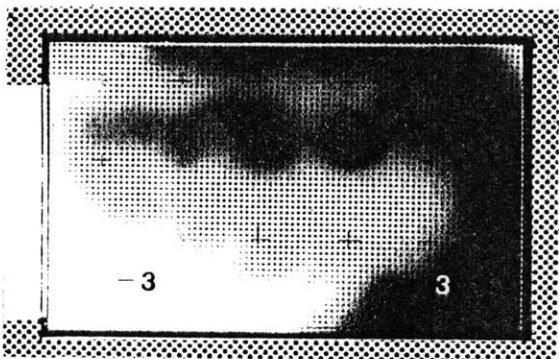


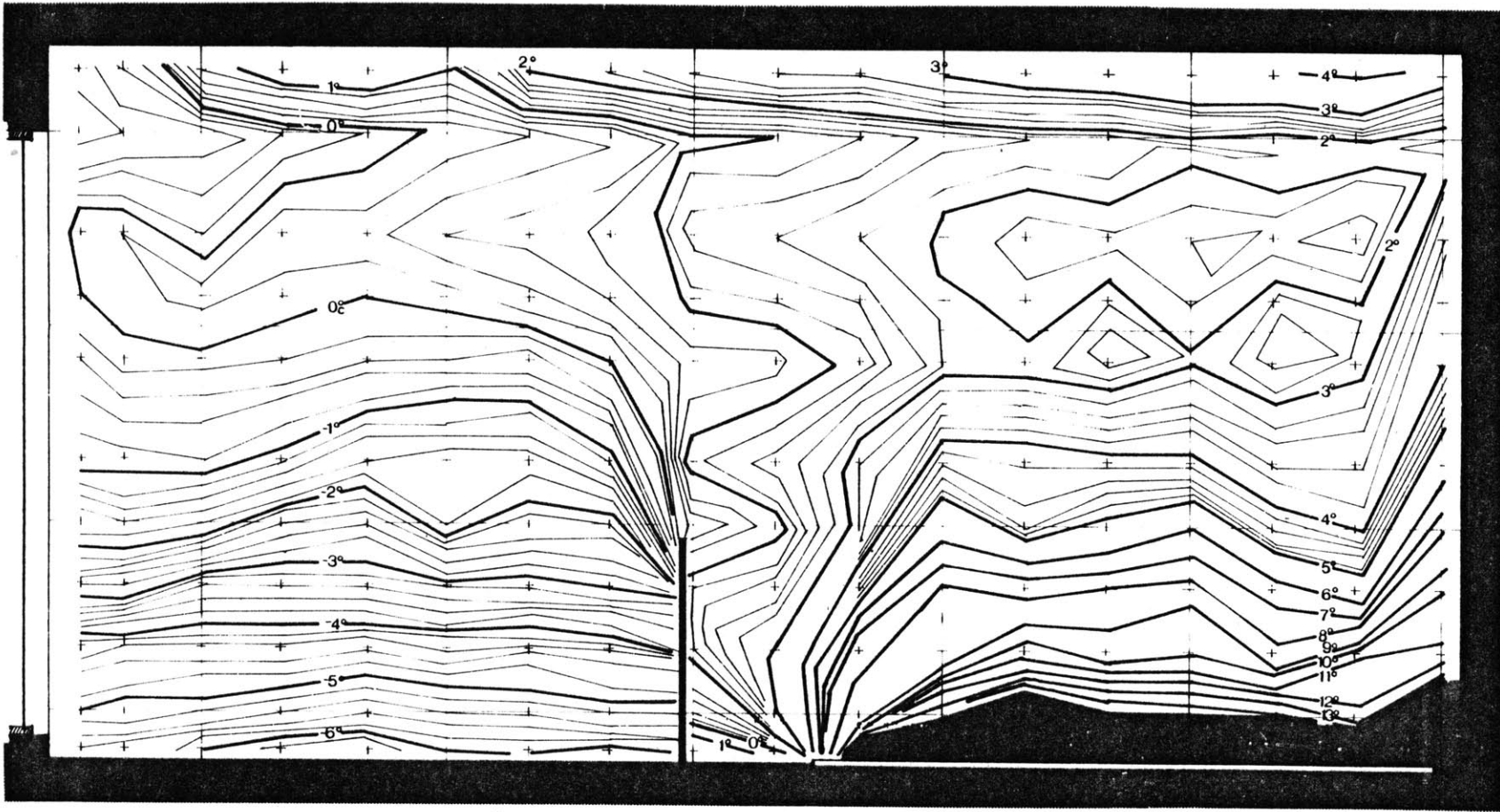
Fig. A-6d. (1/6·8.5) generic air flows.

- 2) a cool air flow generated at the window and flowed towards the heater plate (Fig. A-6c).

Although some generic similarities to test cell flows could be discerned, large differences were detected in some flows. A difference in the warm air flow occurred at the ceiling, where a split flow or possible cellular development occurred, as the plume mixed with the air of the smaller midroom area. On the other hand, the cool air flows, and even the plume were fairly similar to test cell flows. Temperature distributions correlated well but the generic flow (Fig. A-6d), specifically at the ceiling, was not similar to test cell flows. The temperature range was 14°C.

Temperature Field of Configuration B. The temperature field of the model (Fig. A-7a) was different from that of the test cell. Two major flows occurred:

- 1) a warm air flow (Fig. A-7b), generated at the heater, ascended along the rear wall and the front of the heater plate, developed a split cellular flow at the ceiling and dispersed above the window;



**B scale 1/6·8.5**

Fig. A-7a. Temperature field of (1/6·8.5) model.

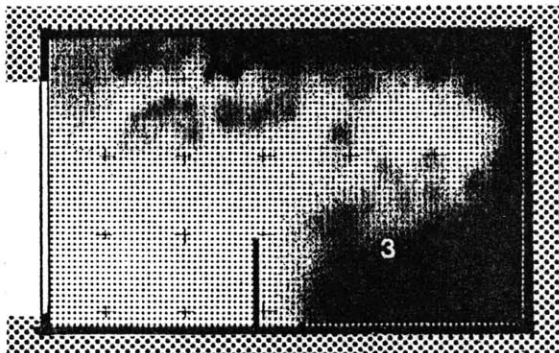


Fig. A-7b. (1/6·8.5) warm air flow, with baffle up.

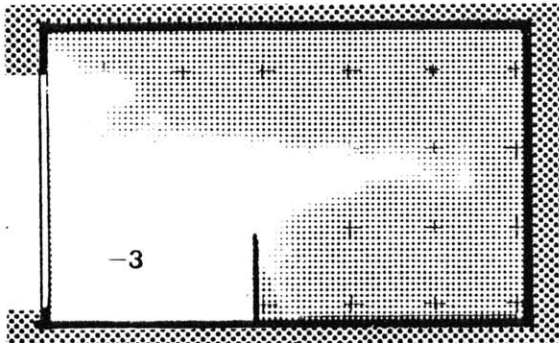


Fig. A-7c. (1/6·8.5) cool air flow.

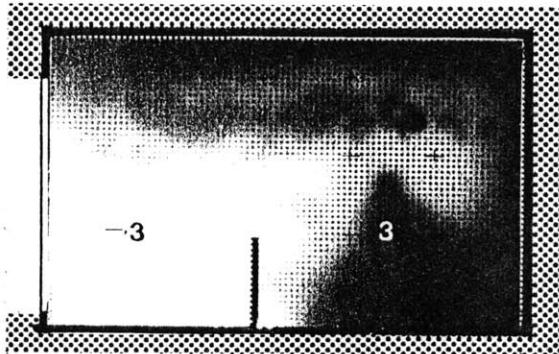


Fig. A-7d. (1/6·8.5) generic air flows.

- 2) a cool air flow (Fig. A-7c) formed at the window and flowed over the cool air pool and baffle until it was entrained in the warm air plume.

Although similarities to test cell flow existed in the model cool air movement, a difference was developed in the warm air flows. This difference was: the thermal rose along the rear wall and a vortex occurred which extended the full length of the model room, creating cellular flows in the midroom "isothermal area".

The generic flows (Fig. A-7d) cannot be considered similar, even though temperature distributions correlated fairly well. The temperature range in the model was 13°C.

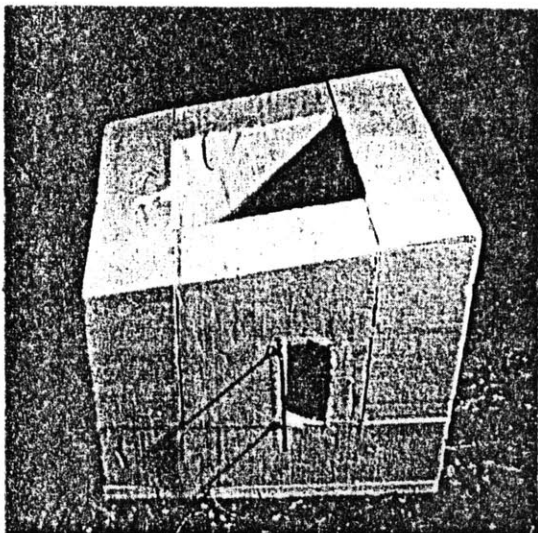


Fig. A-8. (1/12·2.1) scale model indicating thick walls of a small  $D_f$  value

#### THE (1/12·2.1) SCALE MODEL

The model (Fig. A-8) was located 10.2 cm. above the floor, and was built of 4 cm. polyurethane walls with 17.3 cm. ceiling and floor. The window was composed of 0.16 cm. thick plexiglass pieces silicone sealed to wood frames spaced 3.8 cm. from each other.

Heat Loss Test. The windowless heat loss test indicated a conductivity of 0.023 W/M°C. The thickness of the sample may be a reason for the higher than prescribed value. The window increased the heat loss by 14% (0.112 W/C°) over a simple polyurethane cube (0.097 W/C°).

Temperature Field of Configuration A. The temperature field of the model (Fig. A-9a) matched the full scale test cell fields fairly closely. Two major flows were discovered:

- 1) a warm air flow (Fig. A-9b) generated at the heater plate, formed a pronounced wave configuration over the heater, swept along the rear wall and deflected toward the ceiling and,



**A** scale  $1/12 \cdot 2.1$

Fig. A-9a. Temperature field of (1/12·2.1) model, Configuration A

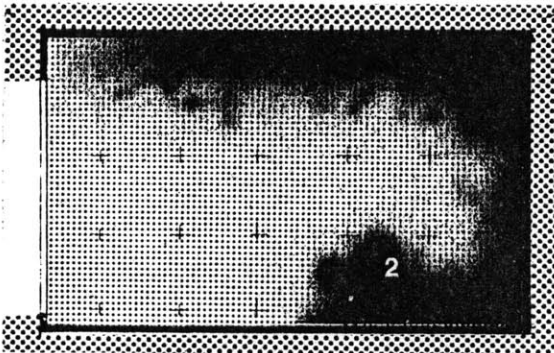


Fig. A-9b. (1/12·2.1)  
warm air flow, Configuration A

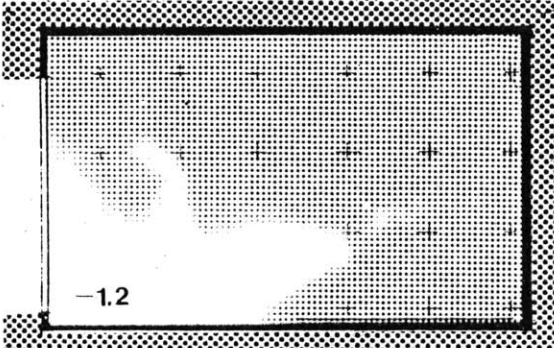


Fig. A-9c. (1/12·2.1) cool  
air flow,

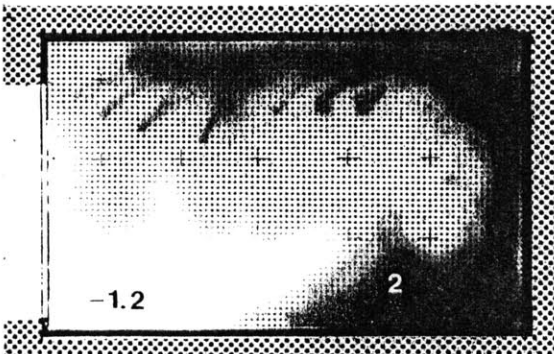


Fig. A-9d. (1/12·2.1) generic  
air flows.

- 2) a cool air flow (Fig. A-9c) which moved down the window and across the floor. Although the generic flows (Fig. A-9d) were similar to those of the test cell, differences in detail could be discerned.

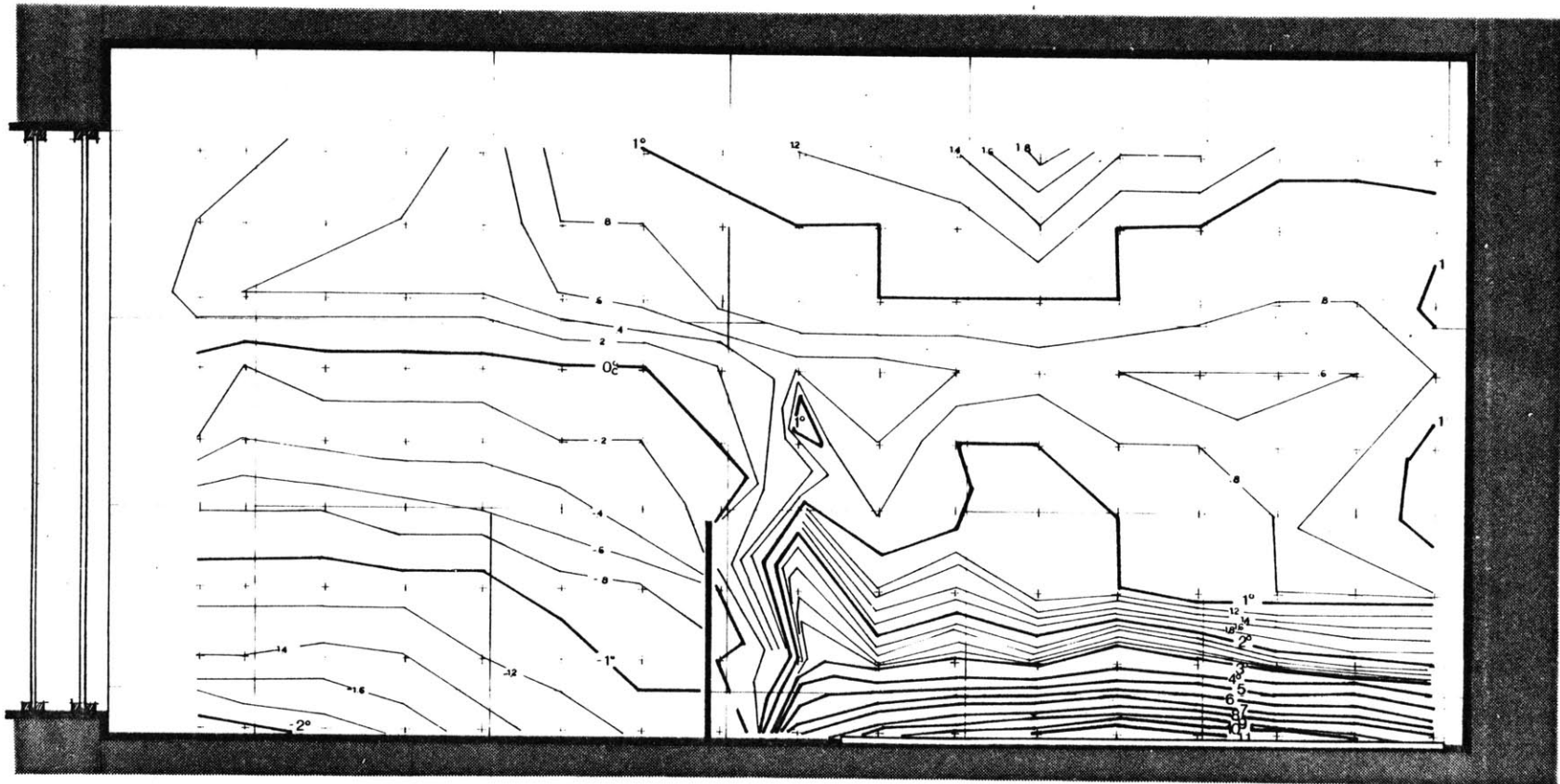
The differences between the warm air flows of the model and those of the test cell occurred at the heater plate where a pronounced wave configuration indicated greater diffusion at that point.

Differences between the model cool air flows and the test cell counterparts occurred at the floor flows where premature diffusion and mixing was interpreted, and a smaller temperature gradient was recorded. The temperature range in the model was 4.9°C.

The Temperature Field of Configuration B. The temperature field observed in the model (Fig. A-10a) was similar to that of the test cell. Two major flows may be identified:

- 1) a warm air flow (Fig. A-10b) generated at the heater that ascended toward the front of the heater plate, split at the ceiling into a flow toward the window and a flow toward the rear of the room, and





**B** scale 1/12·2.1

Fig. A-10a. Temperature field of (1/12·2.1) model, Configuration B.

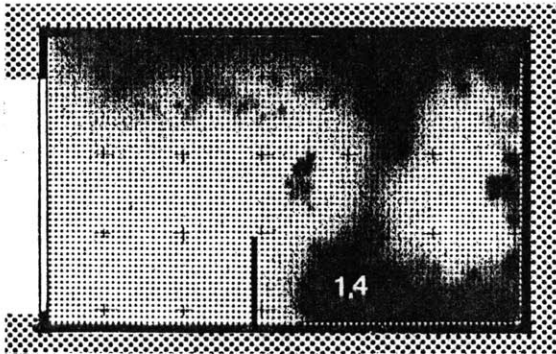


Fig. A-10b. (1/12-2.1)  
warm air flows in  
Configuration B.



Fig. A-10c. (1/12-2.1)  
cool air flows.

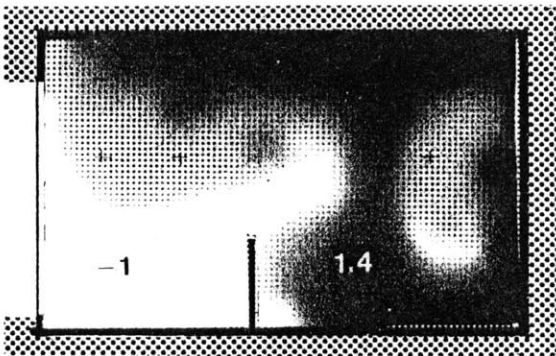


Fig. A-10d. (1/12-2.1)  
generic air flows.

2) a cool air flow (Fig. A-10c) which formed at the window and flowed over and around the baffle.

The generic flow patterns (Fig. A-10d) were similar, but the temperature distributions of the flows exhibited differences. The difference found in the warm air flow was a thicker ceiling flow with greater temperature stratification and the difference found in the cool air flow was a smaller temperature gradient in the pool area.

The temperature range in the model was 3.9°C.

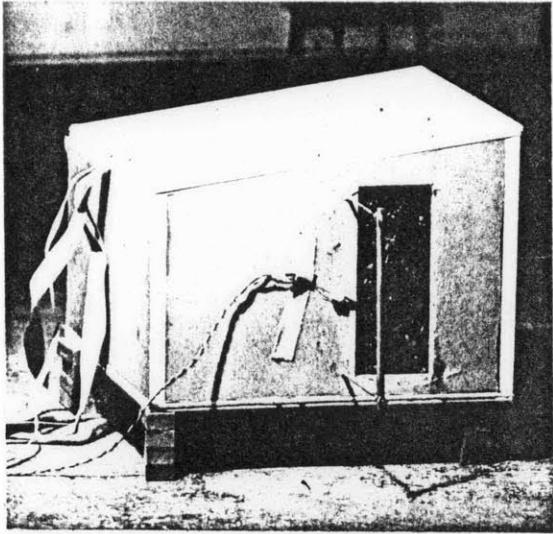


Fig. A-11. (1/12·15.9) model with crimped aluminum window and styrofoam core walls.

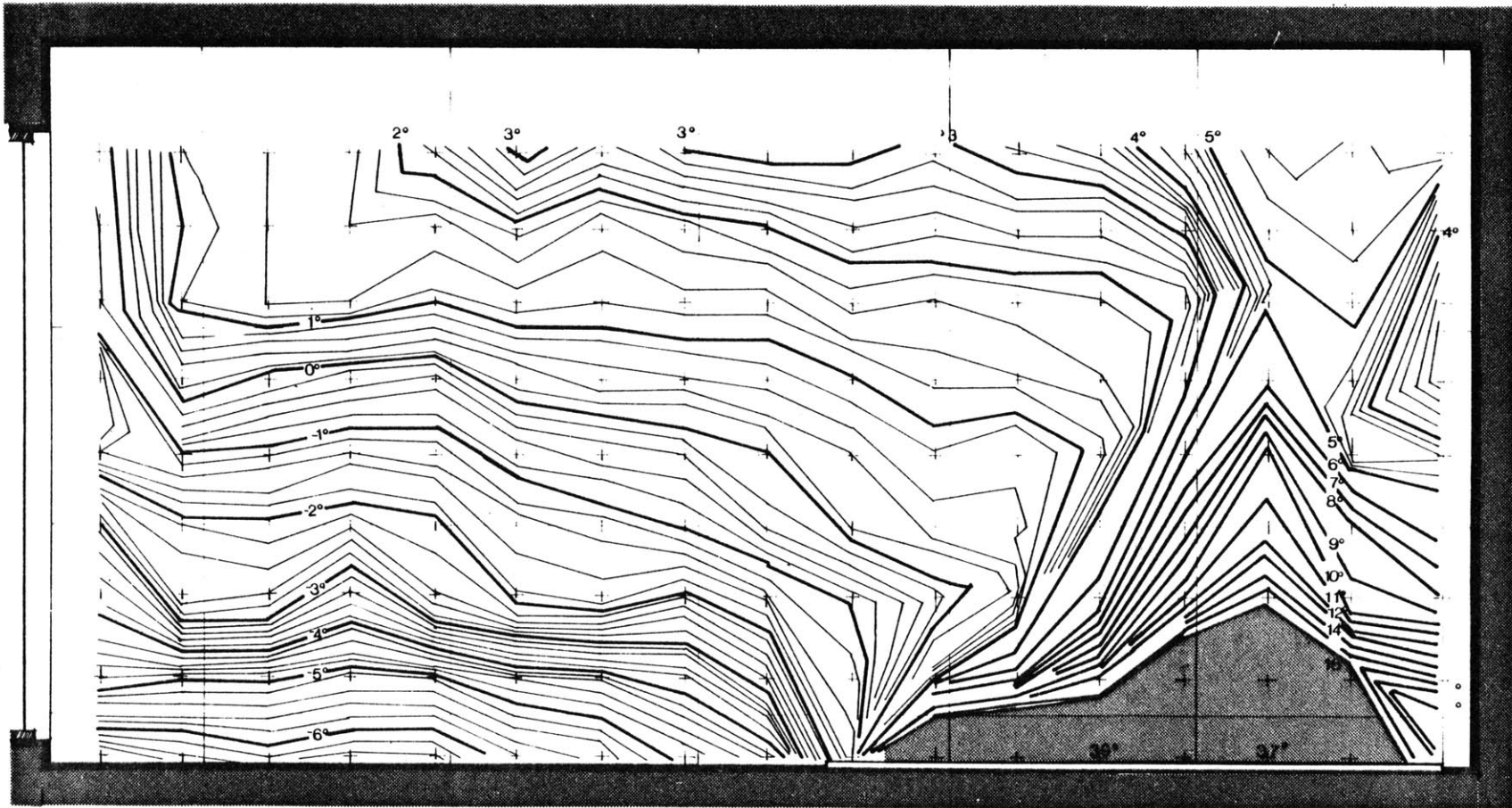
#### THE (1/12·15.9) SCALE MODEL

This scale model (Fig. A-11) bore the greatest resemblance to an architectural model. It was located 10 cm. above the floor, and the walls were constructed of 1.3 cm. styrofoam core board, with floors and ceiling built of 2 cm. foam core. Black aluminum foil of twice the area was crimped into the geometrically scaled window opening.

Heat Loss Test. Heat loss experiments indicated a conductivity of  $0.038 \text{ W/M}^\circ\text{C}$  for the styrofoam core board. This is in agreement with closed-cell styrofoam interpolated for the experimental temperatures (K proprietary =  $0.036 \text{ W/M}^\circ\text{C}$  at  $35^\circ\text{C}$ ). The model heat loss ( $0.85 \text{ W/C}^\circ$ ) with the window was 17% greater than the heat loss without, ( $0.7 \text{ W/C}^\circ$ ).

Temperature Fields of Configuration A. The temperature field of the model (Fig. A-12a) indicates some similarity to the full scale counterpart. Two flows can be discerned:

- 1) a warm air flow (Fig. A-12b) generated at the heater, ascended free from the rear wall, and deflected towards the window where it diffused.



**A** scale  $1/12 \cdot 15.9$

Fig. A-12a. Temperature field of (1/12·15.9) model, Configuration A.

2) a cool air flow (Fig. A-12c) formed at the window and flowed across the floor and over the heater. Although generic similarity to test cell flows was found in most model flows, differences occurred, particularly in warm air flows.

Differences in model warm air flows were:

- 1) the position of the plume was separated from the rear wall and formed a vortex in the rear upper corner upon being deflected at the ceiling.
- 2) the wave configuration had largely disappeared.
- 3) the ceiling flow was thicker. However, the generic flows

(Fig. A-12d) and specifically the cool air plume, were very similar to those occurring in the test cell. The temperature range in the model was 18°C.

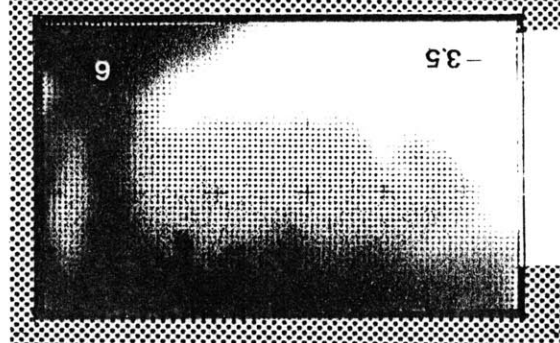
Temperature Field of Configuration B. The model temperature

field (Fig. A-13a) was different from the test cell field. Two major flows are described by the isotherms:

- 1) a warm air flow (Fig. A-13b) ascended at the baffles and split at the ceiling into a flow toward the window and a

generic air flows.

Fig. A-12d. (1/12-15.9)



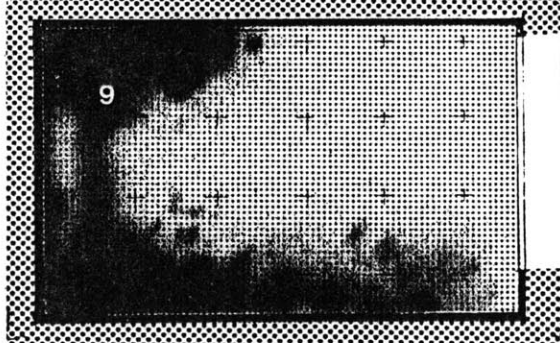
cool air flow.

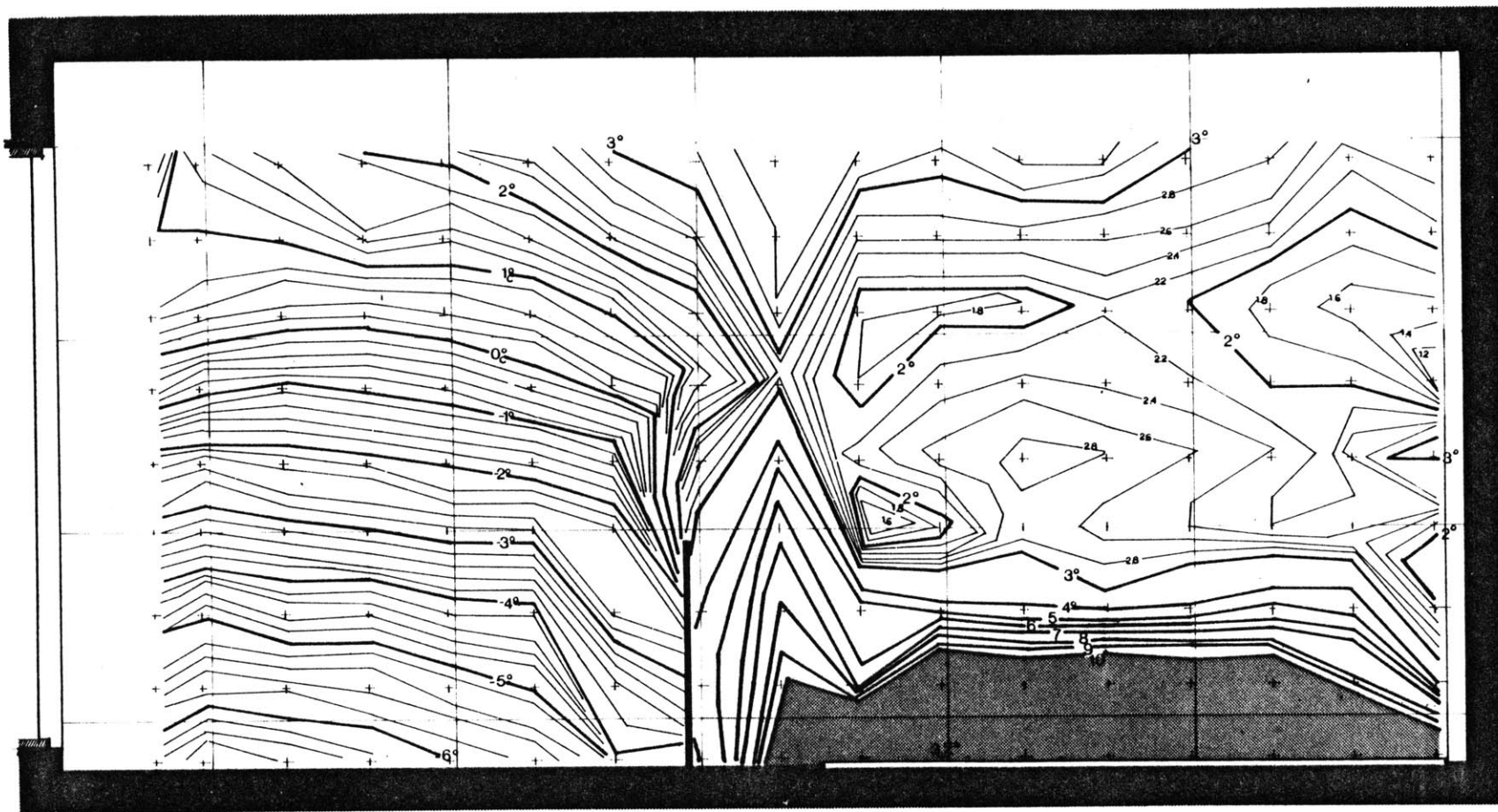
Fig. A-12c. (1/12-15.9)



warm air flow, Configuration A.

Fig. A-12b. (1/12-15.9)





**B** scale 1/12-15.9

Fig. A-13a. Temperature field of (1/12-5.9) model, Configuration B.

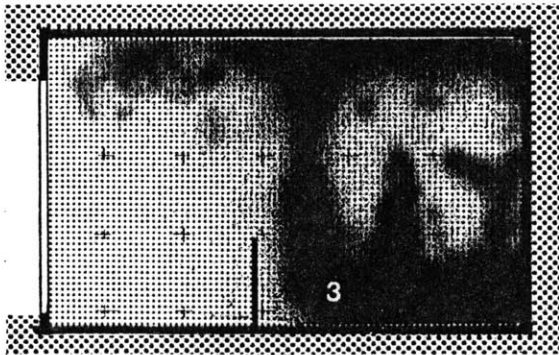


Fig. A-13b. (1/12-15.9)  
warm air flow, Configuration B



Fig. A-13c. (1/12-15.9)  
cool air flow

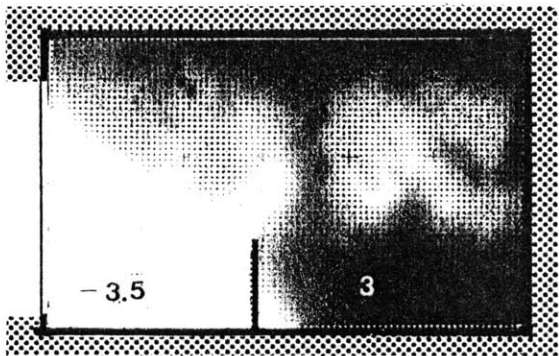


Fig. A-13d. (1/12-15.9)  
generic air flows.

- 2) vortex at the rear wall, and
- 2) a cool air flow (Fig. A-13c) formed at the window, flowed over and around the baffle, and was immediately entrained into the plume.

Although some generic similarities may be established with test cell flows, there is a fundamental difference in flow. The differences in air flows were:

- 1) the position of the plume rise at the baffle,
- 2) the immediate entrainment of cool air into the plume, and
- 3) the formation of a vortex at the window. The generic flows in this model (Fig. A-13d) are seen as deviating from the test cell flows. The temperature range in the model was  $13.6^{\circ}\text{C}$ .

A synopsis of model behaviors is given in Chapter II, Table 4.

## Appendix II

### Experiments and Instrumentation

#### The Ambient Environment

The measurements of test cell and model thermal behaviors were performed in an empty warehouse space. The floor to ceiling height was 3.5M (or 11 ft. 4 in.), while the temperature gradient was ca. 1-1.25°C (1.8-2.25°F). This gradient was minimized by mixing the air; the air velocity around the test cell and models being kept below 5 M/min. During tests, the temperature of the warehouse space was kept within  $\pm 1^\circ\text{C}$  over 24 hr. steady state periods. This fluctuation was reduced to  $\pm 0.5^\circ\text{C}$  during measurement periods. The large floor and ceiling masses of the warehouse had a thermostatic effect on ambient temperature deviations. Fig. A-14 shows the test cell and models in the warehouse space.

#### Temperature Sampling

The air temperatures and the temperature of various surfaces were measured by YSI 44203 series thermistors (Fig. A-15). These thermistors were used in lieu of thermocouples due to the ease with which they could be transferred from one model to the next, without changing or tangling large runs of wiring. Their accuracy is well within the range achieved by thermocouples. Further, the thermis-



Fig. A-14. Test cell, in upper photo, and models, in lower photo, were located in a warehouse space, with temperatures controlled by opening windows.

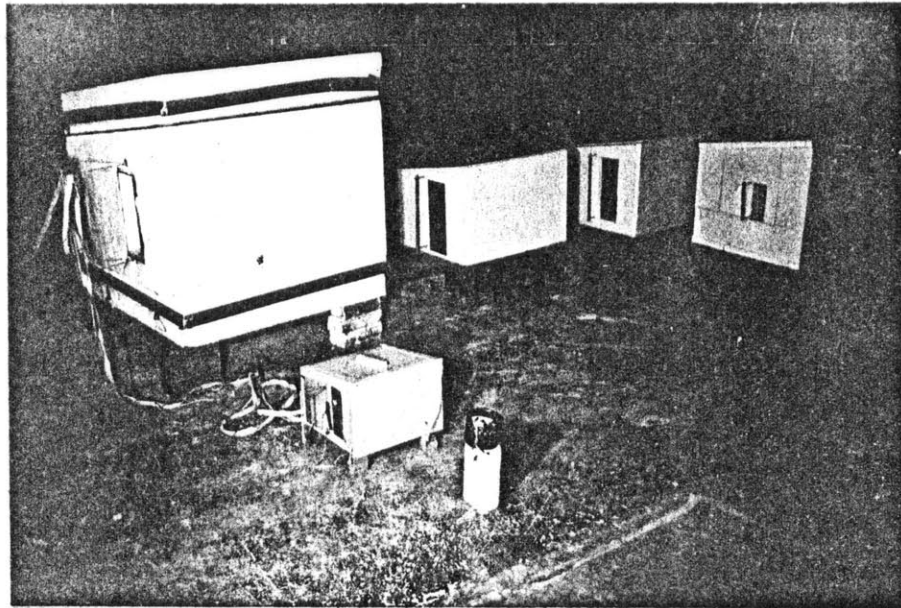
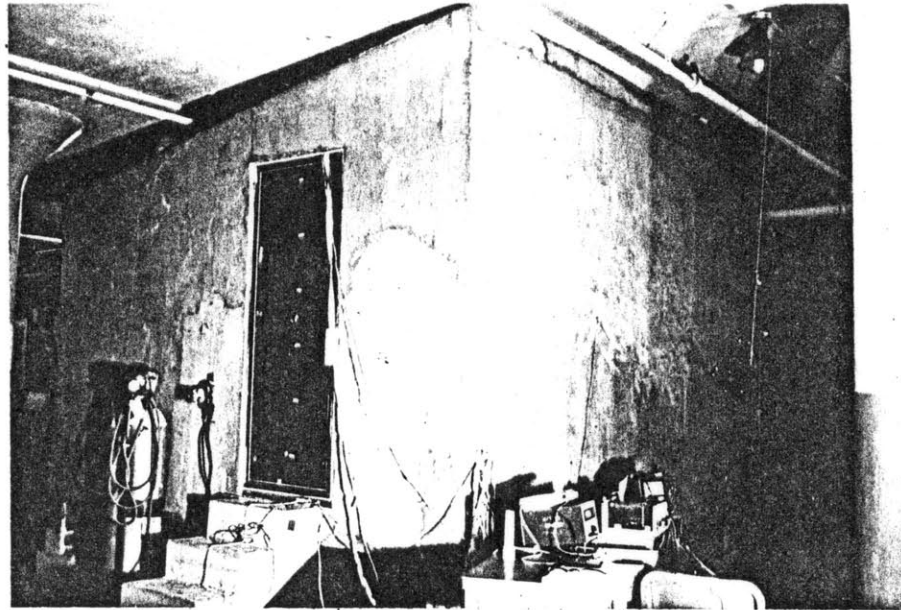


Fig. A-15. YSI 44203  
Thermistor specifications

YSI THERMILINEAR<sup>®</sup> COMPONENT

YSI 44203

RANGE -30° to +50°C

This Thermilinear Thermistor Network is a composite device consisting of resistors and precise thermistors which produce an output voltage linear with temperature, see Fig. 1, or a linear resistance with temperature, see Fig. 2. The precise thermistors can either be the YSI #44018 (as included in the #44203) or they can be a YSI 700 Series Probe since they are electrically identical.

Equations which describe the behavior of the device are: (Refer to Fig. 1)

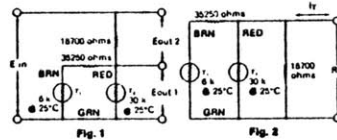
$$E_{out} = (-0.0067966 \text{ Ein})T + 0.65107 \text{ Ein}$$

$$E_{out} = (+0.0067966 \text{ Ein})T + 0.34893 \text{ Ein}$$

$$R_T = (-127.096)T + 12175$$

$$T = ^\circ\text{C}$$

	Voltage Mode	Resistance Mode
Thermistor Absolute Accuracy and Interchangeability:	± 0.15°C	± 0.15°C
Linearity Deviation:	± 0.16°C	± 20.3 ohms
*Ein Max	3 Volts	
*I <sub>T</sub> Max		475 $\mu\text{A}$
Sensitivity:	0.0067966 Ein/°C	127.096 ohms/°C
Load Resistance:	10 Megohm min.	
Time Constant:	The time required for the thermistor to indicate 63% of a new impressed temperature, in well stirred oil, 1 sec.; in free still air, 10 sec.	
Storage Temperature:	-80°C to +120°C (-112° to +250°F)	

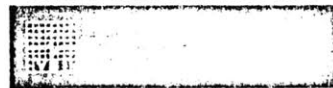


\*Ein Max. I<sub>T</sub> Definition:  
Ein Max. I<sub>T</sub> Max values have been assigned to control the thermistor self-heating errors so that they do not enrage the component error band, i.e., the sum of the linearity deviation plus the probe tolerances.  
Ein Max. I<sub>T</sub> Max values are assigned using a thermistor dissipation constant of 8mW/°C in stirred oil. If better heat-sink methods are used or if an enlargement of the error band is acceptable, Ein Max. I<sub>T</sub> Max values may be exceeded without damage to the thermistor probe.

WARNING

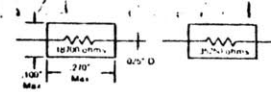
Use heat sinks when soldering or welding to thermistor leads.

U. S. Patent -3316765, Canadian Patent #742790

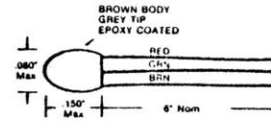


11EM 002480 P/N 844523 C Printed in U.S.A. AB

YSI RESISTOR COMPOSITE 44303



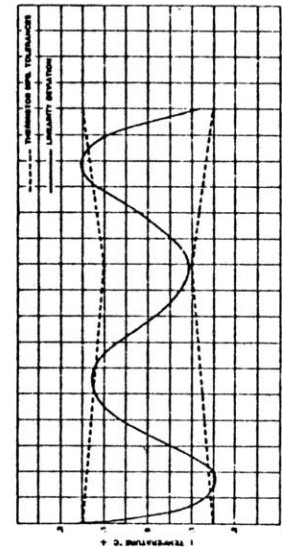
YSI THERMISTOR COMPOSITE 44018



R<sub>T</sub> = (-127.096)T + 12175  
T = ^\circ\text{C}

Temperature (°C)	Resistance (ohms)
-30	10066
-25	15396
-20	14736
-15	13626
-10	12796
-5	12136
0	11536
5	10936
10	10336
15	9736
20	9136
25	8536
30	7936
35	7336
40	6736
45	6136
50	5536

The values tabulated above are computed using nominal thermistor values as called for in the linear equation. The deviations computed for the Linearly Deviation Curve.



The maximum error of this probe is the magnitude, such as the thermistor non-linearity, which the linearly deviation curve is a worst case deviation. Since the linearly deviation is a worst case deviation, it may be subtracted from the error statement by combining the linearity deviation curve at the temperature in question, and making the appropriate adjustment.

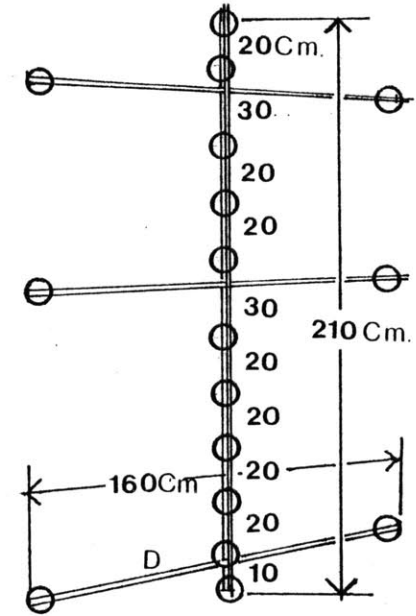
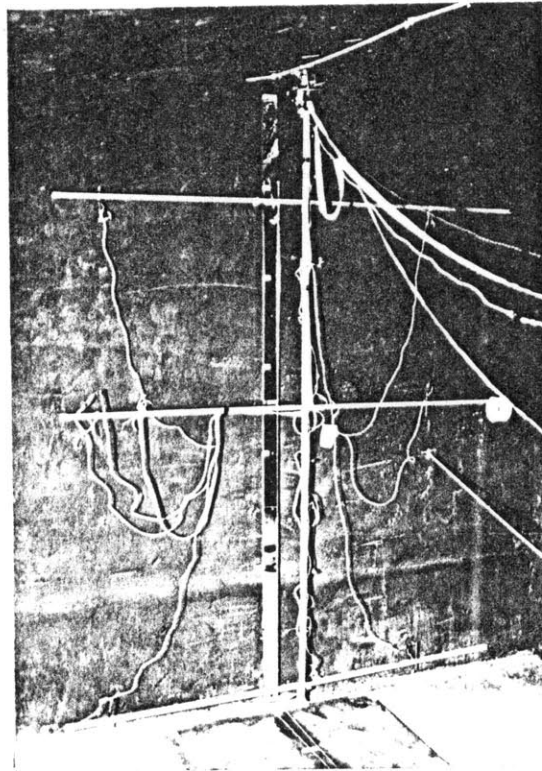


Fig. A-16. Thermistor locations on the boom (at left) are indicated above.

tors were bathed in a 0°C icewater bath to determine the accuracy of the entire sensing and decoding system.

The thermistors were located on a vertical boom at heights shown in Fig. A-16. In the test cell a motorized carriage moving along a ceiling rail carried the temperature boom across the space. In the models, aluminum booms moved along slider mechanisms built into the models. The thermistor beads were isolated from the

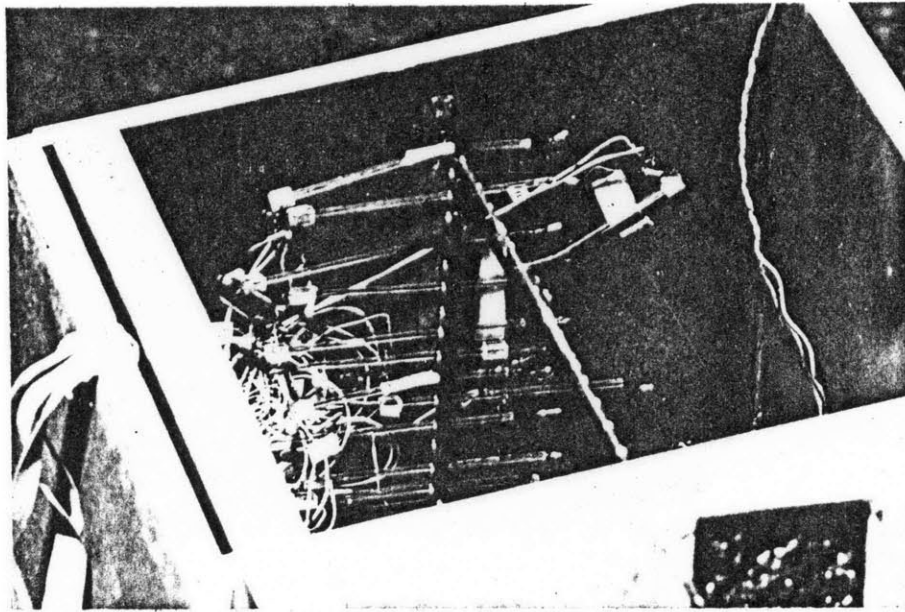


Fig. A-17. Thermistor arrangement on boom in (1/12.9) model.

boom by a glass tube extension. Aluminum foil was crimped around the head to minimize radiation transfer. The thermistors received only a ground and a signal connection; and the ground was pinned to a common ground on the boom. Fig. A-17 indicates thermistors on a model boom.

Typically, a total of 25 thermistors were located in the test cell or in the models: 18 were located on the boom, while 7 thermistors were located on various surfaces, such as the heater plate, the back wall and the window. Three thermistors were located outside

test space: 1 on the window surface, and 2 measuring the ambient air temperature in the warehouse space. A total of 306 temperature samples were taken at 18 points occurring along the plane of boom travel. 198 of these points occurred along the hypothesized plane of convection. (Fig. 2, p. 20) Flat computer cable carried the signal to the multiplexer. Experiments conducted in the (1/6·2) model indicated no significant changes in temperature fields when the attitude of the probe and supporting signal wire was changed from one side of the boom to the other.

The signal from a thermistor was passed along a wire with contiguous grounds to minimize signal noise. A precise low noise power input was required for the thermistors, as a 0.02V change equalled a 1°C change in temperature.

#### Signal Recording and Decoding

Thermistor signals were sequentially passed through a low noise ( $\pm 0.0006V$ ) multiplexer (Fig. A-18 is a circuit diagram for this multiplexer). The multiplexer may be switched to yield any number of sequence lengths and sample times. Multiplexer analog signals were passed to an HP3430A Digital Voltmeter. The voltage was read and manually entered into a Texas Instruments TI 59 calculator

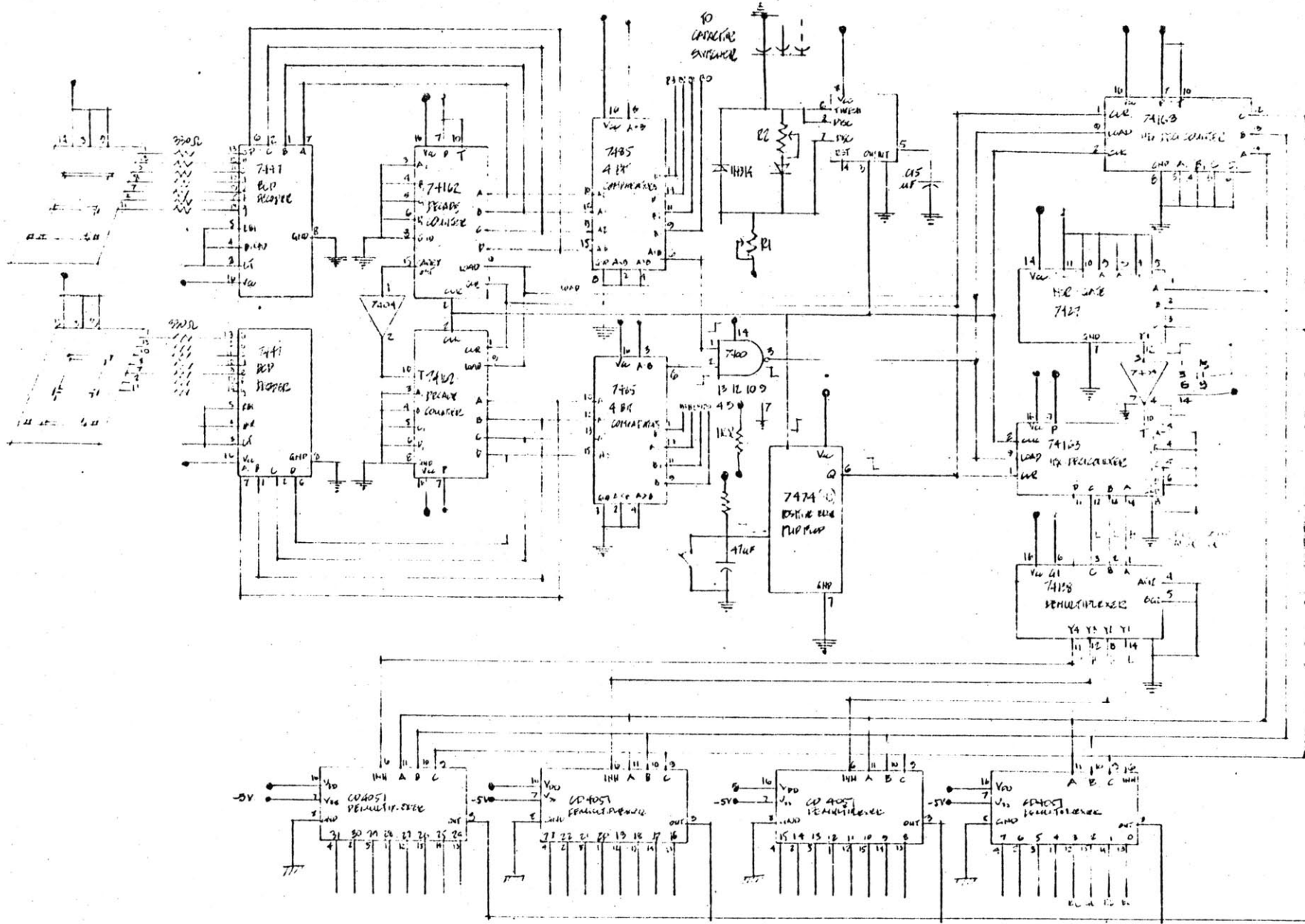


Fig. A-18.  
Low noise multiplexer design

(Fig. A-19). A PC 100A printer provided a written record of the temperatures and the data was also recorded onto magnetic cards.

A linear data interpolation program generated the data base for the isothermal plots. Data strips were mounted on a board, and the isotherms were drawn by joining the similar interpolated values.

#### Velocity Measurements

Velocity was sampled by a directional hot-wire anemometer coupled to a Flowtronic Velocity Meter (Model 55 A1). The lower threshold for accurate readings was ca. 1 M/min. (3.3 ft/min.). This anemometer was used to sample velocities in the test cell along the hypothesized convection plane (Fig. 2, p.20 ). A second meter, allowing vertical movement of the hot wire anemometer, was mounted on a vertical boom . Two sets of measurements were taken; both horizontal and vertical velocities were determined. The signal current was passed on to an HP 412 DC Vacuum Tube Multimeter.

#### Visualization

In order to confirm flows in the test cell, visualization experiments were performed. A number of techniques were attempted, all

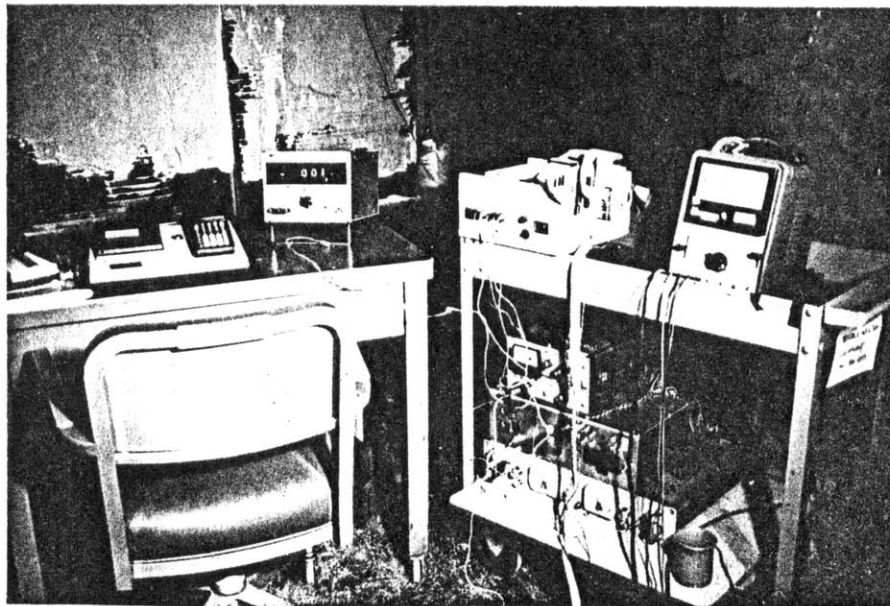


Fig. A-19. Instrumentation used for temperature decoding. TI-59 and voltmeter are located on table. Multiplexer and power supplies on cart.

employing the principle of suspending particles in air to render it visible.<sup>33</sup> Attenuated light sources were then employed to define a specific air movement plane.

Suspended Particles in Air. A number of visualization methods were tried:

- 
33. This in contrast to schlieren photography and interferometry use the different optical properties of various air densities to yield flow patterns.



- 1) Vermiculite dust: Vermiculite was ground into a fine powder and dispersed in the space by means of a fan or compressed gas. The vermiculite powder proved too heavy and settled too quickly. The finer suspended particles provided poor contrast for flow visualization (Fig. A-20).

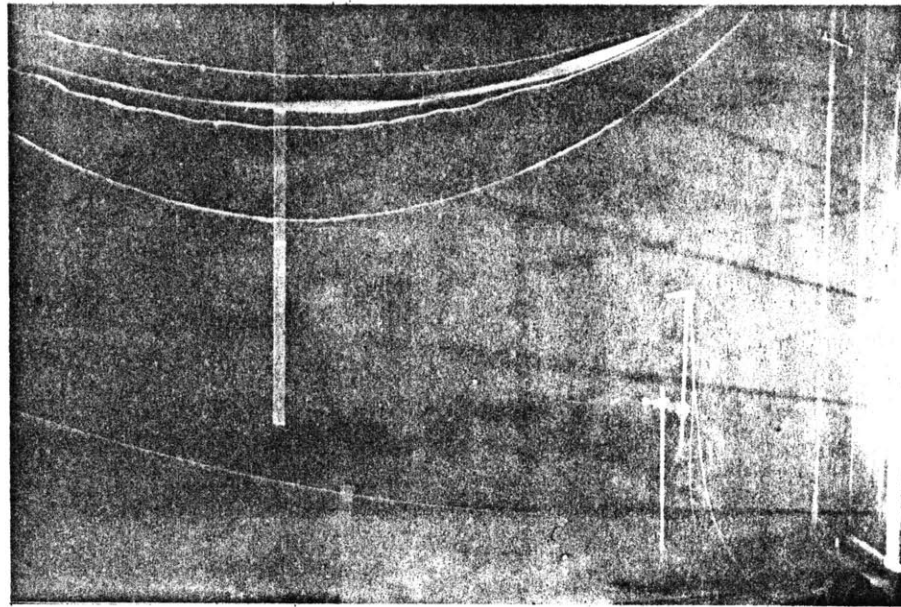


Fig. A-20. Vermiculite dust, lighted by attenuated spotlights, yields poor contrast. Instrumentation cables are located at ceiling.

- 2) Dandelion seed pods: Although these seed pods have high-drag-to-weight ratios, the pods deteriorate quickly after picking and lose their "floating" characteristics.

3) Soap bubbles:<sup>34</sup> Nitrogen and helium were mixed in a SAI Bubble Generator (Model 3). The soap bubble thus formed had neutral buoyancy. Pustefix bubble fluid with glycerine added yielded fairly long life times (1 min.) when blown outside the test cell. The introduction of the bubble into the test cell (Fig. A-21) decreased the life of the bubble to

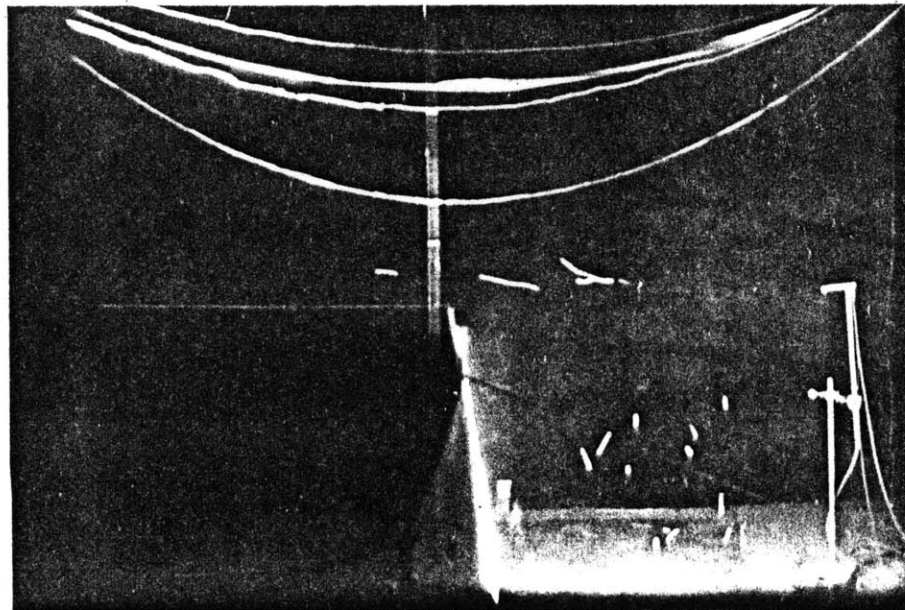


Fig. A-21. Shows traces of soap bubbles with baffle up in the test cell. Bubble wand is seen at right.

---

34. See G. A. Carpenter and L. J. Mailsey, "Visualization Techniques for Studying Air Movement," Building Services Engineer, Vol. 40.

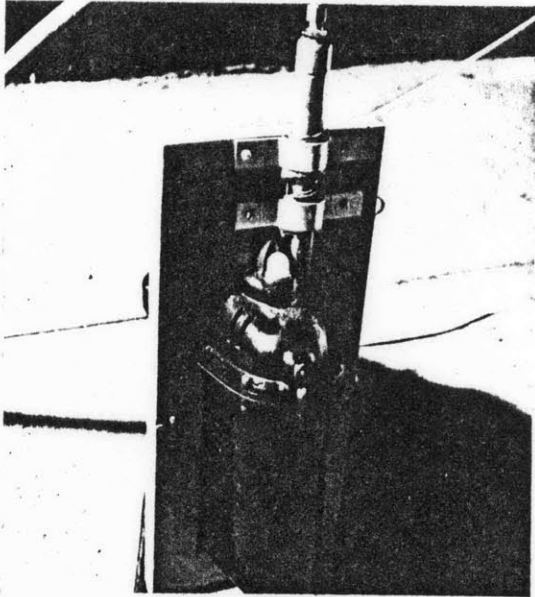


Fig. A-22. Fog juice vaporizer

5-10 seconds, due to the pressure difference between the bubble's internal temperature and the test cell's air temperature. For potentially better results using this technique, the gas cylinders should be kept at temperatures approximating those of the interior space.

- 4) Fog Juice: An esoteric blend of kerosene produces a thick, dense fog when heated in a converted insecticide vaporizer (Fig. A-22). This medium proved to be the most effective for flow visualization yielding contrasting flow images (Fig.A-23).



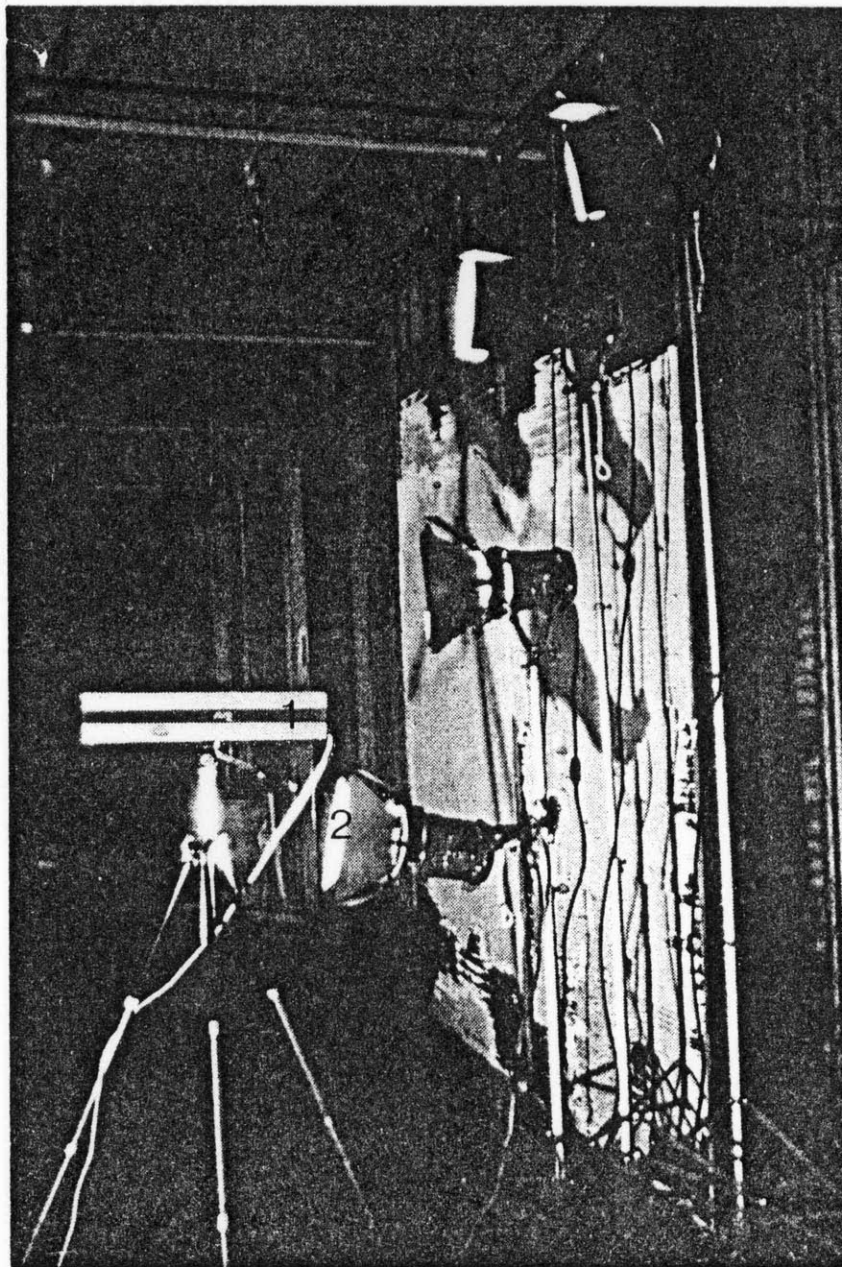
Fig. A-23. Contrasting flows achieved with vaporized fog juice.

Although thermal equilibrium was disturbed by the introduction of the warmer vapour, equilibrium was quickly restored (ca. 1 min.) as the amount of vapour introduced was small (ca. 100 mil/10 min.). The thick white fog dispersed after 5 minutes, and flow patterns after that time were difficult to discern.

Lighting. An attenuated light source was needed to isolate flow in a single plane. Two methods were used (Fig. A-24):

- 1) A laser beam was attenuated by projecting it through a glass rod. This laser (.3 mW) proved too weak to properly illuminate the suspended particles. As the laser light is forward dispersing, an acute viewing angle was maintained between the beam and the viewer, and a distorted view field resulted.
- 2) Baffled quartz incandescent spotlights were attenuated at the window by a foil baffle. The beam identified a 3 in. wide section within the room, clearly illuminating the fog juice, and the air flows. The convection flows were recorded through a viewing port using a Nuvicon video camera.

Fig.A-24. Attenuated lighting for the test cell was attempted with (1) a laser and (2) a series of spotlights attenuated by a baffle at the test cell window.



## Appendix III

### Dimensionless Parameters

Fluid flow is often described by the dimensionless numbers  $Re$ ,  $Sr$ ,  $Pr$ ,  $Gr$ , and  $Nu$ . These numbers are ratios between different fluid properties, or ratios of fluid properties to physical properties of a specific context. The fluid properties are:

$$\text{viscosity } (\mu) = \frac{M}{Lt} \quad (A\cdot1)$$

$$\text{kinematic viscosity } (\nu) = \frac{L^2}{t} \quad (A\cdot2)$$

$$\text{thermal diffusivity } (\kappa) = \frac{L^2}{t} \quad (A\cdot3)$$

$$\text{density } (\rho) = \frac{M}{L^3} \quad (A\cdot4)$$

$$\text{specific heat } (c) = \frac{E}{M} \quad (A\cdot5)$$

where

$M$  = mass

$L$  = length

$t$  = time

$E$  = energy

The physical context is defined by:

time ( $t$ )

length ( $L$ )

temperature ( $T$ )

pressure ( $P$ )

Dimensionless analysis<sup>35</sup> relates particular variables and yields dimensionless numbers which have a specific meaning and application. Empirical studies define value ranges for dimensionless numbers in which the formation of specific boundary layers<sup>36</sup> may be expected. If all the applicable fluid properties and physical contexts describing two dynamic systems have been included in dimensional analysis, and if the dimensionless numbers describing the systems are similar, then the two systems are dynamically similar.<sup>37</sup>

Reynold's Number. The Reynold's number (Re) for convective flows is the ratio of inertia forces to viscous forces.

$$\text{Re} = \frac{\rho V L}{\mu} \quad (\text{A}\cdot\text{6})$$

---

35. See Tritton, p. 70

36. Boundary layer is defined as the area in the fluid flow next to the friction layer where the greatest changes occur in the flow pattern.

37. A model changes the space (L) of a dynamic system. To keep the dimensionless numbers similar in the full scale and the model, another parameter of the system, such as velocity, may have to change.

where

$\rho$  = density

$V$  = velocity of flow

$L$  = characteristic length in the flow

$\mu$  = viscosity

It typically describes forced convection flows. Similitude of the Reynold's number is maintained in wind tunnel experiments by increasing the wind tunnel velocity (where  $V$  in wind tunnel  $\gg V$  at full scale), while decreasing the size (where  $L$  in wind tunnel  $\ll L$  at full scale).

Strouhal Number. The Strouhal number ( $St$ ) is a slowly varying function of  $Re$ . It specifies the frequency of flow variation.

$$St = nL/V$$

where

$n$  = frequency

$L$  = length of cycle

$V$  = velocity of flow

Above an  $Re$  of 200, the transition to turbulent flow takes place and vortex periodicity is lost.



Prandtl Number. The Prandtl number (Pr) is the ratio between the diffusivity of momentum and vorticity, and the diffusivity of heat.

$$\text{Pr} = \frac{\nu}{\kappa} \quad (\text{A}\cdot\text{8})$$

where

$\nu$  = kinematic viscosity

$\kappa$  = thermal diffusivity

In a simple pipe flow the thermal boundary layer occurs before the velocity boundary layer (with air as the fluid).

Grashof Number. The Grashof number (Gr) is a parameter describing natural convection. It is a measure of the relative importance of viscous effects versus inertial effects.

$$\text{Gr} = \frac{g\beta(\Delta T)L^3}{\nu^2} \quad (\text{A}\cdot\text{9})$$

where

$g$  = gravitational force

$\beta$  = coefficient of expansion

$\nu$  = kinematic viscosity

$L$  = characteristic length of heat flux element

$\Delta T$  = temperature difference between bulk air and convection flow

The product of the Grashof number and the Prandtl number (GrPr) is an indication of the convection to conduction ratio. Large GrPr numbers ( $>10^4$ ) indicate the onset of convection.<sup>38</sup> The orientation of the convection spaces and the attitude of the heat flux surface determine the numerical ranges of turbulent versus laminar flow.<sup>39</sup>

Nusselt Number. The Nusselt number (Nu) describes the heat transfer through a surface into or out of a convecting flow. For natural convection:

$$\text{Nu} = C(\text{GrPr})^y \quad (\text{A}\cdot 10)$$

where

C = constant

y = exponent

For hot plates on floors,  $c \sim 0.5$

$y \sim 0.2$

The heat transfer coefficient (h) may be related to the Nusselt number by:

$$h = \frac{\text{Nu}(k)}{L} \quad (\text{A}\cdot 11)$$

---

38. Holman, p. 223

39. W. H. McAdams, Heat Transmission, from ASHRAE Handbook of Fundamentals, p. 40.

where

$k$  = conductivity

$L$  = characteristic length of heat flux element

Dimensionless relationships describing other thermodynamic behaviors within a system may be defined. Rigorous thermal modelling defines dimensionless dynamic wall parameters  $K$ ,  $K_1$ ,  $K_2$ , and  $K_3$ .<sup>40</sup>

$$K = \frac{Nu}{Re \cdot Pr} \cdot \frac{A}{S} \quad (A \cdot 12)$$

$$K_1 = \frac{h_e}{h_i} \quad (A \cdot 13)$$

$$K_2 = h_i \frac{L}{k} \quad (A \cdot 14)$$

$$K_3 = \frac{\rho_w c_w L^2}{k \Delta t} \quad (A \cdot 15)$$

where

$A/S$  = Area/mass flow

$h_i$  = interior wall heat transfer coefficient

$h_e$  = exterior wall heat transfer coefficient

---

40. Suter and Choulat, p. 117

$L$  = wall thickness

$k$  = conductivity

$\rho_w$  = density of wall

$c_w$  = specific heat of wall

$\Delta t$  = time differential

Rigorous similitude in thermal models may be achieved by maintaining the similarity of the above dimensionless parameters in the model and the real world.

## Bibliography

The list of references is classified according to content. A direct reference to the thesis is indicated by an asterisk (\*).

### HEAT TRANSFER AND FLUID MECHANICS

ASHRAE. Handbook of Fundamentals. New York: The American Society of Heating and Refrigerating and Air Conditioning Engineers, 1967.

Brown, Aubrey, I. Introduction to Heat Transfer. New York: McGraw Hill, 1958.

\*Cammerer, W. F. "Insulating Values as a Function of Thickness," in Some Thermophysical Properties of Refrigerants and Insulants. Zurich: International Institute of Refrigeration, 1973.

Gebhart, Benjamin. Heat Transfer. New York: McGraw Hill, 1971.

Grober, H. Fundamentals of Heat Transfer. New York: McGraw Hill, 1971.

\*Holman, J. P. Heat Transfer. New York: McGraw Hill, 1968.

\*Kreith, Frank. Principles of Heat Transfer. Scranton, Ohio: International Textbook Company, 1958.

\*McAdams, W. H. Heat Transmission, 3rd Edition. New York: McGraw Hill, 1954.

Sabersky, R. H. et al. Fluid Flow. New York: MacMillan Company, 1971.

Threlkeld, James L. Thermal Environmental Engineering. Englewood Cliffs, N. J.: Prentice-Hall, 1970.

\*Tritton, D. J. Physical Fluid Dynamics. New York: Van Nostrand Reinhold Company, 1976.

## THERMAL PERFORMANCE OF BUILDINGS

Bassett, C. R. and Pritchard, M. D. W. Environmental Physics: Heating. New York: American Elsevier Publishing Company, Inc., 1969.

\*Bryan, A. D. "Performance Studies of a Working Solar Home," M.Arch.Thesis, MIT Department of Architecture, Cambridge, 1977.

Caudill, W. W. et al. Some General Considerations in the Natural Ventilation of Buildings. Texas Engineering Experiment Station, College Station, Texas, 1951.

E.R.D.A. Passive Solar Heating and Cooling, Conference and Workshop Proceedings, 1976, Albuquerque, New Mexico. Springfield, Virginia; U. S. Dept. of Commerce, 1976.

Howarth, A. T. and Morton, A. S. "Air Movement in an Enclosure with a Single Heated Wall," in Building Services Engineer, Vol. 40, Dec., 1972.

Institution of Mechanical Engineers. Heat and Mass Transfer by Combined Forced and Natural Convection. London: Institution of Mechanical Engineers, Sept., 1971.

Jones, B. W. "Energy and Housing Symposium, Bletchley, England, 1974" in Building Science, Oct., 1974. London: Pergamon Press.

\*McGuiness, William J. and Stein, Benjamin. Mechanical and Electrical Equipment for Buildings. New York: John Wiley and Sons, 1971.

O'Sullivan, P. E. and Cole, R. J. "The Thermal Performance of School Buildings," in Journal of Architectural Research, Vol. 3, no. 2, Feb., 1974.

Peavy, B. A. et al. Dynamic Thermal Performance of an Experimental Masonry Building. Building Science Series 45, July 1973. Washington, D.C. U. S. Dept. of Commerce, National Bureau of Standards.

Stoecler, W. F. Principles for Air Conditioning Practice. New York: Industrial Press, 1967. U. S. Dept. of Housing and Urban Development.

HUD. A HUD Guide, Heat Loss Calculations. Washington, D.C.: Hud, April, 1963.

#### MODELLING THE THERMAL PERFORMANCE OF BUILDINGS

Basnett, P. "Modelling Real Houses" in Journal of Architectural Research, Vol. 3, no. 3, Sept., 1974.

\*Bilsborrow, R. E. and Fricke, F. R. "Simulation of Building Ventilation in Wind Tunnels," in Building Science, Vol. 10, 1975. London: Pergamon Press.

\*Carpenter, G. A. and Maisley, L. J. "Visualization Techniques for Studying Air Movement" in Building Services Engineer, Vol. 40, Dec., 1972.

Chorin, A. J. Numerical Study of Thermal Convection via Fluid Layer Heated from Below. New York: A. E. C. Computing and Applied Mathematics Center, Courant Institute of Mathematical Sciences, New York University, August, 1966.

\*Croome, D. J. and Roberts, B. M. Air Conditioning and Ventilation of Buildings. Oxford: Pergamon Press, 1975.

Holleman, T. R. Air Flow Through Conventional Window Openings. Texas Engineering Experiment Station, College Station, Texas, 1951.

\*Lebens, R. M. "Passive Background and Workbook," M. Arch. A.S. Thesis, MIT Department of Architecture, Cambridge, MA., Jan., 1978.

Parsons, D. et al. Subway Environmental Design Handbook. Washington, D.C.: U. S. Department of Transportation, 1976. Appendix B-1.

\*Peavy, B. A. et al. Comparison of Measured and Computer-Predicted Thermal Performance of a Four Bedroom Wood Frame Townhouse. Building Science Series 57, April, 1975. Washington, D.C.: U. S. Department of Commerce, National Bureau of Standards.

Smith, E. G. The Feasibility of Using Models for Predetermining Natural Ventilation. Texas Engineering Experiment Station, College Station, Texas, 1951.

Snock, C. W. and Tarasuk, J. D. "Heat Transfer from Inflatable Structures," in ASME Papers, 76-WA/HT-97, 1976.

\*Suter, P. and Choulat, C. "Essais sur Modèle Réduit Concernant la Dynamique de Locaux Chauffés à Similitude Rigoureuse," Air Conditioning of Rooms and Vehicles. Paris: International Institute of Refrigeration, 1973.

Thomason, H. E. Solar House Model. New York: Edmund Scientific, 1965.

#### THERMAL COMFORT

Fanger, P. O. Thermal Comfort. Copenhagen: Danish Technical Press, 1970.

Gerlach, K. A. "Environmental Design to Counter Occupational Boredom" in Journal of Architectural Research. Vol. 3, no. 3, Sept., 1974.

Longmore, J. and Ne'eman, E. "The Availability of Sunshine and Human Requirements for Sunlight in Buildings" in Journal of Architectural Research. Vol. 3, no. 2, Jan., 1974.

#### SCIENTIFIC RESEARCH

Wilson, E. Bright, Jr. An Introduction to Scientific Research. New York: McGraw Hill, 1952.